Master's thesis in Physics
Quantum Transport Theory

Spin blockade in Cooper pair splitters

Jami Rönkkö

February 15, 2020

Tutor: Dr. Ciprian Padurariu

Censors: Prof. Kari Rummukainen
Prof. Christian Flindt

UNIVERSITY OF HELSINKI
Department of Physics
Gustaf Hällströmin katu 2, 00560 Helsinki

HELSINGIN YLIOPISTO — HELSINGFORS UNIVERSITET — UNIVERSITY OF HELSINKI

Tiedekunta — Fakultet — Faculty	Laitos — Institution — Department
Faculty of Science	Department of Physics

Tekijä — Författare — Author
Jami Rönkkö

Työn nimi — Arbetets titel — Title

Spin blockade in Cooper pair splitters

Oppiaine — Läroämne — Subject
Quantum Transport Theory

Työn laji — Arbetets art — Level	Aika — Datum — Month and year	Sivumäärä — Sidoantal — Number of pages
Master's thesis in Physics	February 15, 2020	106

Tiivistelmä — Referat — Abstract

Entanglement is a valuable resource for quantum computing and information technologies. A promising way to obtain spin-entangled electrons is the splitting of Cooper pairs residing in superconductors. This is realized by a nanodevice called Cooper pair splitter. A Cooper pair splitter is realized by tunnel-coupling a superconductor to two quantum dots, which are each further tunnel-coupled to separate terminal leads. This setup enables the extraction and splitting of Cooper pairs from the superconductor into the terminals via the quantum dots.

The quantum dots are commonly fabricated from semiconducting materials like InAs and InSb, that can manifest spin-orbit interaction. This thesis studies the effect of spin-orbit interaction on the spin state of the electron pair in the Cooper pair splitter. Activating the spin-orbit effects in a Cooper pair splitter requires a static magnetic field to be applied to the quantum dots. Together with the gate electrodes controlling the electrostatic energy of the quantum dots, the external magnetic field provides a handle for addressing different two-particle spin states.

The spin-orbit interaction can be activated by various combinations of the gate voltage and Zeeman magnetic field, that create resonances between different states of the system. The most interesting coherent evolution, that can be invoked in this way, involves the simultaneous activation of the two spin-polarized triplet states. This gives a rise to an entangled Bell state, $(|\uparrow\uparrow\rangle + |\downarrow\downarrow\rangle)/\sqrt{2}$, that moreover exhibits spin blockade and thus stabilizes entanglement in the Cooper pair splitter.

Secondly, the spin-orbit interaction can be used to bypass suppressed Cooper pair tunneling at a high superconductor-quantum dots detuning. Introducing a large Zeeman magnetic field allows Cooper pairs to tunnel into the dots given that their spin state flips to the triplet $|\downarrow\downarrow\rangle$. Although this regime lacks spin-entanglement, it is of interest for creating triplet Cooper pairs and spin-polarized superconducting currents.

Avainsanat — Nyckelord — Keywords
Cooper pair splitter, spin-orbit coupling, entanglement, spin-current

Säilytyspaikka — Förvaringsställe — Where deposited

Muita tietoja — övriga uppgifter — Additional information

Contents

1. Introduction

Entanglement [1, 2] is a fundamental quantum mechanical property that, in addition of being of immense theoretical interest [3, 4, 5], is an essential resource for encoding quantum information [6, 7, 8, 9]. In short, entanglement signifies non-local correlations between quantum particles. Entanglement is of particular interest in quantum information processing, that utilizes spatially separated entangled particles, so called Einstein-Podolsky-Rosen-pairs [10], for new kind of computing and communication [9, 11]. The production of photon EPR-pairs, where the photon polarization is the entangled quantity, has been first realized in 1970s [12, 13]. In contrast, despite the abundance of entanglement in solid-state physics [14], the controlled production of spin-entangled electrons remains a challenge.

Accessing individual electrons has become possible as a result of nanotechnology reaching ever smaller length scales [15]. The propagation of electrons in nanoscale metal or semiconductor structures involves quantum effects, such as quantization of energy levels, and is studied in the field of quantum transport [16, 17]. In nanodevices, electric current can be shrunken down to individual events of electrons hopping across insulating barriers. Moreover, the flow of electrons through isolated pieces of semiconducting islands can become blockaded as the Coulomb repulsion of electrons in them prevents further electrons from tunneling in. This effect, known as the Coulomb blockade, proves to be useful for production of entangled electron pairs in a solid state setting [18, 19].

Superconductors are a naturally occurring source of entangled pairs [20]. A metal becomes superconducting when, below its critical temperature, its conduction electrons pair up as Cooper pairs propagating with zero energy dissipation. The Cooper pairs of a conventional superconductor [21] occupy a specific two-electron state known as the spin-singlet [22]. The wavefunction of the singlet is a quantum superposition of the spin 'up-down' and 'down-up' states, $(|\uparrow\downarrow\rangle - |\downarrow\uparrow\rangle)/\frac{1}{\sqrt{2}}$. The state is spin-entangled since if one spin is known, the other one is also determined, as it must be opposite. In the ground state of a superconductor, all conduction electrons are bound as Coopers pairs [23]. Hence, a superconductor principally yields electrons only in pairs to remain in its ground state.

This insight motivates the subject of this thesis, a nanodevice called Cooper pair splitter [24, 25]. A Cooper pair splitter essentially consists of a superconductor separated by insulating tunneling barriers from two single-level quantum dots, each of which are further coupled to separate terminal leads. Quantum dots [26, 27] are tiny, less than 100 nm in width, semiconductors that have significantly discrete electron energy levels as a result of quantum confinement. In a single-level quantum dot, or a resonant level, only one energy level is available for electrons. The Coulomb blockade can be utilized to block the tunneling of a second electron on the resonant level [24], making it effectively a box that fits only one electron at a time. In a Cooper pair splitter, this forces the Cooper pairs to split between the two quantum dots upon tunneling. Hence, a voltage bias can be used to generate flow of entangled electron pairs directed from the superconductor to each of the leads. The idea of such a device was first proposed in 2001 [24] and realized in 2009 [25].

There are no spin-flips involved in the conventional model of Cooper pair splitter [24], so the spins of the electron pair will remain in the singlet state throughout the transport from the superconductor to the leads. It is known [28, 29], however, that electrons traversing through certain semiconductors, such as indium arsenide

(InAs) [30] can experience spin-flips caused by an effect known as spin-orbit interaction [31, 32, 33]. Since the quantum dots of a Cooper pair splitter are semiconductors with potential to exhibit spin-orbit coupling, and the quantity of interest is the entangled spin of the electrons, it seems natural to ask what effects the spin-orbit interaction would have on the operation of a Cooper pair splitter?

This motivates the research questions of this thesis: How does active spin-orbit interaction in the quantum dots of a Cooper pair splitter affect the spin state of the electron pairs? To what degree can the spin state be manipulated? What happens to the entanglement?

It turns out, that the spin-orbit interaction can indeed give rise to spin-rotations for the electron pairs in the dots. An external static magnetic field is required to break the time reversal symmetry that normally mitigates spin-orbit effects in solids. This Zeeman magnetic field and the capacitive gate detuning of the dot energy levels function as handles to the coherent evolution of the spin states. By tuning these handles, different two-particle spin states can be made degenerate in the presence of an active spin-orbit interaction. This causes the electron spins to rotate in the dots and introduces the spin-triplet states in the Cooper pair splitter. Employing a time-dependent gate detuning would allow spin-manipulation at the dots, in a fashion of the electric dipole spin resonance (EDRS) method [34].

This thesis presents a scheme for verifying the spin-flips, that take the electrons on the quantum dots from the singlet state, $(|\uparrow\downarrow\rangle - |\downarrow\uparrow\rangle)/\frac{1}{\sqrt{2}}$, to polarized triplet states, $|\uparrow\uparrow\rangle$ and $|\downarrow\downarrow\rangle$. In the conventional operation regime of the device [24], the tunneling rate between quantum dots and terminal leads is fast and the dot occupation time is vanishing. This leaves no time for measuring the state of the electron pair on the well isolated dots before the electrons are lost in the reservoirs of the terminal leads. In order to give time for the spin-flips and their measurement, the transport through the Cooper pair splitter needs to be slowed down by reducing

the dots-to-terminals tunneling rate.

In the limit where the dots-to-terminals tunneling rate is much slower than the superconductor-to-dots tunneling rate, the time evolution of the superconductor-coupled double quantum dot can be observed. The coherent evolution results firstly from the superconductor-coupling, that hybridizes the empty dot state (singlet pair in the superconductor) and the singlet pair on the dots and secondly on the spin-orbit coupling, that introduces the triplet states via spin-flips. The fact that only electrons in a spin-singlet state can enter the superconductor leads to a spin blockade [35] for electron pairs in a triplet state. When occupying a triplet state, an electron pair remains trapped in the quantum dots, until it rotates back to the singlet state able to realize a tunneling back to the superconductor.

Thus, observing the effects of spin blockade on the quantum dots amounts to proving that spin-flips have taken place. The average occupation, and hence electric charge, on the double dot increase due to spin blockade. This means that instead of directly measuring the spins of the electrons, which is more challenging, it suffices to measure the average charge. By using a quantum point contact [36, 37], an efficient capacitive real-time measurement can be performed. Alternatively, the slow connection to terminal leads can be utilized in tunneling spectroscopy approach for probing the charge state on the dots.

In addition to the way to verify the spin-orbit interaction in the Cooper pair splitter, a couple of interesting coherent states are discussed. In particular, at a zero detuning between the superconductor and dots, the two polarized triplet states can be addressed simultaneously giving rise to an equal superposition state, $(|\uparrow\uparrow\rangle + |\downarrow\downarrow\rangle)/\sqrt{2}$. Being product states, the polarized triplets generally ruin the entanglement in a Cooper pair splitter. However, remarkably, the equal superposition of polarized triplets is maximally entangled and also especially long-lived due to the spin blockade. Hence, the occupation of this triplet state increases the average time

the quantum dots hold entangled electrons.

Away from the zero-detuning regime, the polarized triplets can only be addressed individually, by specific values of Zeeman magnetic field which enable spin-rotations due to spin-orbit coupling to only one of the triplets. Despite ruining the entanglement of electron pairs, the ability of accessing the individual triplets turns the Cooper pair splitter into a source of spin-polarized electrons [38]. The extreme case occurs in a regime of high detuning, where the ordinary Cooper pair transport between superconductor and dots becomes near completely suppressed. Using high external magnetic field, a degeneracy between the polarized triplet, $|\downarrow\downarrow\rangle$, and the empty dot state can be reached, allowing spin-orbit coupling to mix the two. In view of this, the Cooper pair splitter could thus be used as a source of pair-wise emitted spin-polarized electrons.

The structure of the thesis is the following. The first three chapters, after the introduction, each discuss some physical phenomenon, that together create the physics of a Cooper pair splitter. In short, these phenomena are the electron tunneling in the dynamic Coulomb blockade regime (Chapter 2), two-particle spin states (Chapter 3) and superconductor-normal metal junction (Chapter 4).

Chapter 5 discusses the double quantum dot-regulated electron transport through the conventional Cooper pair splitter. In Chapter 6 the reader is familiarized with the spin-orbit interaction. The main results of the thesis, the evolution of the spin state leading to a spin blockade is discussed in Chapter 7.

In Chapter 8 a measure called concurrence is used to quantify the entanglement on the double quantum dot. Finally, in Chapter 9, two charge based detection schemes are suggested for indirect measurement of the spin state and its concurrence. The concluding Chapter 10 presents some discussion and future implications of the main results.

2. Coulomb blockade

Cooper pair splitters operate in an exotic conductance regime known as the dynamic Coulomb blockade regime [16, 17]. In most of the solid state physics, the celebrated free-electron model [39] can be used to accurately model electrons by non-interacting quasiparticles known as solid-state electrons. However, many nanodevices include components where electrons are localized close to each other. In such setups, the free-electron model is no longer applicable. Instead, the Coulomb interaction leads to a concept of charging energy, that renders the energy spectrum of charge carriers discrete [40]. Electron localization occurs in parts of a nanostructure separated from the rest of it by weakly conducting tunnel barriers, where an electron can be trapped for a time.

The fundamental unit of conductance in electron transport is the conductance quantum $G_Q = 2e^2/h$. It is the conductance of a channel that allows only two electrons of opposite spins to enter at a time, with transmission probability of one [41]. It is, therefore, the minimum conductance for a spin degenerate ballistic nanoconductor. Non-ballistic channels i.e. those with transmission probability less than one, have conductance less than the conductance quantum. A barrier with conductance $G \ll G_Q$ will stagnate the electron flow to an occasional trickling and stack up electrons on the other side. Such low conductance characterises the dynamic Coulomb blockade regime reviewed in this chapter.

2.1 Charging energy

The isolated parts of a Coulomb nanostructure, called *islands*, form the center for the physics in the dynamic Coulomb blockade regime. On an island, an excess electron, whose charge is not countered by a positive nucleus, generates an electric field around itself. This electric field possesses electrostatic energy $E_{el} = e^2/2C$, where C is the capacitance of the island. An island with N number of excess electrons has a charge eN and electrostatic energy

$$E_{el} = \frac{e^2}{2C}N^2, \tag{2.1}$$

where $E_C \equiv \frac{e^2}{2C}$ is termed the *charging energy*. Adding Nth electron to an island with a charge $e(N-1)$ increases the electrostatic energy by $\Delta E_{el} = E_C N^2 - E_C(N-1)^2 = E_C(2N-1)$. This extra energy needs to be provided to surpass the Coulomb repulsion when adding an electron to a charged island. The uncompensated charging energy will block a current from flowing, giving rise to a *Coulomb blockade* [42].

The charging energy E_C is inversely proportional to the capacitance of the island and is therefore determined by the size and separation of the island. For macroscopic islands the large capacitance leads to a vanishing charging energy. In the opposing limit, as one reduces the size of the island to the length scales of the De Broglie wavelength of an electron, another energy scale has to be taken into consideration. As the island gets smaller, the discreteness of electron energy levels becomes more prominent by the virtue of increased quantum confinement so that the interval between energy levels, the mean level spacing δ_S, has to be considered. Only two electrons can fit to a single energy level, which means that subsequent electrons have to go to a higher empty level with δ_S more energy. This energy has to be provided as an extra part of the addition energy on top of the charging energy E_C.

Comparison of the charging energy and mean level spacing for a 100 nm island

with 10^9 atoms yields $E_C/\delta_S \approx N_{atoms}^{2/3}$ [17]. Hence, the contribution of the discreteness of energy levels to the addition energy is vanishing compared to the charging energy if the island consists of a large number of atoms. This *metallic island* limit is assumed in this chapter in order to illuminate the basic concepts of the dynamic Coulomb blockade regime. The opposite limit, where $\delta_S \gg E_C$, is discussed in Sec. 5.1. Properties of such *quantum dots* prove to be essential to the operation of Cooper pair splitters.

2.2 Capacitance circuits

A coulomb nanostructure can be conceptually represented by a DC electric circuit consisting of capacitors and voltage sources. In this picture, the islands are formed by plates of two or more capacitors, so that one of the adjacent plates of each capacitor is part of the island while the second plate belongs to circuit elements connected to the island, as illustrated in the left side of Fig. 2.1. The gaps between capacitor plates describe tunneling barriers defined both by their capacitance and conductance. Electron transmission is represented as occasional leaking of these capacitors: given enough energy an electron can hop across the capacitor plates creating a tiny current. The tunnel barriers separate the islands from the rest of the nanodevice, where electrons follow the metallic free electron model [39]. These lead electrodes (reservoirs of delocalized electrons) correspond to anodes and cathodes of voltage sources in the circuit. The difference in electric potential between the source and drain leads, represented by the bias voltage V_b will drive current through island, if it is not prevented by the Coulomb blockade.

In addition to islands and leads, *gate electrodes* have an important role in the Coulomb capacitance circuits. A gate is connected to a separately adjustable voltage source V_g and is placed farther from the island than source and drain leads in the realization of the circuit. This results in a weak coupling that suppresses electron

tunneling between the island and gate. As the gate is coupled only capacitively to the island, no electron transfer may take place between them. Instead, the function of a gate is to affect the electrostatic energy of an island by inducing charge, that can trigger or prevent electron tunneling between the island and other leads.

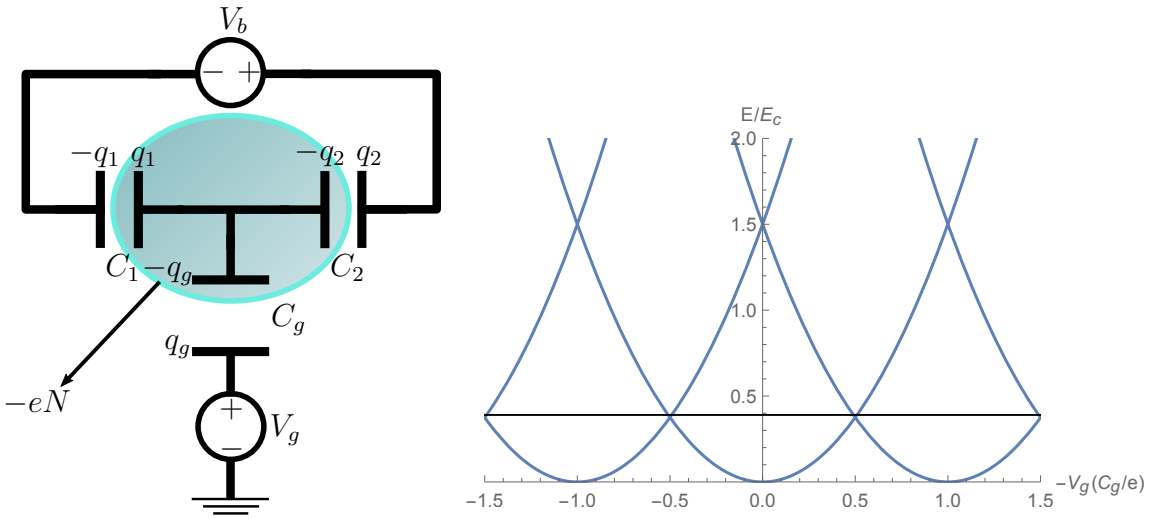

Figure 2.1: (Color online.) Single electron transistor. **Left:** Electric circuit corresponding to an elementary Coulomb device consisting of a single island coupled to source, drain and gate electrodes. The charge on the island is quantized as multiples of the elementary charge $-eN$. The gate electrode is used to manipulate the electrostatic energy of the island to govern the electron transport through it from the source to the drain. **Right:** The electrostatic energy E_{el} (2.2) of the island in units of charging energy E_C for various charge states N as a function of the gate voltage V_g in units of $-e/C_g$. The three parabolas correspond to having $-1, 0$ and 1 excess electrons on the island. The energy of the system is minimum below the horizontal line, which implies that electron transfers become preferable as the gate voltage reaches degeneracy points $V_g = \pm 0.5e/C_g$.

2.3 Gate electrodes

The electrostatic energy of an isolated island, $E_{el} = E_C N^2$, will be modified by voltage sources of the circuit that it is part of. Voltage will cause charge to accumulate on the capacitor plates adjacent to the island, which generates electric fields. These electric fields will increase the island's electrostatic energy as they induce a charge q on it. The electrostatic energy accounting for this induced charge can be written as

$$E_{el} = E_C(N - \frac{q}{e})^2, \tag{2.2}$$

where the charging energy includes a sum over capacitances of all circuit elements connected to the island, $E_C \equiv e^2/2\sum C_i$. Likewise, the induced charge $q \equiv -\sum C_i V_i$ is generally contributed to by all adjacent elements. It is, however, often convenient to choose antisymmetric bias voltage $V_{\text{sources}} = -V_{\text{drains}}$, so that source and drain contributions cancel in the above sum, making the induced charge depend solely on the gate voltage V_g.

Note that while the electrostatic energy of Eq. (2.2) is now continuous due to the gate voltage $q = -C_g V_g$, the charge on the island is always an integer multiple of the electron charge, $-eN$. The result of this can be illustrated by plotting the electrostatic energy versus the gate voltage for different numbers of excess electrons N. Such plot yields a set of parabolas each reaching zero energy at the minimum vertex and shifted by integer number from each other, as displayed in the right panel of Fig. 2.1. Clearly the island has minimal energy whenever the gate voltage is an integer multiple of e/C_g corresponding to the number of excess electrons. Lowering (increasing negative) V_g boosts the electrostatic energy of an island in charge state N until it reaches a degeneracy point with a state of $N + 1$ electrons as the corresponding parabolas cross. At this point the Coulomb blockade is lifted and a tunneling of an electron to the island is allowed. Further decrease of V_g will

allow another electron to enter after a full period of e/C_g. Likewise, raising the gate voltage will lead to electrons periodically tunneling away from the island in order to relax the electrostatic energy.

Hence, the charge quantization of the island causes its electrostatic energy to be a periodic function of the gate voltage. This presents a useful tool to control the number of electrons on the islands as well as deny or allow tunneling by the use of Coulomb blockade. Although the electron tunneling is a quantum mechanical effect, the dynamics of the transport in the dynamic Coulomb blockade regime are governed by concepts from classical physics such as energy conservation and probability balance, as will be discussed next.

2.4 Sequential tunneling

The state of an island is characterized by the number of excess electrons in it. This charge state changes when electrons tunnel between the island and other parts of a nanodevice. Because of the weakly conducting connections $G \ll G_Q$, nanosystem spends most of its time in one of the well defined charge states. Tunneling occurs rarely and is dominated by the most probable case of a single-electron transfer.

Consider the single electron transistor portrayed in Fig. 2.1. The device consists of an island connected to three electrodes: a source (on the left), a drain (on the right) and a gate. A single electron transfer between charge states N and $N+1$ or $N-1$ is possible if it complies with the energy conservation principle. In other words energy can only be dissipated, not increased, unless it is brought from outside as heat or work. This corresponds to the difference of the energies of the initial and final states of a process being negative, $\Delta E < 0$. Assuming vanishing thermal fluctuations, only the difference in the electric potentials across the tunneling barrier and a change in the electrostatic energy of the island contribute to the electron addition energy of the tunneling event. An island in charge state N holds electrostatic

energy given by Eq. (2.2). Therefore, the energy difference between states N and $N \pm 1$, is

$$\Delta E = E_{el}(N \pm 1) - E_{el}(N) \mp eV_{L/R}. \tag{2.3}$$

The last term $eV_{L/R}$ represents the energy gained (paid) from extracting (adding) an electron from the left or right lead with electric potentials V_L and V_R respectively. There are two tunable parameters dictating whether tunneling process is allowed or not: the gate voltage V_g governing the electrostatic energy E_{el} and the bias voltage $V_b = V_L - V_R$ responsible for the different chemical potentials of the left and right leads $eV_b = e(V_L - V_R)$.

Now, there are four possible single electron transfers: an electron tunneling to or from the left lead and an electron tunneling to or from the right lead. Whether the energy difference (2.3) for each of these transports is negative or not dictates the transport regimes of the device. Consider such bias voltage V_b and gate voltage V_g, that $\Delta E < 0$ for an electron tunneling from the left reservoir to the island and from the island to the right reservoir, while $\Delta E > 0$ for the opposite transfers. There is now a current running from left to right as the island oscillates between charge states $N = 0$ and $N = 1$. See the region marked as $0 \rightleftharpoons 1$ in Fig. 2.2.

The region where the energy costs for all single electron transfers are negative is Coulomb blockaded. When the bias and gate voltages of the system are within this regime, the charge state of the island remains unchanged and there is no current. In the $V_g - V_b$ plane, the conditions $\Delta E > 0$ for various transfers are represented by slanted lines. For the single electron transistor considered earlier with symmetric bias voltage $V_L = -V_R = V_b/2$, these lines form the typical diamond pattern seen in the middle of Fig. 2.2 known as the *Coulomb diamonds*. In order to produce such plots, one has to know the electric current as a function of the two voltages. This is achieved by utilizing the *master equation* approach.

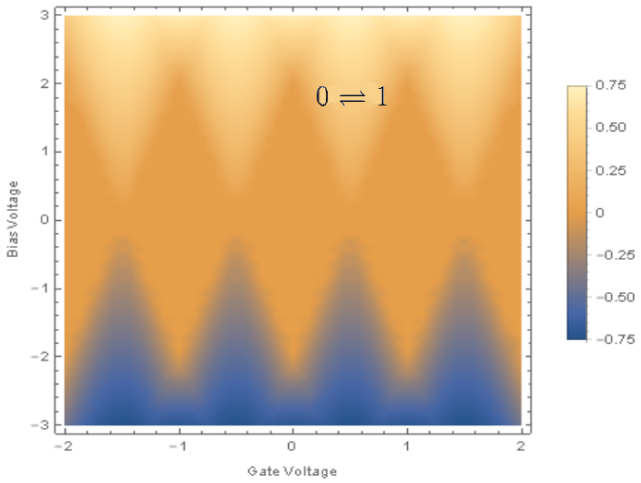

Figure 2.2: (Color online.) Coulomb blockade. The colours represent the current (2.7) through a metallic island as a function of bias V_b and gate voltages V_g, calculated from the master equation (2.5). Sequential tunneling is blocked within the rhombuses centered at zero bias voltage, known as the Coulomb diamonds. Each diamond corresponds to a different discrete charge state. In the regions around the diamonds, there is a finite current, carried by single electron transfers either from left to right or in the opposite direction for opposite bias voltage. The region responsible for transitions between charge states $N = 0$ and $N = 1$ is labelled in the picture as an example.

2.5 The master equation and current

The time evolution of the charge states of Coulomb nanostructures and the resulting current can be solved by considerations of probability balance. Since the charge states are classical non-coherent states, classical reasoning suffices to deduce their evolution. An electron transition from a charge state to another, given that it is allowed by the energy conservation, is realized if some electron actually undergoes a tunneling event. To quantify the probabilistic nature of electron transitions, rate $\Gamma_{\alpha\to\beta}$ is introduced. It equals the probability per unit time that electron tunnels

from a charge state α to β.

The probability of an island to be in a charge state N is denoted by the occupation probability distribution $P(N)$. Assigning the charge states with classical probability distributions is possible because the island has time to relax into incoherence after every tunneling event. The state of the island changes only due to charges either leaving or arriving from the neighbouring charge states $N+1$ and $N-1$. It is convenient to label states with α and β so that the states α evolve to neighbouring charge states β at a tunneling rate $\Gamma_{\alpha\to\beta}$. The time evolution of a charge state α is then written as

$$\frac{d}{dt}P(\alpha) = -\sum_{\beta}^{M}\Gamma_{\alpha\to\beta}P(\alpha) + \sum_{\beta}^{M}\Gamma_{\beta\to\alpha}P(\beta), \tag{2.4}$$

where the rates taking the system away from the initial charge state are assigned with a minus sign and M is the total number of charge states. This balance equation is called the master equation. For practical purposes it is easiest to write it as a matrix equation

$$\frac{d}{dt}P_{\alpha} = \sum_{\beta}^{M}\hat{\Gamma}_{\alpha\beta}P_{\beta}. \tag{2.5}$$

The diagonal elements of the matrix $\hat{\Gamma}$ contain rates from state α to other states and the off-diagonal elements contain rates, that bring the system to state α, corresponding respectively to the first and second terms in Eq. (2.4).

The rates Γ do not change in time as long as the capacitances, bias and gate voltages in the circuit are kept constant. There exists, therefore, a set of stationary solutions to the master equation, $\{P^0(\alpha)\}$. These time-independent solutions, $\frac{d}{dt}P^0(\alpha) = 0$, correspond to a situation where the incoming and outgoing terms cancel in the right hand side of Eq. (2.4). With the aid of condition $\sum_{\alpha}^{M}P(\alpha) = 1$ i.e. the sum of all occupation probabilities is unity, the steady states can be straightforwardly found. In the matrix formalism of the master equation, finding the steady

states corresponds to finding an eigenvector associated with the zero eigenvalue,

$$\sum_{\beta}^{M} \hat{\Gamma}_{\alpha\beta} P^0_\beta = 0. \tag{2.6}$$

The components of the eigenvector P^0_β are the steady probabilities $P^0(N), P^0(N \pm 1), P^0(N \pm 2)...$, that can be solved as a function of the rates $\Gamma_{\alpha\to\beta}$.

The state transitions evoke a tiny current in the nanocircuit as each electron hop transfers elementary charge across a tunneling barrier. The stationary current through the circuit is found by considering rates at any junction of the device. As long as the steady states $P^0(\alpha)$ are used and there is no splitting of the current in the circuit, charge conservation ensures that the same current goes through all junctions. The stationary current through a given junction is a sum of the competing contributions of electrons going both to and from any of the stationary states

$$I = e \sum_{\alpha} (\Gamma_{\alpha\to\alpha+1} - \Gamma_{\alpha\to\alpha-1}) P^0(\alpha). \tag{2.7}$$

As an example of solving the stationary current using the master equation, consider transfer through a simple lead-island-lead structure with the left lead having higher chemical potential so that the electrons move from left to right. Consider for simplicity only charge states N and $N+1$. Tunneling from the left lead to the island changes the charge state from N to $N+1$ with rate Γ_L and tunneling from the island to the right lead brings it back to state N with rate Γ_R. Therefore, the charge state of the island oscillates between N and $N+1$ as electrons pass through the junctions. The time derivatives of stationary solutions of the master equation are zero,

$$\begin{cases} \frac{dP^0(N)}{dt} = \Gamma_R P^0(N+1) - \Gamma_L P^0(N) = 0 \\ \frac{dP^0(N+1)}{dt} = \Gamma_L P^0(N) - \Gamma_R P^0(N+1) = 0. \end{cases}$$

With the help of unity condition, the stationary occupation probabilities $P^0(N) = \Gamma_R/(\Gamma_R + \Gamma_L)$ and $P^0(N+1) = \Gamma_L/(\Gamma_R + \Gamma_L)$ are readily solved and the current (through the left junction) is obtained from the Eq. (2.7) as

$$I_L = e\Gamma_L P^0(N) = e\frac{\Gamma_L\Gamma_R}{\Gamma_R + \Gamma_L}. \tag{2.8}$$

By virtue of the charge conservation, the same current goes through both junctions, $I_R = I_L$. To conclude the analysis of the sequential tunneling at the Coulomb blockade regime, the classical description must finally give way to the quantum theory for the determination of the rates $\Gamma_{\alpha\to\beta}$.

2.6 Tunneling rates

To obtain actual values for the stationary current in Coulomb nanostructures from Eq. (2.7) the rates $\Gamma_{\alpha\to\beta}$ must be known in terms of the circuit parameters. That is achieved by the quantum mechanical perturbation theory [43], known in this context as the tunneling Hamiltonian method [44]. Establishing the states of the islands and leads of the circuit, with their individual quantum states labeled by i and l, respectively, as the unperturbed Hamiltonian $\hat{H}_0 = \sum_i \hat{H}_i + \sum_l \hat{H}_l$ and the tunneling events as small perturbations given by Hamiltonian $\hat{H}_T$, enables a perturbative approach to the analysis of the tunneling dynamics. Convenient formalism for the Hamiltonians is the second quantization (see e.g. [44]), centered around the creation and annihilation operators $\hat{a}^\dagger_{l,\sigma}$ and $\hat{a}_{l,\sigma}$. The individual energy states of a lead or island are expressed using the Dirac notation $|n\rangle_{l,\sigma}$, where n gives the number of electrons in a given energy state l with a spin σ. Each l is associated with two σ's because of the two possible spin orientations $\sigma = \{\uparrow, \downarrow\}$. Due to the Pauli exclusion principle, each energy level can have up to one fermion so that n must be either 0 or 1. This simplifies the effect of the creation and annihilation operators for electrons to four following operations.

The creation operator $\hat{a}^\dagger_{l,\sigma}$ acts on the corresponding empty state $|0\rangle_{l,\sigma}$ by adding one electron to it $\hat{a}^\dagger_{l,\sigma}|0\rangle_{l,\sigma} = |1\rangle_{l,\sigma}$. In accordance with the Pauli exclu-

sion principle, acting with a creation operator on a filled state destroys the state $\hat{a}^{\dagger}_{l,\sigma}|1\rangle_{l,\sigma} = 0$. Annihilation operator conversely removes an electron from an occupied state $\hat{a}_{l,\sigma}|1\rangle_{l,\sigma} = |0\rangle_{l,\sigma}$ and destroys an empty state $\hat{a}_{l,\sigma}|0\rangle_{l,\sigma} = 0$. The combination of creation and annihilation operators acting on the same state is dubbed the number operator, $\hat{a}^{\dagger}_{l,\sigma}\hat{a}_{l,\sigma} \equiv \hat{n}_{l,\sigma}$. Furthermore, the antisymmetry property of fermions [44] is accounted for by the anti-commutation relations satisfied by the fermionic creation and annihilation operators

$$\begin{aligned}\{\hat{a}^{\dagger}_{l,\sigma}, \hat{a}_{k,\sigma'}\} &= \hat{a}^{\dagger}_{l,\sigma}\hat{a}_{k,\sigma'} + \hat{a}_{k,\sigma'}\hat{a}^{\dagger}_{l,\sigma} = \delta_{l,k}\delta_{\sigma,\sigma'} \\ \{\hat{a}^{\dagger}_{l,\sigma}, \hat{a}^{\dagger}_{k,\sigma'}\} &= \{\hat{a}_{l,\sigma}, \hat{a}_{k,\sigma'}\} = 0.\end{aligned} \tag{2.9}$$

Expressed in the second quantization formalism, the Hamiltonian of a lead is the sum of energies of individual occupied electrons states l up to the Fermi level,

$$\hat{H}_l = \sum_{l\sigma} \epsilon_l \hat{a}^{\dagger}_{l\sigma}\hat{a}_{l\sigma}. \tag{2.10}$$

Each single level energy ϵ_l is doubly degenerate due to two allowed spin orientations $\sigma = \{\uparrow, \downarrow\}$. In islands the interactions of localized electrons are accounted by inclusion of interaction term in the Hamiltonian,

$$\hat{H}_I = \sum_{i\sigma} \epsilon_i \hat{a}^{\dagger}_{i\sigma}\hat{a}_{i\sigma} + \hat{H}_{int}. \tag{2.11}$$

In case of an island with a high density of states, such as those considered throughout this section, the interaction term is simply the electrostatic energy of Eq. (2.2)

$$\hat{H}_{int} \equiv E_{el}(\hat{N}) = E_C(\hat{N} + \frac{C_g V_g}{e})^2, \tag{2.12}$$

where again $E_C = e^2/2C$ is the charging energy and the latter term in the parenthesis stands for the energy contributed by the gate electrode. $\hat{N}$ is the number operator of the whole island, i.e. it gives the total number of electrons on the island $\hat{N} = \sum_{i,\sigma} \hat{a}^{\dagger}_{i\sigma}\hat{a}_{i\sigma}$.

The energy contribution of a single electron to the total energy is small for an island and even more so for a metallic lead. It is therefore clear that the tunneling events transferring one electron between the island and lead change the initial energies only slightly, and it is safe to treat them as perturbations. *The tunneling Hamiltonian* of a sequential tunneling across a tunneling barrier is

$$\hat{H}_T = \sum_{lr\sigma} (T_{lr}\hat{a}^\dagger_{l\sigma}\hat{a}_{r\sigma} + T^*_{lr}\hat{a}_{l\sigma}\hat{a}^\dagger_{r\sigma}), \tag{2.13}$$

where the first term removes an electron from left side of the barrier and adds one to the right side, while the second term is its Hermitian conjugate representing the opposite process. $T_{l,r}$ gives the amplitude of the tunneling coupling i.e. the overlap of the wavefunctions of the electron states l and r separated by a tunneling barrier. In practice, solving such an overlap integral requires microscopic knowledge of the specific quantum states and is hard to achieve. It turns out, however, that the sum of $T_{l,r}$'s can be related to the conductance of the junction and thus solved indirectly [17].

The rate $\Gamma_{\alpha\to\beta}$ can be solved by applying a famous result from the quantum mechanics for calculating transition rates between energy eigenstates known as *the Fermi's golden rule* [45, 46]. It yields the probability of transition per unit time from a specific state of the system to a continuum of other states, initiated by a weak perturbation [45]. The first order perturbation provides a rate

$$\Gamma_{\alpha\to\beta} = \frac{2\pi}{\hbar}\left|\langle f_\beta|\, \hat{H}_T\, |i_\alpha\rangle\right|^2 \delta(E_{f_\beta} - E_{i_\alpha}), \tag{2.14}$$

where $|i_\alpha\rangle$ and $|f_\beta\rangle$ are the initial and final states with α and β excess electrons and E_{i_α} and E_{f_β} are energies of these states. The squared absolute value of the tunneling matrix element included in the Fermi's golden rule makes it phase independent i.e. incoherent in the first order. Physically this follows from the destructive interference between transitions to various continuous states that abolish any time and phase-dependence [47]. This approach is valid in the dynamic Coulomb blockade regime

because the electron waiting times between tunneling events are considerably longer than the coherence times of the electrons and thus there can be no coherence between successive tunneling events [44]. If the driving perturbation is time-independent, the resulting transitions will be between states equal in energy, which is ensured in the Fermi's golden rule (2.14) by a delta function.

2.6.1 Tunnelling rate from a lead to an island

As a practical example, consider an electron tunneling from a source lead to an island. The relevant parts of the unperturbed Hamiltonian of the system are the ones describing the energies of the lead and island,

$$\begin{aligned}\hat{H}_0 &= \hat{H}_L + \hat{H}_I, \text{ with} \\ \hat{H}_L &= \sum_{l\sigma} \epsilon_l \hat{a}^\dagger_{l\sigma} \hat{a}_{l\sigma} \text{ and} \\ \hat{H}_I &= \sum_{k\sigma} \epsilon_{k\sigma} \hat{d}^\dagger_{k\sigma} \hat{d}_{k\sigma} + E_{el}(\hat{N}).\end{aligned} \tag{2.15}$$

The tunneling Hamiltonian is

$$\hat{H}_T = \sum_{lk\sigma} (T_{lk} \hat{d}^\dagger_{k\sigma} \hat{a}_{l\sigma} + T^*_{lk} \hat{a}^\dagger_{l\sigma} \hat{d}_{k\sigma}). \tag{2.16}$$

The charge state of the island changes from $|N\rangle_{i_I}$ to $|N+1\rangle_{f_I}$ as a result of the tunneling while the lead loses an electron going from $|n\rangle_{i_L}$ to $|n-1\rangle_{f_L}$. Since the lead and island states are independent, the initial and final states of the tunneling event can be written as direct products $|i_N\rangle = |N\rangle_{i_I} \otimes |n\rangle_{i_L}$ and $|f_{N+1}\rangle = |N+1\rangle_{f_I} \otimes |n-1\rangle_{f_L}$. The final state can be further rewritten using creation and annihilation operators as $|N+1\rangle_f = \hat{d}^\dagger_{k\sigma} |N\rangle_{i_I} \otimes \hat{a}_{l\sigma} |n\rangle_{i_L}$. Both the lead and island have multiple electron energy states, that can all realize a tunneling (as long as the energy condition is met) so the rate has to be a sum over all these states. Inserting the tunneling Hamiltonian (2.16) into Fermi's golden rule (2.14) with a summation over the initial

and final states (written in terms of initial states) gives

$$\Gamma_{N\to N+1} = \frac{2\pi}{\hbar}\sum_i \left|\sum_{l\sigma} T_{lk} \langle n|_{i_L} \otimes \langle N|_{i_I} \hat{d}_{k\sigma}\hat{a}^\dagger_{l\sigma}\hat{d}^\dagger_{k\sigma}\hat{a}_{l\sigma} |N\rangle_{i_I} \otimes |n\rangle_{i_L}\right|^2 P(i_N) \times \delta(E_{|N+1\rangle_f} - E_{|N\rangle_i}). \tag{2.17}$$

Here the rate has been weighted with the probability of the system being in the initial state $P(i_N) = P(i_l)P(i_k)$. Using the anti-commutation relation $\{\hat{d}^\dagger_{k\sigma}, \hat{d}_{k'\sigma'}\} = \delta_{kk'\sigma\sigma'}$ and writing the creation and annihilation operators as number operators $\hat{a}^\dagger_{l\sigma}\hat{a}_{l\sigma} = \hat{N}_{l\sigma}$ and $\hat{d}^\dagger_{k\sigma}\hat{d}_{k\sigma} = \hat{N}_{k\sigma}$ gives, after some rearranging,

$$\Gamma_{N\to N+1} = \frac{2\pi}{\hbar}\sum_i \sum_{lk\sigma} |T_{lk}|^2 \left|\langle n|_{i_L} \hat{n}_{l\sigma} |n\rangle_{i_L}\right|^2 P(i_l) \left|\langle N|_{i_I} (1-\hat{n}_{k\sigma}) |N\rangle_{i_I}\right|^2 P(i_k) \times \delta(E_{|N+1\rangle_f} - E_{|N\rangle_i}). \tag{2.18}$$

Note that $\hat{N}_{l\sigma} |n\rangle_{i_L}$ and $\hat{N}_{k\sigma} |N\rangle_{i_I} = 0$ or 1 due to the fermionic nature of electrons, which demands that each energy level can have only up to one particle with a certain spin. Consequently, the squares can be omitted from the matrix elements in Eq. 2.18. Since electron states in the metallic leads are extended, the sums over the occupations weighted by the occupation probabilities in the above equation are given by Fermi-Dirac distributions: $\sum_{i,\sigma} \langle n|_{i_L} \hat{n}_{l\sigma} |n\rangle_{i_L} P(i_l) = n_F(\epsilon_l)$ and $\sum_{i,\sigma} \langle N|_{i_I} 1 - \hat{n}_{k\sigma} |N\rangle_{i_I} P(i_k) = 1 - n_F(\epsilon_k)$. The rate simplifies to

$$\Gamma_{N\to N+1} = \frac{2\pi}{\hbar}\sum_{lk} |T_{lk}|^2 n_F(\epsilon_l)(1-n_F(\epsilon_k))\delta(E_{|N+1\rangle_f} - E_{|N\rangle_i}). \tag{2.19}$$

The energies of the final and initial states appearing inside the delta function are evaluated by taking expectation values of the non-interactive Hamiltonian (2.15) of the system in these states

$$E_{|N+1\rangle_f} = \langle n-1|_{f_L} \otimes \langle N+1|_{f_I} (\hat{H}_L + \hat{H}_I) |N+1\rangle_{f_I} \otimes |n-1\rangle_{f_L} \tag{2.20}$$

and

$$E_{|N\rangle_i} = \langle n|_{i_L} \otimes \langle N|_{i_I} (\hat{H}_L + \hat{H}_I) |N\rangle_{i_I} \otimes |n\rangle_{i_L}\,. \tag{2.21}$$

This yields,

$$E_{|N+1\rangle_f} = \langle n-1|_{f_L} \otimes \langle N+1|_{f_I} \sum_{l\sigma} \epsilon_l \hat{a}^\dagger_{l\sigma}\hat{a}_{l\sigma} + \sum_{k\sigma} \epsilon_k \hat{d}^\dagger_{k\sigma}\hat{d}_{k\sigma} + E_{el}(\hat{N}_{k\sigma}) \, |N+1\rangle_{f_I} \otimes |n-1\rangle_{f_L}$$
$$= \sum_{l\sigma}^{n-1} \epsilon_l + \sum_{k\sigma}^{N+1} \epsilon_k + E_{el}(N+1) \tag{2.22}$$

and

$$E_{|N\rangle_i} = \langle n|_L \otimes \langle N|_{i_L} \sum_{l\sigma} \epsilon_l \hat{a}^\dagger_{l\sigma}\hat{a}_{l\sigma} + \sum_{k\sigma} \epsilon_k \hat{d}^\dagger_{k\sigma}\hat{d}_{k\sigma} + E_{el}(\hat{N}_{k\sigma}) \, |N\rangle_{i_I} \otimes |n\rangle_{i_L}$$
$$= \sum_{l\sigma}^{n} \epsilon_l + \sum_{k\sigma}^{N} \epsilon_k + E_{el}(N). \tag{2.23}$$

The energy condition for the delta function is hence the difference

$$E_{|N+1\rangle_f} - E_{|N\rangle_i} = E_{el}(N+1) - E_{el}(N) + \epsilon_k - \epsilon_l$$
$$\equiv \Delta E_{el}(+1) + \epsilon_k - \epsilon_l. \tag{2.24}$$

Now, assuming continuous density of states in the lead, the sums over energy states can be substituted by integrals over the energies weighted with the densities of states $\rho(\epsilon_l)$ and $\rho(\epsilon_k)$

$$\sum_{lk} \to \int d\epsilon_l d\epsilon_k \rho(\epsilon_l)\rho(\epsilon_k). \tag{2.25}$$

The Eq. (2.19) reads then

$$\Gamma_{N\to N+1} = \frac{2\pi}{\hbar} \int d\epsilon_l d\epsilon_k \rho(\epsilon_l)\rho(\epsilon_k))|T_{lk}|^2 n_F(\epsilon_l)(1-n_F(\epsilon_k))\delta(\Delta E_{el}(+1) + \epsilon_k - \epsilon_l). \tag{2.26}$$

Assuming the combination of the densities of states and tunneling probability $\rho(\epsilon_l)\rho(\epsilon_k)|T_{lk}|^2$ to be constant, integration over ϵ_l yields

$$\Gamma_{N\to N+1} = \frac{2\pi}{\hbar}\rho(\epsilon_l)\rho(\epsilon_k)|T_{lk}|^2 \int d\epsilon_k n_F(\Delta E_{el}(+1) + \epsilon_k)(1-n_F(\epsilon_k)). \tag{2.27}$$

The constants can be labelled as the tunneling density of states $\gamma_0 \equiv \frac{2\pi}{\hbar}\rho(\epsilon_l)\rho(\epsilon_k)|T_{lk}|^2$, whose value can be solved from the conductance of the tunneling barrier [17].

In the limit of low temperature, the Fermi-Dirac distribution is a step function: $\lim_{T\to 0} n_F(\epsilon_{l,k}) \to 1-\theta(\epsilon_{l,k}-\mu_{L,I}) = \theta(-\epsilon_{l,k}+\mu_{L,I})$, where $\mu_{L,I}$ is the Fermi energy of the lead/island. This simplifies the rate (2.27) to

$$\Gamma_{N\to N+1} = \gamma_0 \int d\epsilon_k \theta(-\Delta E_{el}(+1) - \epsilon_k + \mu_L)(1-\theta(-\epsilon_k+\mu_k)). \tag{2.28}$$

The step functions dictate which values of ϵ_k provide non-zero contribution to the integral and hence set new effective limits of integration. The integral is then a trivial one:

$$\Gamma_{N\to N+1} = \gamma_0 \int_{\mu_k}^{\mu_l - \Delta E_c(+1)} d\epsilon_k = \gamma_0(\mu_l - \mu_k - \Delta E_{el}(+1)). \tag{2.29}$$

The difference of the lead and island Fermi energies can be linked to the bias voltage between them, $\mu_l - \mu_k = eV_b$. As mentioned earlier, the tunneling density of states γ_0 can be connected to the conductance of the tunneling junction, which allows the rate to be finally written in a form characterized completely by the circuit parameters

$$\Gamma_{N\to N+1} = \frac{G}{2\pi^2 G_Q}(eV_b - \Delta E_{el}(+1)), \tag{2.30}$$

where the gate voltage V_g acts through the electrostatic energy difference $\Delta E_{el}(+1) = 2E_c(N+\frac{1}{2}-\frac{CV_g}{e})$. The bias voltage multiplied by the electron charge eV_b has to be positive for the electrons to go from the lead to island, and larger than the change in electrostatic energy, $eV_b > \Delta E_{el}(+1)$, for the process to be in congruence with the energy conservation principle. Once these conditions are fulfilled, the sequential tunneling rate between an island and lead manifests a simple linear dependence on the voltage bias. This is in contrast with quantum dots, that will be encountered in Sec. 5.1, whose transition rate is bias-independent.

2.7 Coherent transport

The complex phase of the probability amplitude (matter wave) of a quantum state has an important role in quantum mechanics. Though the phases of individual quan-

tum states have no physical significance, since they cancel out when probabilities are derived from corresponding probability amplitudes by taking squared moduli, phases become relevant when considering multiple quantum states. Different states are able to interfere in a manner typical to waves, and the effect of this interference is determined by the difference of the phases of the subsystems, a quantity called the *relative phase*. The interference manifests as an increase or decrease of the classically expected probability for a given outcome, depending on whether the matter waves interfere creatively or destructively. Notable interference manifest only if the phases of different amplitudes are *coherent* i.e. they have a constant relative phase.

The phase of a wavepacket representing an electron can change as a result of collisions. Inelastic collisions and collisions occurring at random times ruin the coherence of electron waves as they disturb the relative phase [48]. In nanostructures such disturbances originate commonly from thermal vibrations of the lattice or electron-electron interactions. Two electrons will therefore lose their coherence as their phases change differently while travelling in a lattice. This is characterized by a phase coherence time, the average time after which an electron loses its original phase and no interference effects are to be expected.

Since in the dynamic Coulomb blockade regime the tunneling frequency is slower than the phase coherence time, it is reasonable to assume the transport to be dominated by *incoherent* single electron tunneling. However, as the potential barriers become weaker and the waiting times decrease, the coherent correlations between tunneling events gain importance. Electron *co-tunneling* describes coherent transport at the dynamic Coulomb blockade regime as a correlated transfer of two or more electrons. As will be explained next, it enables a tiny current to flow even when sequential tunneling is forbidden, and can therefore be important even deep in the Coulomb blockade regime where $G \ll G_Q$.

For electrons in Cooper pair splitters, co-tunneling is an unwanted transport

that one wishes to suppress. However, the extraction of Cooper pairs from the superconductor is realized by another coherent mode of transport, the Andreev reflection. This process occurring at the interface of superconducting and normal conducting materials, will be described in Sec. 4.3.1.

2.8 Co-tunneling

Classically, tunneling processes have to obey the energy conservation: electron transfer cannot increase the total energy of the system without outside work. However, the uncertainty relation, $\Delta E \Delta t \geq \hbar/2$, between energy and time yields time interval, $\Delta t \approx \hbar/(2\Delta E)$, during which the energy does not need to be conserved. This opens a possibility for an electron co-tunneling: a chain of tunneling events, that although ultimately conserves energy, passes through states that violate energy conservation.

An elementary example of such an event is a co-tunneling of an electron from a reservoir to another via an intermediate island. An electron can tunnel in to the island from the left lead and reside there for a time $\Delta t \approx \hbar/(2\Delta E)$, within which another electron can tunnel to the right lead, relaxing the island to its initial charge state. Unless the second electron tunnels away from the very same energy level of the island, that was previously excited by the initial tunneling, the co-tunneling process leaves an electron-hole exciton on the island. Such processes are called *inelastic* co-tunneling, since the energy of the transported electron in the drain lead is lower than the energy of the initial electron in the source. The energy lost during the transport equals the energy of the exciton created on the island. In contrast, in the *elastic* co-tunneling process, no energy is dissipated as the same energy level both receives and loses an electron on the island. Therefore, not only the charge state but also energy of the island remains unchanged after an elastic co-tunneling transport.

The rate of two electron co-tunneling is obtained from the Fermi's golden rule (2.14), by substituting the tunneling Hamiltonian (2.13) with a higher order

perturbation involving two subsequent tunnelings via an intermediate state. Since the intermediate state cannot be realized for a time longer than is allowed by the uncertainty principle, it is called a virtual state. Formally, the tunneling matrix $\hat{H}_T$ is replaced by a *T-matrix* containing a series of terms each describing tunneling processes with increasing number of virtual states. Up to second order, the T-matrix reads [44]

$$\hat{T} = \hat{H}_T + \hat{H}_T \frac{1}{E_i - \hat{H}_0} \hat{H}_T. \tag{2.31}$$

The first term is the usual single electron tunneling Hamiltonian and the second term corresponds to a co-tunneling via virtual state realized by two single electron transfers. E_i is the initial energy and $\hat{H}_0$ is the unperturbed Hamiltonian of the system. For the simple lead-island-lead junction, considered above, the co-tunneling rate from a source to drain is obtained from the Fermi's golden rule using the second term of the above T-matrix

$$\Gamma_{co}^{(2)} = \frac{2\pi}{\hbar} \sum_{f_\beta i_\alpha} \left| \langle f_\beta | \hat{H}_T \frac{1}{E_i - \hat{H}_0} \hat{H}_T | i_\alpha \rangle \right|^2 P(i_\alpha) \delta(E_{f_\beta} - E_{i_\alpha}). \tag{2.32}$$

Operating on the initial state with the first tunneling Hamiltonian yields two possible virtual states: either electron enters the island from the source or leaves it by tunneling to the drain, taking the system to a virtual charge state $|\nu_{N+1}\rangle$ or $|\nu_{N-1}\rangle$, respectively. The reciprocal of the energy difference of initial and virtual states, $\frac{1}{E_i - \hat{H}_0}$, suppresses processes that involve high energy virtual states. The second tunneling Hamiltonian in Eq. (2.32) restores the system back to its original charge state $|i_N\rangle$, by either removing the excess charge to the drain lead or bringing electron from the source lead back to the island, depending which tunneling had occurred initially. The matrix element inside the squares in Eq. (2.32) hence composes of two terms corresponding to the two ways to realize the electron transport through the junction

i.e.

$$\Gamma_{co}^{(2)} = \frac{2\pi}{\hbar} \sum_{f_\beta i_\alpha} \left| \langle f_\beta | \left(\hat{H}_{TR} \frac{1}{E_i - \hat{H}_0} \hat{H}_{TL} + \hat{H}_{TL} \frac{1}{E_i - \hat{H}_0} \hat{H}_{TR} \right) | i_\alpha \rangle \right|^2 P(i_\alpha) \delta(E_{f_\beta} - E_{i_\alpha}). \tag{2.33}$$

Because the sum of these two ways of transport appears within the square of the absolute value, their contributions do not simply add up in the classical sense but rather interfere like waves, embodying the coherence of the process.

The elastic co-tunneling, mentioned above, leaves no excitons on the island since both transfers happen through the same energy level. The rate of such a process is contributed by all available discrete levels of the island, that is $\sim E_C/\delta_S$ levels. The phase shifts from transports via different energy levels are random and thus average to zero for the total rate. This leads to a strong destructive interference and suppression of the elastic co-tunneling rate by factor of $\sim \delta_S/E_C$ [17]. Hence, for a metallic island with neglectable energy level spacing δ_S, co-tunneling is dominantly inelastic [44]. For the quantum dots encountered in Sec. 5.1, the elastic co-tunneling dominates, as the energy levels are notably discrete.

3. Spin states

Historically, the electric charge of an electron has been the primary property used to encode, store, transmit and process information. The other intrinsic property of all particles, spin angular momentum, has remained mostly untapped until recently. Excluding few passive commercial innovations such as magnetic read heads for reading data and MRAM (magnetic random-access memory) storage, the *spintronic* devices are only in early development phase [49].

Though controlling the spin degree of freedom requires more sophisticated techniques than charge-based manipulation, adopting spin as a basis of data processing has indisputable benefits. In addition to possible increase in processing speed and device density, a major advantage comes from a reduced heat dissipation. This follows from the possibility to alter electron's spin degree of freedom without physically moving the electron, whereas traditional electronics relies on moving the charged electron around. Quantum information technology serves as a more recent motivator for spintronics, since the long coherence time of spin states makes them promising storages for quantum information.

This chapter reviews the formalism of the electron spin and especially the formulation of a two-spin system, which models the electron pairs processed by the Cooper pair splitters. The formalism introduced here can be appreciated to full extend in Ch. 7, where spin-orbit interaction is used to induce spin-flips that transform the spin-singlet, the natural state of a Cooper pair, into other spin states.

3.1 Electron spin

Particle's spin angular momentum exhibits the same properties as its orbital angular momentum: it has a magnitude and orientation and it obeys same quantum mechanical restrictions. However, unlike orbiting, the spin cannot be linked quantitatively to any physical motion, nor can its magnitude be changed [49]. Spin has therefore to be understood as a fundamental intrinsic property like a mass or charge. The relativistic quantum mechanics, as formulated by Dirac [33], dictate the existence of particle's intrinsic angular momentum quantized in half-integers.

The spin is described by a three component operator $\hat{S} = (\hat{S}_x, \hat{S}_y, \hat{S}_z)$. The rotational invariance sets (see e.g. [50]) restrictions to the components of all quantum mechanical angular momenta, including spin, as commutation relations

$$[\hat{S}_y, \hat{S}_z] = i\hbar\hat{S}_x, \qquad [\hat{S}_z, \hat{S}_x] = i\hbar\hat{S}_y, \qquad [\hat{S}_x, \hat{S}_y] = i\hbar\hat{S}_z. \tag{3.1}$$

These relations imply the uncertainty between the values of spin measured along different axes. In other words, the components of spin $\hat{S}$ are conjugate variables in a same way as momentum and position.

As for the orbital angular momentum, the square of total spin $\hat{S}^2 = \hat{S}_x^2 + \hat{S}_y^2 + \hat{S}_z^2$ commutes with each of the components $\hat{S}_{x,y,z}$, which makes their eigenvalues s and m_s good quantum numbers of a spin state $|s, m_s\rangle$. As will be seen later, the z-component is the most convenient choice and together with the square of the total spin, they satisfy simultaneously the eigenvalue equations

$$\hat{S}^2 |s, m_s\rangle = \hbar^2 s(s+1) |s, m_s\rangle \quad ; \quad \hat{S}_z |s, m_s\rangle = \hbar m_s |s, m_s\rangle . \tag{3.2}$$

Furthermore, m_s is quantized to values ranging from $-s$ to s by integer steps [50]. The components of a spin s are hence allowed to have only $2s + 1$ different values. The spin quantum number of an electron is $s = 1/2$. Thus, measuring the spin along any axis will always give either $m_s = +\hbar/2$ or $m_s = -\hbar/2$. It follows that

the spin operators $\hat{S}_{x,y,z}$ must have two eigenvalues i.e. they can be represented by a 2×2 matrices. A group of matrices with eigenvalues $\pm\hbar/2$ fulfilling the relations of Eqs. (3.2) and (3.1) for spin $s = 1/2$ are

$$\hat{S}_x = \frac{\hbar}{2}\hat{\sigma}_x, \qquad \hat{S}_y = \frac{\hbar}{2}\hat{\sigma}_y, \qquad \hat{S}_z = \frac{\hbar}{2}\hat{\sigma}_z, \tag{3.3}$$

where the dimensionless matrices

$$\hat{\sigma}_x \equiv \begin{bmatrix} 0 & 1 \\ 1 & 0 \end{bmatrix}, \qquad \hat{\sigma}_y \equiv \begin{bmatrix} 0 & -i \\ i & 0 \end{bmatrix}, \qquad \hat{\sigma}_z \equiv \begin{bmatrix} 1 & 0 \\ 0 & -1 \end{bmatrix} \tag{3.4}$$

are called the *Pauli matrices* after Wolfgang Pauli. The total spin operator can be written using the Pauli matrices as

$$\hat{S} = \frac{\hbar}{2}\vec{\sigma}, \tag{3.5}$$

where $\vec{\sigma} \equiv (\hat{\sigma}_x, \hat{\sigma}_y, \hat{\sigma}_z)$ is the Pauli vector.

The form of Pauli matrices makes it easiest to consider measurements performed along the z-axis. The eigenvectors of the spin operator $\hat{S}_z$ corresponding to eigenvalues $m_s = +\hbar/2$ and $m_s = -\hbar/2$ are conveniently,

$$|\frac{1}{2}, \frac{1}{2}\rangle_z = \begin{bmatrix} 1 \\ 0 \end{bmatrix} \quad \text{and} \quad |\frac{1}{2}, -\frac{1}{2}\rangle_z = \begin{bmatrix} 0 \\ 1 \end{bmatrix}. \tag{3.6}$$

It is a conventional notation to label the states as $|\frac{1}{2}, \frac{1}{2}\rangle \equiv |\uparrow\rangle$ and $|\frac{1}{2}, -\frac{1}{2}\rangle \equiv |\downarrow\rangle$, reflecting the vertical orientation of z-axis and that vectors projected on it can point either up or down. The eigenvectors of the two remaining Pauli matrices written in a basis spanned by $|\uparrow\rangle$ and $|\downarrow\rangle$ read

$$|\frac{1}{2}, \pm\frac{1}{2}\rangle_x = \frac{1}{\sqrt{2}}\begin{bmatrix} 1 \\ \pm 1 \end{bmatrix} \quad \text{and} \quad |\frac{1}{2}, \pm\frac{1}{2}\rangle_y = \frac{1}{\sqrt{2}}\begin{bmatrix} 1 \\ \pm i \end{bmatrix}, \tag{3.7}$$

with the same eigenvalues $\pm\hbar/2$. Two component spin wavefunctions, like the elementary ones above, are called *spinors*. The spinor of a particle contains full

information of its spin state, which is to say that the direction of an arbitrary spin, described by a spinor $|\psi_{s,m_s}\rangle = a\,|\uparrow\rangle + b\,|\downarrow\rangle$, can be determined as a polarization vector

$$\vec{M} \equiv (\langle\hat{S}_x\rangle, \langle\hat{S}_y\rangle, \langle\hat{S}_z\rangle), \tag{3.8}$$

where $\langle\hat{S}_{x,y,z}\rangle = \langle\psi_{s,m_s}|\,\hat{S}_{x,y,z}\,|\psi_{s,m_s}\rangle$ are the expectation values of its spin along different coordinate axes.

3.1.1 The Zeeman effect

The concept of a particle as a charged object with intrinsic angular momentum provokes one to wonder whether this spinning charge also induces a magnetic field. Indeed, the proof for spin-induced magnetic moment was obtained for silver atoms in the famous Stern-Gerlach experiment in 1922 [51]. Since then, the magnetic dipole moment of electron has become one of the most accurately measured properties of an elementary particle [52].

Classically, the magnetic dipole moment of a spinning charge is just the spin angular momentum times the gyromagnetic ratio, $\vec{\mu}_e = \gamma\vec{S}$. For a quantum mechanical particle, the classical gyromagnetic ratio $\gamma = q/2m$ needs to be modified by a proportionality constant known as the g-factor [53] to account for the fact that the spin cannot be rigorously identified with a classical notion of a rotating body. The spin magnetic dipole moment of an electron is therefore

$$\vec{\mu}_e = -\frac{e g_e}{2m_e}\vec{S}. \tag{3.9}$$

Writing the spin operator in terms of Pauli matrices $\vec{S} = \frac{\hbar}{2}\vec{\sigma}$ and noting that the electron spin g-factor has approximate value of $g_e \simeq 2$ [52], modifies Eq. (3.9) to

$$\vec{\mu}_e \simeq -\frac{e\hbar}{2m_e}\vec{\sigma}. \tag{3.10}$$

The remaining proportionality factor between the magnetic moment and spin is known as the *Bohr magneton*. It is approximately the magnitude of a spin magnetic moment of a single electron

$$\mu_B = \frac{e\hbar}{2m_e}. \tag{3.11}$$

The operator associated with the interaction energy of electron's magnetic moment and external magnetic field $\vec{B}$ is the Zeeman Hamiltonian

$$\hat{H}_Z = \mu_B \vec{\sigma} \cdot \vec{B}. \tag{3.12}$$

This interaction between spin's magnetic dipole and static external magnetic field is the elementary handle to spin control. In the absence of a magnetic field, spin has no effect to the energy of a particle and its orientation remains irrelevant. The Zeeman interaction shifts the energy of a particle, making the state with spin opposite (since electron has a negative gyromacnetic ratio) to external magnetic field energetically favorable. Thus the *spin-splitting*, discovered by Pieter Zeeman [54], enables one to distinguish between different spin states.

3.2 Two-particle spin states

Since the Cooper pair splitter deals with pairs of electrons, the spin formalism is to be expanded to cover two-particle systems. In the formalism of the quantum many-body physics [44], the pair of electrons is assigned with a single wavefunction that describes both particles

$$\Psi(\vec{r}_1, \vec{r}_2, \vec{s}_1, \vec{s}_2,) = \psi(\vec{r}_1, \vec{r}_2) \left|\vec{s}_1, \vec{s}_2\right\rangle . \tag{3.13}$$

The orbital (position related) part of the wavefunction $\psi(\vec{r}_1, \vec{r}_2)$ has to be included for symmetry consideration reasons typical to many-body quantum mechanics. The state of the system is described by the positions $\vec{r}_{1/2}$ and spin orientations $\vec{s}_{1/2}$ of

the particles. Concentrating first only on the spin part $|\vec{s}_1, \vec{s}_2\rangle$, it seems that the obvious choice for the basis vectors, in terms of the z-basis introduced in the previous section, would be

$$\begin{aligned} |\uparrow\uparrow\rangle &\equiv |\uparrow\rangle_1 \otimes |\uparrow\rangle_2 , \\ |\uparrow\downarrow\rangle &\equiv |\uparrow\rangle_1 \otimes |\downarrow\rangle_2 , \\ |\downarrow\uparrow\rangle &\equiv |\downarrow\rangle_1 \otimes |\uparrow\rangle_2 , \\ |\downarrow\downarrow\rangle &\equiv |\downarrow\rangle_1 \otimes |\downarrow\rangle_2 , \end{aligned} \tag{3.14}$$

where the symbol $\otimes$ stands for the *tensor product* defined as

$$\begin{bmatrix} a \\ b \end{bmatrix} \otimes \begin{bmatrix} c \\ d \end{bmatrix} \equiv \begin{bmatrix} ac \\ ad \\ bc \\ bd \end{bmatrix} . \tag{3.15}$$

The four vectors of Eq. (3.14) span the four dimensional Hilbert space $\mathbb{C}^4 = \mathbb{C}^2 \otimes \mathbb{C}^2$, composed of two single-particle Hilbert spaces. The ordered basis $\{|\uparrow\uparrow\rangle , |\uparrow\downarrow\rangle , |\downarrow\uparrow\rangle , |\downarrow\downarrow\rangle\}$ corresponds to the four possible permutations of the spin-up and spin-down orientations of the particles 1 and 2.

In this basis the spin operator for the particle 1 is constructed as a *Kronecker product* of the 2×2 Pauli vector and unit matrix

$$\vec{\sigma}_1 = \vec{\sigma} \otimes \hat{I}, \tag{3.16}$$

where the the Kronecker product [55] of matrices $\hat{A}$ and $\hat{B}$ is defined as

$$\hat{A} \otimes \hat{B} \equiv \begin{bmatrix} A_{11}\hat{B} & A_{12}\hat{B} \\ A_{21}\hat{B} & A_{22}\hat{B} \end{bmatrix} . \tag{3.17}$$

Conversely, the spin operator for the second particle is the Kronecker product

$$\vec{\sigma}_2 = \hat{I} \otimes \vec{\sigma}. \tag{3.18}$$

Any operators acting on the two-particle states can be expressed using the spin-specific 4×4 Pauli matrices of Eqs. (3.16) and (3.18). Take for instance the Zeeman interaction for a two-particle system. By choosing the z-axis to be aligned with the magnetic field $\vec{B}=(0,0,B)$, the Zeeman Hamiltonian (3.12) is generalized for two electrons as a matrix in the ordered basis $\{|\uparrow\uparrow\rangle, |\uparrow\downarrow\rangle, |\downarrow\uparrow\rangle, |\downarrow\downarrow\rangle\}$ as

$$
\begin{aligned}
\hat{H}_Z &= \sum_{l=\{1,2\}} \mu_B \vec{\sigma_l}\cdot(0,0,B) \\
&= \mu_B B_Z(\hat{\sigma}_z\otimes\hat{I}+\hat{I}\otimes\hat{\sigma}_z) \\
&= \mu_B B_Z\Big(\begin{bmatrix}1&0\\0&-1\end{bmatrix}\otimes\begin{bmatrix}1&0\\0&1\end{bmatrix}+\begin{bmatrix}1&0\\0&1\end{bmatrix}\otimes\begin{bmatrix}1&0\\0&-1\end{bmatrix}\Big) \\
&= \mu_B B\Big(\begin{bmatrix}1\cdot\begin{bmatrix}1&0\\0&1\end{bmatrix} & 0\cdot\begin{bmatrix}1&0\\0&1\end{bmatrix}\\ 0\cdot\begin{bmatrix}1&0\\0&1\end{bmatrix} & -1\cdot\begin{bmatrix}1&0\\0&1\end{bmatrix}\end{bmatrix}+\begin{bmatrix}1\cdot\begin{bmatrix}1&0\\0&-1\end{bmatrix} & 0\cdot\begin{bmatrix}1&0\\0&-1\end{bmatrix}\\ 0\cdot\begin{bmatrix}1&0\\0&-1\end{bmatrix} & 1\cdot\begin{bmatrix}1&0\\0&-1\end{bmatrix}\end{bmatrix}\Big) \\
&= \mu_B B\Big(\begin{bmatrix}1&0&0&0\\0&1&0&0\\0&0&-1&0\\0&0&0&-1\end{bmatrix}+\Big(\begin{bmatrix}1&0&0&0\\0&-1&0&0\\0&0&1&0\\0&0&0&-1\end{bmatrix}\Big) \\
&= \mu_B B\begin{vmatrix}2&0&0&0\\0&0&0&0\\0&0&0&0\\0&0&0&-2\end{vmatrix} \\
&= 2\mu_B B\,|\uparrow\uparrow\rangle\langle\uparrow\uparrow| - 2\mu_B B\,|\downarrow\downarrow\rangle\langle\downarrow\downarrow|\,, \qquad (3.19)
\end{aligned}
$$

where in the last line the matrix is written as an outer product of its (non-zero) basis vectors. As seen, when considering the two spins as a composite system, the Zeeman interaction only affects the spin-aligned states. The energy of anti-aligned

states $|\uparrow\downarrow\rangle$ and $|\downarrow\uparrow\rangle$ does not change in a magnetic field, as the contributions of the two spins are equal and opposite.

3.3 Singlet-triplet basis

The trivial basis for spin states of two-electron system (3.14), introduced above, has a subtle flaw in it. It does not take into account the indistinguishable nature of quantum particles. Particularly, the states $|\uparrow\downarrow\rangle$ and $|\downarrow\uparrow\rangle$ imply that the first electron is in spin-up state and the second is in spin-down state or vice versa. One cannot fundamentally label electrons like that, since they cannot be distinguished in any way and there is no means of tracking their movement between measurements. It is therefore more rigorous to say simply that one of the electrons is in spin-up state and the other one in spin-down state [43].

This can be incorporated in the two-particle spinor by writing it in a way that is non-committal as to which electron occupies which state i.e. combining the two midmost states of Eq. (3.14) either as

$$\begin{aligned} &\frac{1}{\sqrt{2}}(|\uparrow\downarrow\rangle + |\downarrow\uparrow\rangle) \\ &\text{or} \\ &\frac{1}{\sqrt{2}}(|\uparrow\downarrow\rangle - |\downarrow\uparrow\rangle), \end{aligned} \tag{3.20}$$

where the coefficient $\frac{1}{\sqrt{2}}$ normalizes the states. It turns out that these two superposition states together with the two spin-aligned states of Eq. (3.14) form an orthogonal basis for vectors in $\mathbb{C}^4$ Hilbert space. This set of vectors is called the *singlet-triplet*

basis:

$$
\begin{aligned}
|S\rangle &= \frac{1}{\sqrt{2}}(|\uparrow\downarrow\rangle - |\downarrow\uparrow\rangle), \\
|T_0\rangle &= \frac{1}{\sqrt{2}}(|\uparrow\downarrow\rangle + |\downarrow\uparrow\rangle), \\
|T_+\rangle &= |\uparrow\uparrow\rangle\,, \\
|T_-\rangle &= |\downarrow\downarrow\rangle\,,
\end{aligned} \tag{3.21}
$$

where $|S\rangle$ is the singlet and $|T_0\rangle$, $|T_+\rangle$ and $|T_-\rangle$ are called the neutral and polarized triplet states, respectively. An important distinction, as will be seen in the next section, is that the singlet state is antisymmetric under the exchange of the spins, whereas the triplet states are symmetric.

3.3.1 Exchange interaction

The fact that electrons are fundamentally indistinguishable does not actually matter if they are located far apart. Only if two particles are close enough for their wavefunctions to overlap, the indistinguishability manifests as an effective force called the *exchange interaction*. Being based on the same *symmetrization requirement* [43],

$$\Psi(\vec{r}_1, \vec{r}_2, \vec{s}_1, \vec{s}_2) = \pm\Psi(\vec{r}_2, \vec{r}_1, \vec{s}_2, \vec{s}_1), \tag{3.22}$$

as the Pauli exclusion principle, the exchange interaction differentiates between two types of particles. The total wavefunction of a many particle system has to be either symmetric (bosons) or antisymmetric (fermions) under the simultaneous exchange of both positions and spins of any two particles. For a system of two fermionic electrons, this means that the total wavefunction (3.13) has to change sign when the electrons are interchanged i.e.

$$\psi(\vec{r}_1, \vec{r}_2)\,|\vec{s}_1, \vec{s}_2\rangle = -\psi(\vec{r}_2, \vec{r}_1)\,|\vec{s}_2, \vec{s}_1\rangle\,. \tag{3.23}$$

As a consequence, either the orbital part $\psi(\vec{r}_1, \vec{r}_2)$ of a two-electron wavefunction is symmetric and the spin part $|\vec{s}_1, \vec{s}_2\rangle$ is antisymmetric (singlet)

$$\Psi = \frac{1}{\sqrt{2}}(\psi(\vec{r}_1)\psi(\vec{r}_2) + \psi(\vec{r}_2)\psi(\vec{r}_1))\frac{1}{\sqrt{2}}(|\uparrow\downarrow\rangle - |\downarrow\uparrow\rangle) \tag{3.24}$$

or the orbital part is antisymmetric and the spin part is one of the symmetric triplet states

$$\Psi = \frac{1}{\sqrt{2}}(\psi(\vec{r}_1)\psi(\vec{r}_2) - \psi(\vec{r}_2)\psi(\vec{r}_1))\,|T_{0/+/-}\rangle\,. \tag{3.25}$$

The sign of the pseudo-force produced by the exchange interaction depends on the orbital part of a two-electron wavefunction [56, 57]. If the orbital part is symmetric, the electrons feel a repulsion and if it is antisymmetric, they feel an attraction. The symmetry or anti-symmetry of a two-electron orbital wavefunction is directly linked to their spin configuration (Eqs. (3.24) and (3.25)). Hence, the energies of the singlet and triplet states will become non-degenerate due to the exchange interaction, given that the electrons are close enough for their wavefunctions to overlap.

In truth, this is not the situation in a Cooper pair splitter, where the paired electrons are located in separate islands. However, as will be shown Sec. 4.1, the Cooper pairs themselves are naturally in the spin-singlet state. This alone makes the singlet-triplet basis an optimal choice when examining the operation of a Cooper pair splitter. Moreover, since there is a coupling between the superconductor and quantum dots only when the electrons on dots are in the spin-singlet state, an effective exchange interaction lifts the energy degeneracy of the singlet and triplets; see Sec. 7.2.

To conclude, the spin state of an electron pair on the quantum dots of a Cooper pair splitter is best described in the singlet-triplet basis. The two-particle Zeeman Hamiltonian (3.19) carries over unchanged from the trivial basis to the singlet-triplet

basis

$$\begin{aligned}\hat{H}_Z &= \sum_{l=\{1,2\}} \mu_B \vec{\sigma}_l \cdot \vec{B} \\ &= 2\mu_B B \left|T_+\right\rangle \left\langle T_+\right| - 2\mu_B B \left|T_-\right\rangle \left\langle T_-\right| . \end{aligned} \tag{3.26}$$

Evidently, the energies of the singlet and neutral triplet states are unaffected by an external magnetic field, whereas the polarized triplets experience equal and opposite shift in energy. This will lift the remaining degeneracy of the two-electron states as all three triplets have different energy from each other and the singlet state. The evolution of spin states that follows from these state separations will be discussed in Ch. 7.

The following chapter introduces the superconducting state of metal as a source of spin-entangled Cooper pairs. Particularly, the way these pairs are exchanged across a barrier between superconducting and normal conducting material will be reviewed.

4. Superconductors

Superconductivity was discovered by H. Kamerlingh Onnes [58], who noticed in the year 1911 that the electric resistivity of mercury suddenly vanishes below 4.2 kelvin. It was soon realized that certain metals undergo a phase transition at cold temperatures under critical value T_c into a new peculiar state, characterized by this ability to maintain electric current with zero energy dissipation.

Microscopic explanation for the superconductivity was still lacking almost 50 years after its discovery. There were striking similarities between the non-dissipative supercurrent and zero-viscosity flow of superfluid helium, observed in 1938 by P. L. Kapitza [59]. Lev Landau formulated a theory for the helium superfluidity [60] in 1941, defining a threshold value v_c for the flow velocity, under which viscosity will appear. When applied to the Fermi liquid formed of metal's conduction electrons, Landau's theory yields $v_c = 0$, implying viscosity for any flow velocity in the Fermi system. Thus, Landau's theory explains the behaviour of bosonic helium atoms but not fermionic electrons. As demonstrated next, this problem is solved if there is a way for electrons to form composite bosons in the superconducting state.

4.1 Cooper pairs

In 1950, a new discovery named the isotope effect was made independently by Maxwell and Reynolds et al. [61, 62]. The critical temperature T_c was found to depend on the mass of a metal's lattice-ions. This implies that the microscopic

description of superconductivity must include the crystal lattice of metals in addition to the free electrons. Indeed, at the same time Fröhlich [63] had come up with an idea of electron-phonon interactions leading to an effective attraction between electrons. Indeed, in 1956, Leon Cooper showed that a pair of electrons above the Fermi surface will form a bound state in the presence of an attractive interaction [22].

Though quantum mechanical by nature, the concept of the *Cooper pairs* can be classically motivated. An electron moving in a crystal lattice attracts the positive lattice-ions, which creates a local concentration of positive charge around it. Another electron can feel attraction to this positive charge concentration. Since the negative charges of the electrons are screened by other electrons and lattice-ions of the metal, this attraction can overcome the Coulomb repulsion on a long distance. The electrons can thus be weakly attracted to each other to form shortlived, long-distance pairs. The following sub-section contains a prove that the pairing of electrons is indeed energetically favorable, assuming arbitrarily weak attractive potential.

4.1.1 Electron pairing

A Cooper pair is stable, if its energy is lower than the energy of the electrons in the ground state of the metal, the so-called Fermi sea. Consider a metal in the ground state with all energy levels filled up to the Fermi surface and none above it (no excitations). Let there be two elementary quasiparticle excitations experiencing Cooper pairing. The total momentum of the bound pair must be zero, suggesting the pair should consists of excitations with equal and opposite momenta. Since the momentum of an electron excitation (slightly above Fermi surface) is different from hole's (slightly below Fermi surface), only quasiparticles of same kind can form Cooper pairs [64]. For the sake of brevity, the particles forming a Cooper pair

are here referred to as electrons, keeping in mind that they could as well be hole excitations of the Fermi sea.

To describe two-electron excitations as a pair, they are assigned with a two-particle wavefunction. The electrons in metals can be approximated to be plane waves. Hence, a suitable ansatz for the orbital wavefunction of the pair is (see e.g. [65])

$$\psi_0(\vec{r}_1, \vec{r}_2) = \sum_k c_k e^{i\vec{k}\cdot\vec{r}_1} e^{-i\vec{k}\cdot\vec{r}_2}, \tag{4.1}$$

where c_k are the probability amplitudes for the first electron having momentum $\hbar\vec{k}$ and the second one having $-\hbar\vec{k}$. The states below the Fermi surface are all filled, so $c_k = 0$ for $\vec{k} < \vec{k}_F$. By virtue of the Euler formula, the orbital wavefunction can be rewritten as

$$\psi_0(\vec{r}_1, \vec{r}_2) = \sum_k c_k e^{i\vec{k}\cdot(\vec{r}_1-\vec{r}_2)} = \sum_k c_k(\cos\Big(\vec{k}\cdot(\vec{r}_1-\vec{r}_2)\Big) + i\sin\Big(\vec{k}\cdot(\vec{r}_1-\vec{r}_2)\Big)). \tag{4.2}$$

The total wavefunction of fermions $\Psi = \psi(\vec{r})\psi_{spin}$ has to be antisymmetric with respect to interchange of two particles (3.23). The cosine term in Eq. (4.2) is symmetric under the exchange of $\vec{r}_1$ and $\vec{r}_2$, whereas the sine term is antisymmetric under the exchange. In view of this, only one of the terms of the ansatz can be part of the actual wavefunction. The cosine term grows as the distance $\vec{r}_1 - \vec{r}_2$ between the paired electrons gets smaller

$$\lim_{\vec{r}_1-\vec{r}_2\to 0} \cos(\vec{r}_1 - \vec{r}_2) = 1, \tag{4.3}$$

corresponding to a higher probability of finding the electrons close to each other. Hence, the wavefunction being proportional to the cosine is in congruence with the assumed attractive interaction, and the sine term is to be omitted from the ansatz (4.2).

To fulfil overall antisymmetry, the spin wavefunction accompanying the symmetric cosine term has to be the antisymmetric spin-singlet (3.3.1). The total wave-

function of the paired electrons is then

$$\Psi_0 = \sum_k c_k \cos\Big(\vec{k}\cdot(\vec{r}_1 - \vec{r}_2)\Big)\frac{1}{\sqrt{2}}(|\uparrow\downarrow\rangle - |\downarrow\uparrow\rangle). \tag{4.4}$$

Demonstrably, the Cooper pair has the minimum energy when formed of two electrons (or holes) with equal and opposite momentum and spin. The energy of this singlet can be solved from the two-particle Schrödinger equation

$$(\hat{H}_1 + \hat{H}_2 + V(\vec{r}_1, \vec{r}_2))\Psi_0 = E\Psi_0, \tag{4.5}$$

where the Hamiltonians $\hat{H}_{1,2} = \hbar^2\hat{k}_{1,2}^2/2m$ give the energy of the free excited electrons counted from the Fermi level ($E_F = 0$). Since the electrons forming a Cooper pair have wave vectors of equal magnitude $\left|\vec{k}\right| = \left|-\vec{k}\right|$, they have the same energy

$$\hat{H}_{1,2}\Psi_0 = \epsilon_k\Psi_0. \tag{4.6}$$

Inserting Eq. (4.4) into the two-particle Schrödinger equation (4.5) yields an equation for the probability amplitude c_k

$$2\epsilon_k c_k + \sum_{k'=0} V_{kk'}c_{k'} = Ec_k, \tag{4.7}$$

where $V_{kk'}$ is a matrix element of the interaction between electron states k and k'. It can be approximated as

$$V_{kk'} = \begin{cases} -V, \text{ for } |\epsilon_k| < \hbar\omega_D \text{ and } |\epsilon'_k| < \hbar\omega_D \\ \\ 0, \text{ otherwise.} \end{cases}$$

The negative potential $-V$ is approximated to be constant on an energy strip near the Fermi level and vanishing beyond a cut-off energy $\hbar\omega_D$, corresponding to the maximal lattice vibration frequency ω_D, called the Debye frequency [66]. Since the attraction is mediated by lattice vibrations, electrons further than $|\hbar\omega_D|$ away from the Fermi surface have too much energy to be paired by the attractive potential. By

inserting this approximate potential into Eq. (4.7), the amplitude c_k can be solved as

$$c_k = V \sum_{k'=0} \frac{c_{k'}}{E - 2\epsilon_k}. \tag{4.8}$$

Introducing $\sum_k$ to both sides of the equation and then cancelling $\sum_k c_k$ and $\sum_{k'} c_{k'}$ yields

$$1 = V \sum_{k=0} \frac{1}{E - 2\epsilon_k}. \tag{4.9}$$

The summation over states k can be replaced by an integration over energies ϵ_k

$$\sum_{k=0} \to N(0) \int_0^{\hbar\omega_D} d\epsilon_k, \tag{4.10}$$

where $N(0)$ is the electron density of states at the Fermi level for one spin polarization. The integration results in

$$1 = \frac{VN(0)}{2} \ln \frac{E - 2\hbar\omega_D}{E}. \tag{4.11}$$

The binding energy of the Cooper pair can be solved from this, in the limit of weak interaction $VN(0) \ll 1$, to be

$$E = -2\hbar\omega_D e^{-2/N(0)V}. \tag{4.12}$$

Therefore, such bound states are indeed energetically favourable to the ground state of Fermi sea ($E_F = 0$). Note that these bound states are not generally possible in three dimensions unless the binding interaction $-V$ exceeds a certain threshold. The bonding due to a weak attractive interaction (such as the phonon mediated coupling) is possible only because the existence of the Fermi sea structure [67].

4.1.2 Formation of the condensate

The Cooper pairs continue forming among electrons withing a strip of $\pm\hbar\omega_D$ from the Fermi surface, until equilibrium between the emergent and old phase is reached.

Electrons deeper in the Fermi sea remain unaffected and bound to their ions as they do in the normally conducting state. The equilibrium occurs when the state of the Fermi sea has changed enough not to support the anomalous formation of bound states under weak attraction in three dimensions [65]. At this point, macroscopic amount of electrons is bound into pairs of zero total momentum and a *coherent condensate* of Cooper pairs has emerged.

To understand why the Cooper pairs condense into a single quantum state, it is enlightening to consider the spatial extension of the pair. Distance between the paired electrons can be approximated from their momentum by the use of the uncertainty principle as

$$\xi \equiv \delta r \propto \frac{\hbar}{\delta p} \propto \frac{\hbar v_F}{\Delta}, \tag{4.13}$$

where the Fermi velocity of an electron is $v_f \approx 10^6$m/s and the gap energy Δ can be connected to the critical temperature (at which the pair breaks): $E_k \propto k_B T_c \approx 10^{-22}$J ($T_c \approx 10$K). The approximation yields $\xi \approx 1\mu$m [17], which by far exceeds the interparticle distance of the excitations in metal, causing the Cooper pairs in the metal to be highly overlapping. Though individual electrons are forbidden by the exclusion principle to enter the same quantum state, Cooper pairs have a total spin of zero (implying bosonic behaviour) and thus are unrestricted by it. Therefore, they all occupy the same minimum energy quantum state of zero total momentum and are described by a macroscopic wavefunction.

4.2 Gap energy

When a Cooper pair is broken, the binding energy of Eq. (4.12) is split evenly between the constituent particles

$$\Delta \equiv -E/2 = \hbar\omega_D e^{-2/N(0)V}. \tag{4.14}$$

As will be demonstrated shortly, this energy known as the *gap energy* Δ, is a key concept in the theory of superconductors.

The microscopic theory of superconductivity was finally developed by Bardeen, Cooper and Schieffer in 1957 [23]. The BCS theory approaches metal as a many-body state of electrons, and approximates all interactions by a mean-field. Then it applies a variational Hartree-Fock method to formulate the new ground state for superconducting metal as a phase-coherent superposition of Cooper pairs. As well as allowing the derivation of thermal and transport properties of superconductors, BCS theory reproduces the gap energy as a complex parameter

$$\Delta(\vec{r}) = |\Delta(\vec{r})|e^{i\varphi(\vec{r})}. \tag{4.15}$$

The modulus of the gap energy is generally constant, $|\Delta(\vec{r})| = |\Delta|$. By comparing Eq. (4.15) to Eq. (4.14), the absolute value of the gap energy can be associated with the Debye energy $|\Delta| = \hbar\omega_D$, and the phase with the inverse of the product of the density of states and binding potential, $i\varphi(\vec{r}) = -2/N(0)V$.

4.2.1 Excitations

The excitations of the superconducting ground state are not simple electron or hole excitations like in normal metals. They are superpositions of the two, called Bogoliubov quasiparticles after Nikolay Bogoliubov who developed an alternative approach for obtaining the results of BCS theory [68]. These excitations have energy

$$E_k = \pm\sqrt{\epsilon_k^2 + |\Delta|^2}, \tag{4.16}$$

where ϵ_k is energy of an excitation in the normally conducting state. The gap energy Δ appears as a minimum energy for all excitations in the superconducting state. In normal metals any amount of energy is enough to excite the Fermi sea ground state by sending an electron to a vacant state above the Fermi surface. Superconductors contrast this by requiring a minimum energy of Δ to excite the ground state. This

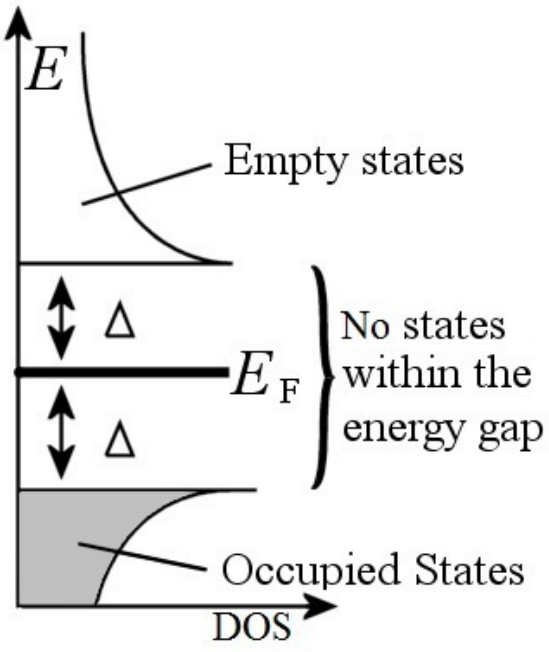

Figure 4.1: Energy spectrum of a superconductor. The figure shows the density of states vs. energy. The gap energy Δ defines a region around the Fermi level E_F, where excitations cannot occur. Reproduced from [69].

creates a gap to the energy spectrum of excitations i.e. an energy interval where no excitations can occur (see Fig. 4.1). The gap energy depends on the temperature reaching maximum value of $\Delta(0) = 1.76 k_B T_c$ at the absolute zero (see e.g. [67]). At the critical temperature T_c, the thermal fluctuations have enough energy to break Cooper pairs, and the superconducting condensate ceases to exist.

Important concequence of the gap energy is the complete suppression of single electron tunneling events at sub-gap energies. An electron can only tunnel into a superconductor provided it holds enough energy to reach the allowed energy levels with energy Δ above the ground state energy. Electrons tunneling in with energy $E_k = \Delta$ join the condensate directly, while more energetic electrons become quasi-particle excitations [65]. Thus, single electron tunneling to a superconductor is forbidden unless the gap energy is matched by a thermal or electric source.

4.3 The proximity effect and Andreev reflection

The purpose of a Cooper pair splitter is to extract spin-entangled singlets from the ground state of a superconductor and gather the split electrons to separate output terminals. One thus needs to understand the physics at the junction of a superconductor and normal conductor. Two ultimately equivalent descriptions, the more phenomenological approach known as the *proximity effect* and the previously mentioned Andreev reflection are frequently used to characterize the interface.

The concept of proximity effect was developed in the 1960s by de Gennes [70, 71] and Werthamer [72]. The distance ξ between particles forming a Cooper pair, derived in Eq. (4.13), is called the superconducting *coherence length*. Electrons can be located within ξ of a superconductor without loosing coherence with the superconducting ground state. This enables electrons located in a normal conductor adjacent to a superconductor to remain in a bound pair state. The lattice vibrations of ordinary conductors are strong enough to break the pairing, causing Cooper pairs outside superconductors to have a short lifetime of order $\hbar/\Delta$. This penetration and subsequent breaking of Cooper pairs in normal conductors occurs even if the Fermi level of the metal is within the superconducting energy gap Δ and sequential tunneling is forbidden (see. sec. 4.2.1).

The same transfer of $2e$ charge across the interface of an ordinary and superconductor can be described in an alternative way. In a superconductor, there are no states available for Bogoliubov quasiparticles at energies below the gap energy Δ. An electron with excitation energy $\epsilon < \Delta$ in the normal conductor, is able to enter the superconductor only jointly with another electron of opposite spin and quasimomentum, by forming a Cooper pair that directly joins the condensate. The electron with opposite quasimomentum $\vec{k'} = -\vec{k}$ resides below the Fermi surface. As the new Cooper pair is formed, a hole excitation is left in the Fermi sea with quasimomentum $\vec{k}$ i.e. equal to the momentum of the initial electron excitation.

4.3.1 Andreev reflection

The above process can be viewed as an unusual scattering event: an electron from the conductor gets reflected back as a hole from the interface of the superconductor. This specular reflection is called the *Andreev reflection* [73]. Since the hole and electron have an opposite charge, a total of $2e$ is lost from the normal conductor. This charge deficit is compensated by a creation of a Cooper pair in the superconductor.

Here the charge transfers in the proximity effect and Andreev reflection were explained as happening in opposite directions: proximity effect dispatching $2e$ as a Cooper pair in to the normal conductor and the Andreev reflection transferring it to the superconductor. Actually, both of these processes work either way. The inverse proximity effect describes normal conducting electron states extending over the interface into the superconductor, where they join the condensate in pairs. For the Andreev reflection, the inverse process is a hole excitation reflected back as an electron excitation, accompanied by a removal of a Cooper pair from the superconducting condensate.

The phases of the electron and hole waves are correlated in the Andreev reflection. This phase coherence (see Sec. 2.7) vanishes shortly after the scattering as the electron and hole move in the normal conductor with slightly different momenta. The coherence length, introduced in the context of proximity effect, matches exactly the distance the electron and hole can travel before their phase coherence is lost [74]. It is therefore clear that the proximity effect and Andreev scattering are equivalent in explaining the charge transfer between a superconductor and normal state conductor.

4.3.2 Crossed Andreev reflection

The Andreev reflection can be conceptualized as a simultaneous tunneling of two electrons from normal conductor into a superconductor and the inverse Andreev

reflection as its opposite: the transport of a Cooper pair from the superconductor to normal conductor, where it splits to a pair of electrons. The situation where the electrons each tunnel from (into) a different normal state electrode is called *crossed Andreev reflection* [75]. It is the same process as the direct Andreev reflection in every respect, except for the spatial separation of the electrons in their respective normal conductors. Hence, this process is also known as the non-local Andreev reflection.

For the crossed Andreev reflection to be possible, the distance between the separated normal conductors cannot be much longer than the superconducting coherence length ξ. As long as both electrons remain within $\sim \xi$ from the superconductor during the transport, the electron pair can feel the pairing potential and join (leave) the condensate in the superconductor, regardless of the electrons being located in different leads at the beginning (end) of the transport.

This is the mechanism behind the extraction of Cooper pairs in Cooper pair splitters achieving the production of spatially separated entangled electrons. As will be seen in the next chapter, the crossed Andreev reflection competes with its direct counterpart, and additionally, with the elastic co-tunnelling (Sec. 2.8) in the conventional setup of a Cooper pair splitter. The defining building block of Cooper pair splitters, the one that enables exploiting the crossed Andreev reflection, is the *double quantum dot*. The next chapter addresses this nanostructure, and the way it governs the electron transport in the Cooper pair splitter.

5. Electron transport in a Cooper pair splitter

5.1 Quantum dots

As discussed in Ch. 2, isolation of (semi)conducting parts of a nanodevice by tunneling barriers leads to electron confinement in the isolated island. In this situtation, the number of excess electrons on the island becomes an important factor, since the Coulomb force of individual electrons affects whether new electrons can enter the island. In Sec. 2.1, the discreteness of an island's energy levels was ignored on the grounds of the charging energy being much larger than the energy level spacing, $E_C \gg \delta_S$. This is the case with islands larger than approximately 100 nm in width. Islands smaller than that have noticeable discreteness of their electron energy levels, and are termed *quantum dots* [26, 27].

5.1.1 Quantization of energy levels

Non-negligible energy level spacings of the quantized levels raise the energy cost of adding an electron to new energy level by δ_S. To see how the quantum mechanical effect of discrete energy levels comes about, consider a toy system representing an island: an electron bound to a two dimensional infinite potential well. Solving the corresponding Schrödinger equation is an elementary practice in quantum mechanics

(see e.g. [43]). The solutions of the Schrödinger equation are standing waves

$$\psi(x,y) = \frac{1}{\sqrt{L_x L_y}} \sin\left(\frac{n_x \pi x}{L_x}\right) \sin\left(\frac{n_y \pi y}{L_y}\right), \tag{5.1}$$

where the possible waveforms are labelled by quantum numbers n_x and n_y. The eigenenergies corresponding to these electron eigenstates are

$$E_{n_x,n_y} = \frac{\pi^2 \hbar^2}{2m}\left(\frac{n_x^2}{L_x^2} + \frac{n_y^2}{L_y^2}\right). \tag{5.2}$$

The quantum numbers $n_{x,y}$ are linked to a corresponding wave number by

$$k_{x,y} = \frac{\pi n_{x,y}}{L_{x,y}}, \tag{5.3}$$

where $L_{x,y}$ are the dimensions of the island. In order to solve the density of states ω of the island for some energy interval $E_1 - E_2$, one finds out the number of states within the interval. For the sake of convenience, let $n_{x,y}$ be continuous, so that the number of states is given by the integral

$$N = 2\int_{E_1(n_x,n_y)}^{E_2(n_x,n_y)} dn_x dn_y, \tag{5.4}$$

where the factor of two comes from the spin degeneracy. Changing integration variables from $n_{x,y}$ to $k_{x,y}$, using (5.3), and transforming Cartesian coordinates to polar coordinates $\int dk_x dk_y \to \int dk d\theta\ k$, yields

$$N = 2\frac{L_x L_y}{\pi^2} \int_{\sqrt{2mE_1}/\hbar}^{\sqrt{2mE_2}/\hbar} k dk \int_0^{\pi/2} d\theta = \frac{L_x L_y m}{\pi \hbar^2}(E_2 - E_1). \tag{5.5}$$

The density of states i.e. number of states N per energy $E_2 - E_1$ is then

$$\omega = \frac{L_x L_y m}{\pi \hbar^2}. \tag{5.6}$$

Evidently, reducing the size of the island $L_x L_y$ leads to a smaller density of states and thus larger mean level spacing $\delta_s \equiv \omega^{-1}$. The spacing of the energy levels can thus be controlled by varying the size of a quantum dot. This enables control over electrical and optical properties of the dot. The possibility to precisely adjust the

wavelength of photons emitted by quantum dots [76] has already yielded commercial applications, like televisions with ultra deep colors [77]. In the field of electron transport, quantum dots are frequently used to confine individual electrons on certain discrete levels [78].

To maintain the quantization of energy levels in a quantum dot part of a larger nanodevice, any couplings between the dot and rest of the device need to be sufficiently weak. If a quantum dot is coupled too strongly to neighbouring (semi)conductors, the discrete states of the dot will mix with the continuous states of extended electrons of its neighbours. The limit of sufficient isolation of the discrete dot levels can be stated formally as a requirement: the conductance of the gap between the dot and connected electron reservoir has to be significantly smaller than the conductance quantum $G \ll G_Q$. Since the same condition ensures that the charging energy dictates electron transport (see Ch. 2), the discreteness of quantum dots is guaranteed to hold in nanodevices, that operate in the dynamic Coulomb blockade regime.

In Cooper pair splitters, the separation of energy levels of quantum dots is taken to its extreme. Controlled extraction of an individual electron from a superconductor can be realized into a quantum dot, when there is only single energy level available for it. The details of creating such single level quantum dots or *resonant levels* are discussed next.

5.1.2 Resonant level

A quantum dot acts as a resonant level when its mean level spacing is larger than the electric and thermal energy available for electrons in the nanostructure, $\delta_s > \min(k_B T, eV_{\text{bias}})$. Electrons from the rest of the nanodevice can then only tunnel into resonant level whose energy is within $k_B T$ or eV_{bias} of their own energy. Evidently, because of the Pauli exclusion, this level can be occupied at most by two

electrons (with opposite spins). This is reduced to only one allowed electron, if the charging energy of the first electron on a resonant level is large enough to prevent the second electron from tunneling in, $E_C > \min(k_B T, eV_{\text{bias}})$. Just like larger Coulomb blockade islands, the chemical potential of a quantum dot can be controlled by a gate electrode (Sec. 2.3).

5.2 Transport through a double quantum dot

The conventional Cooper pair splitter uses two resonant level quantum dots to regulate the electron flow from s-type superconductor into two terminal leads. It makes sense to conceptualize to the two adjacent resonant levels as a *double quantum dot*, since they operate mostly as a single component. By virtue of the Coulomb blockade, only one Cooper pair can occupy the double dot at time (one electron per dot). From the double quantum dot, the electrons can independently tunnel further to the terminal leads. Only at this point the dots have to be considered individually as the dot-lead tunneling is not synchronized like the superconductor-dots tunneling. Hence, one of the dots can be occupied while other one is left empty by a sequential tunneling process into a lead.

These two main transport events for electrons in the Cooper pair splitter are quite different in nature. The first event, superconductor-dots tunneling, is a coherent exchange of electrons between the superconductor and the double quantum dot (crossed Andreev reflection, Sec. 4.3.2). The second kind, tunneling events between the dots and leads, are a form of incoherent tunneling as described in Sec. 2.4. A brief overview of these tunneling events is now in place, before this chapter is concluded by energy hierarchy considerations for maximally efficient Cooper pair splitting.

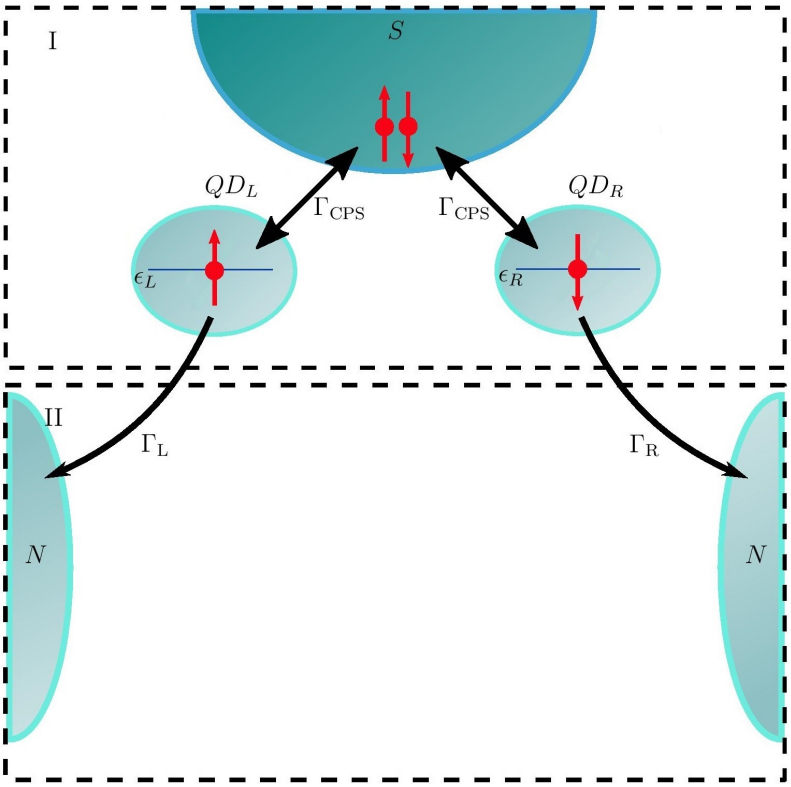

Figure 5.1: (Color online.) Cooper pair splitter. **Part I:** Superconductor (S) and two quantum dots ($DQ_{L,R}$) form the coherent part of the device. The coupling Γ_{CPS} denotes the amplitude of crossed Andreev reflection, that hybridises the states of an electron pair in the superconductor (empty state) and an electron pair in the double quantum dot(singlet state). The dot energy levels ϵ_L and ϵ_R (note $\epsilon_L + \epsilon_R = \nu$) can be individually controlled by gate electrodes (not shown in the picture). **Part II:** The two normal metal terminals (N) enable the final splitting of a Cooper pair. The incoherent single-electron transports with rates $\Gamma_{L,R}$ are directed from the dots to leads by biasing the chemical energy of the leads below that of the dots.

5.2.1 Superconductor to quantum dots

As stated earlier in Sec. 4.1.2, in the ground state of a superconductor, all conduction electrons are collected as Cooper pairs at a same energy level. This chemical

potential of the superconductor μ_S, is a convenient choice as the reference potential of the Cooper pair splitter, $\mu_S = 0$. Now, if located within the superconducting coherence length of each other and the superconductor, the quantum dots can accept Cooper pairs from the coherent condensate via the crossed Andreev reflection.

Higher level formal description of the transport between the superconductor and double quantum dot is given by a two level quantum system, whose time evolution is encoded in the Hamiltonian

$$\hat{H}_{S,DQD} = \begin{bmatrix} \mu_S & \Gamma_{\mathrm{CPS}} \\ \Gamma^*_{\mathrm{CPS}} & \mu_{DQD} \end{bmatrix}, \tag{5.7}$$

where $\mu_S = 0$ and μ_{DQD} are the chemical potential of the superconductor and the double quantum dot, respectively, and Γ_{CPS} is the amplitude of the crossed Andreev reflection. The diagonal elements of the Hamiltonian are the energies of the system in the two possible states (Cooper pair in the superconductor or Cooper pair in the dots). The off-diagonal amplitudes Γ_{CPS} couple these states by enabling population transport between the superconductor and dots.

Labelling the states of the system as $|0\rangle$ (empty dots) and $|S\rangle$ (spin-singlet in the dots), the solved eigenstates of the Hamiltonian (5.7) are

$$|S_-\rangle = a\,|0\rangle - b\,|S\rangle \qquad ; \qquad |S_+\rangle = c\,|0\rangle + d\,|S\rangle\,, \tag{5.8}$$

with some coefficients a, b, c, d. When the chemical potential of the double quantum dot matches that of the superconductor, $\mu_{DQD} = \mu_S = 0$, the eigenstates $|S_+\rangle$ and $|S_-\rangle$ both become equal superpositions of $|0\rangle$ and $|S\rangle$ i.e. the coefficients a, b, c, d become all equal to $1/\sqrt{2}$. Then the original states $|0\rangle$ and $|S\rangle$ are said to be completely *mixed*, as the Cooper pair exchange is maximised and happens equally to both directions between the superconductor and the dots, leaving the two-level quantum system oscillating between the two initial states.

This phenomenon is an instance of *resonant transport*, where coherent particle exchange is maximized at an energy resonance (here $\mu_{DQD} = \mu_S$). The width of

the resonance peak i.e. amount of particle exchange at slightly off-resonant energy values, is determined by the strength of the coupling (here the crossed Andreev reflection amplitude Γ_{CPS}). An important feature of the resonant transport is the two-way nature of the tunneling. At the resonance, Cooper pairs are continuously transported back and forth across the tunneling barrier. The usual way of directing electron flow, voltage bias, does not work in this case as it brings the system off-resonance and thus suppresses the transport rate. However, the probabilistic time evolution of a coherent system can be solved from the Schrödinger equation (see Sec. 7.1.2), making it possible to predict when the Cooper pair is likely to reside in the dots.

5.2.2 Quantum dots to lead terminals

Each quantum dot is coupled to a different normal metal lead by a tunneling barrier with conductance less than the conductance quantum, $G \ll G_Q$. Hence, the dynamics of the two junctions are driven by sequential tunneling on the dynamic Coulomb blockade regime. The tunneling rate across dot-lead junction resembles the case of island-lead tunneling derived in Sec. 2.4. The main difference is that, as long as the energy conservation is satisfied, the transition rate between a single level quantum dot and a lead does not depend on the energy difference between the initial and final states of the transport. For an island-lead junction, growing energy difference means that more energy states are able to realize the tunneling from the island. Clearly this is not the case for a dot with just a single relevant energy level, so the transport rate does not change with increasing energy.

The tunneling rate can be again written in terms of the conductance of the tunnel barrier G; see Ref. [17]. In the limit of vanishing temperature the rate is

$$\Gamma_{\mathrm{dot}\to\mathrm{lead},} = \frac{\delta_S}{\hbar}\frac{G}{G_Q}\Theta(-\Delta E), \tag{5.9}$$

where $\Theta(-\Delta E)$ is the Heaviside step-function. Even for resonant levels, as a consequence of there being multiple states in the lead, any information of the electron phase gets averaged out and the transport is incoherent. The two sequential transport processes are not a priori synchronized, and can thus leave the double quantum dot occupied with only one electron for a time. As will be specified next, in the conventional Cooper pair splitting regime this situation is avoided since the rate of these sequential tunnelings is the smallest relevant time scale and hence, the system spends practically no time in a singly occupied state.

However, the purpose of this thesis is to study spin-orbit effects in the quantum dots, and too fast dot-to-lead rates leave no time for measuring the electron pair in the dots. In view of this, the next section presents first the conventional way of setting system parameters for optimised Cooper pair splitting, and introduces then a slight change, that allows verifying spin-orbit effects on the quantum dots by making the dot-states long-lasting.

5.3 Energy hierarchy of Cooper pair splitters

Now that all the relevant phenomena related to a conventional Cooper pair splitter has been addressed, it is time to discuss what should be the relative strengths of various phenomena when aiming at the optimal performance. Achieving the desired split flow of pairwise entangled electrons from the superconductor via the quantum dots to the two leads requires careful tuning of the system parameters.

Gathering from all the topics discussed this far, the relevant system parameters include (all in the units of energy): the temperature k_BT, the superconducting gap Δ, the charging energy E_C and the level spacing δ_S of the quantum dots, the chemical potentials of all the components μ_S, μ_{dot1}, μ_{dot2}, μ_{lead1}, μ_{lead2}, as well as the transport amplitudes $\Gamma_{\mathrm{CPS}}, \Gamma_L$ and Γ_R. Finally, the spatial separation of the quantum dots d is to be compared to the coherence length of a Cooper pair ξ.

The optimal energy hierarchy presented here is suggested by [24]. The aim is to reach maximal efficiency of Cooper pair splitting by suppressing unwanted transport phenomena. Indeed, splitting efficiency of $\sim 100\%$ is reported in [79]. Firstly, as mentioned in Sec. 4.2.1, a large superconducting gap Δ prevents tunneling that would result in an excited quasiparticle state in the superconductor. With high Δ in place, the superconductor can only exchange electrons with the quantum dots via the Andreev reflection. Now, the Andreev reflection is a coherent transport process, and thus yields maximal electron exchange when the energies of the participating energy levels coincide. Therefore, the chemical potential of the superconductor should match the chemical potentials of the quantum dots, $\mu_S = \mu_{\mathrm{dot1}} = \mu_{\mathrm{dot2}}$. This is achieved by tunable gate electrodes individually coupled to the dots.

The reason for the inclusion of double quantum dot between the superconductor and the leads is to suppress the direct Andreev reflection, where a Cooper pair tunnels into a single lead, in favour of the crossed Andreev reflection that produces split pair into two different leads. In view of this, a pair of resonant level quantum dots is needed between the superconductor and leads to kill out the direct Andreev process. As stated in Sec. 5.1.2, single level dots are produced by combining high charging energy E_C and level spacing δ_S, with weak tunnel-couplings i.e. low conductance between the dots and superconductor as well as the dots and leads.

Low coupling strengths, $\Gamma_{\mathrm{CPS,L,R}} < E_C, \delta_S$, fulfil the conductance restriction, $G_l \ll G_Q$, placing the device in the dynamic Coulomb blockade regime. Furthermore, for the crossed Andreev reflection to be possible, the quantum dots cannot be placed farther than the coherence length of a Cooper pair ξ apart from each other. With separation longer than ξ, the crossed Andreev reflection becomes suppressed exponentially.

The chemical potential of the leads is to be set lower than the superconductor's and dots', by a bias voltage fulfilling $\Delta\mu = \mu_s - \mu_l > 0$, in order to have a stationary

flow of outbound electrons. The temperature of the system is naturally expected to be low for superconductivity to occur. Low temperature also excludes unwanted thermally activated transport, e.g. between the leads and dots, that happen when $k_BT > \Delta\mu$.

Lastly, at the transport resonance of the crossed Andreev reflection, $\mu_S = \mu_{\text{dots}}$, the opposite process carrying electrons from the dots to superconductor, happens at an equal rate. To mitigate the transport towards the wrong direction, the energies associated with the dot-lead couplings $\Gamma_{L,R}$ should be considerably larger than the energy of the superconductor-dots coupling Γ_{CPS}. Consequently, the rate of the dot-lead transport is much faster than the dots-superconductor transport, and the dots will be emptied into the terminal leads as soon as they become occupied by a Cooper pair. This renders the electron occupancy of the double quantum dot to a mere virtual state in a complete transport event, that extracts and splits a Cooper pair from the superconductor to separate electrons into the terminal leads.

5.3.1 Regime of long-lived dot-states

For studying the spin-orbit interaction in a Cooper pair splitter, the mere virtual occupation of the quantum dots is insufficient. To obtain time-averaged charge measurements (Ch. 9), the occupation time of the pair in the dots must be increased. This is achieved by weakening the coupling between the dots and the terminal leads. In the limit where $\Gamma_{\text{CPS}} \gg \Gamma_{L,R}$, the coherent transport between the superconductor and dots occurs much faster than the tunneling from dots to leads.

Keeping rest of the system parameters unchanged from the conventional regime of Cooper pair splitter and inverting the tunnel coupling strengths ($\Gamma_{\text{CPS}} \gg \Gamma_{L,R}$ to $\Gamma_{L,R} \gg \Gamma_{\text{CPS}}$), yields an operational regime, called here the *regime of long-lived dot-states*, that allows time-averaged measurements to be performed on the superconductor-dot system. The active spin-orbit interaction expands the two di-

mensional Hilbert space of the empty and singlet state with the spin-triplet states (3.21), rendering the state of the electron pair in general into a coherent superposition of the now five basis states, $\{|0\rangle, |S\rangle, |T_0\rangle, |T_+\rangle, |T_-\rangle\}$. In this regime, the single electron tunnelings to the terminal leads can be used for tunneling spectroscopy. It is noteworthy, that the regime of long-lasting dot-states includes in principle also the singly occupied double quantum dot: there is a time between the two sequential dot-to-lead tunnelings when only one electron resides on the dots, and can realize co-tunneling processes between the dots through the superconductor. As shown in Ch. 9, this transport can be excluded by introducing detuning between the quantum dots.

In the coming chapters, the state of the electron pair is studied as a delocalized entity in the superconductor-quantum dots system while the near decoupled terminal leads are left out of the picture. This enables a convenient analysis of the coherent evolution of the system. However, prior to that, the mechanism responsible for the non-trivial time evolution of the system, the spin-orbit interaction, will be discussed.

6. Spin-orbit interaction

The coupling of magnetic fields to the spin of a particle is fairly straightforward and intuitive process (see Sec. 3.1.1). This coupling is utilized in contemporary spin-electrical devices such magnetic memory and MRI. Less obvious is the coupling between electric fields and spin. This relativistic effect is termed *spin-orbit interaction*, since it was discovered by observing electrons in orbital motion in hydrogen atoms [31, 32].

Before discussing the spin-orbit effect in a Cooper pair splitter, a physical description of the spin-orbit phenomenon is in place. The mechanism of spin-orbit coupling will be introduced first in conceptually simpler case of a hydrogen atom, before delving into its manifestation in crystalline (semi)conductors. The rigorous derivation of the spin-orbit coupling will be left out, as it requires relativistic quantum theory, arising as a term in the Dirac equation [33].

6.1 Hydrogen atom

The spin-orbit coupling was originally invented to explain an observed shift in spectral lines of hydrogen atom. Semi-classical understanding of the effect can be obtained by considering the Bohr's hydrogen model in the rest frame of the electron. In this frame of reference, the stationary electron is orbited by the proton, whose charge creates a magnetic field $\vec{B}$. The electron has a magnetic dipole moment $\vec{\mu}$ due to its spin, and thus feels a torque aligning it with the magnetic field of the

proton. As before (Sec. 3.12), the energy associated with this torque is given by the Hamiltonian

$$\hat{H}_{SO} = -\vec{\mu} \cdot \vec{B}. \tag{6.1}$$

By identifying the circling proton as a current loop with effective current $I = e/T$, where T is the period of the proton, the magnitude of the generated magnetic field can be obtained from the Biot-Savart law

$$B = \frac{\mu_0 I}{2r}. \tag{6.2}$$

Inserting this into Eq. (6.1) and introducing the angular momentum of the electron (returning for a moment to the usual frame of reference) $L = rm_e v = 2\pi m_e r^2/T$, as well as eliminating the vacuum permeability μ_0 in favour of the vacuum permittivity ϵ_0 via $c = 1/\sqrt{\mu_0 \epsilon_0}$, yields the magnetic field [43]

$$\vec{B} = \frac{1}{4\pi\epsilon_0} \frac{e}{m_e c^2 r^3} \vec{L}. \tag{6.3}$$

The magnetic field points to the same direction as the angular momentum generating it, i.e. perpendicular to the plane of the proton movement. The magnetic moment $\vec{\mu}$ of an electron is given by Eq. (3.9) as

$$\vec{\mu} = -\frac{e g_e}{2m_e} \vec{S}. \tag{6.4}$$

Inserting this to the Eq. (6.1) along with the effective magnetic field of Eq. (6.3) gives

$$\hat{H}_{SO} = \frac{g_e}{8\pi\epsilon_0} \frac{e^2}{m_e^2 c^2 r^3} \vec{S} \cdot \vec{L}. \tag{6.5}$$

This result is based only on classical reasoning, apart from the g_e correction for electron spin. In truth, Eq. (6.5) is in need of a further non-classical correction. In actuality, the orbiting electron cannot be assigned with a constant inertial frame because of its centripetal acceleration. Proper relativistic considerations modify the

result with an additional factor of 1/2, known as the Thomas precession correction [31, 32].

In order to highlight the effect of the spin-orbit Hamiltonian (6.5), the spin-operator can be written in terms of Pauli matrices and the angular momentum can be set along z-axis. The Hamiltonian reads then (including the Thomas precession factor)

$$\hat{H}_{SO} = \frac{g_e \hbar}{32\pi\epsilon_0} \frac{e^2 L}{m_e^2 c^2 r^3} \begin{bmatrix} 1 & 0 \\ 0 & -1 \end{bmatrix}. \tag{6.6}$$

Evidently, a splitting of $|\uparrow\rangle$ and $|\downarrow\rangle$ states occurs, just as if there was an external Zeeman magnetic field; see Sec. 3.1.1. This explains the extra spectral lines in the spectrum of hydrogen atom.

The effective magnetic field, resulting from the spin-orbit coupling, means that the spin of an electron can be addressed not only by magnetic but also electric fields. The same phenomenon affects also the conduction electrons in solids, with few complications arising from the geometry of the crystalline lattice.

6.2 Spin-orbit coupling in solids

The delocalized conduction electrons moving in a crystalline solid feel the spin-orbit interaction while traversing the electric field produced by the lattice-ions. Again, the electric field is perceived as an effective magnetic field by the electrons in their rest-frame. However, whereas electrons orbiting an atom are subjected to a radial electric field, the field of a symmetric crystal follows the periodic isotropy of the lattice. Consequently, the net-electric field felt by an electron in a symmetric lattice adds to zero, nullifying the effect of the spin-orbit coupling [17].

The combination of the inversion symmetry of the lattice and the time-reversal symmetry of spin-orbit coupling ensures the persistence of spin degeneracy [17].

Reversing time causes both the electron's momentum (wave vector) and the spin to change sign. Evidently, this leaves the spin-orbit energy $\hat{H}_{SO} \propto \vec{k} \cdot \vec{S}$ unchanged. The energy of the electron obeys, therefore, the symmetry: $E(\vec{S}, \vec{k}) = E(-\vec{S}, -\vec{k})$. Combined with the inversion symmetry of the lattice, $E(\vec{k}) = E(-\vec{k})$, this invariance under time-reversal leads to a spin degenerate system. Electrons with the same wave vector but opposite spins will be equal in energy

$$E(\vec{S}, \vec{k}) = E(-\vec{S}, \vec{k}). \tag{6.7}$$

Therefore, in solids the spin-orbit effect manifest only when there is some asymmetries or impurities in the lattice structure. Active spin-orbit effects are present most commonly in solids wherein the inversion symmetry is broken either with respect to the center of the bulk or along some axis. The former case leads to a so-called Dresselhaus spin-orbit interaction [28]. In lattices with only uniaxial bulk symmetry or at the surface of a solid, the inversion symmetry is violated in the direction perpendicular to the special axis/surface, which gives rise to a Rashba spin-orbit effect [80].

Once the degeneracy of Eq. (6.7) is broken e.g. by the Rashba or Dresselhaus effects, spin-flip transitions can take place between the split sub-levels. An electron moving in a non-symmetric potential landscape of a *spin-active solid*, experiences changes of velocity and electric field, that create a varying spin-orbit magnetic field. In such materials, spins of the mobile electrons are subjected to constant rotations. Spin-orbit length λ_{SO} is defined as the average distance the electron needs to traverse for its spin to rotate π radians [81]. Spin-orbit length thus serves as a measure of the strength of the spin-orbit coupling, with shorter λ_{SO} indicating stronger interaction.

6.3 Spin-orbit coupling in quantum dots

Being tiny bits of semiconducting solid, quantum dots (Sec. 5.1) exhibit spin-orbit interaction via the mechanism described above. However, the localization of electrons in a minute dot leads to a suppression of spin-orbit interactions. As the width of a quantum dot λ_d is typically less than the spin-orbit length λ_{SO}, a suppression of a power of λ_d/λ_{SO} generally abolishes any spin-orbit effects. The Rashba and Dresselhaus interactions are not strong enough to significantly lift the degeneracy of opposing spin states in quantum dots. Hence, an external magnetic field is needed to achieve noteworthy spin-orbit effects.

For indium arsenide (InAs), the amplitude of spin-orbit coupling is found to be proportional to the Zeeman effect with a factor of ≈ 0.1 [82]. This gives rise to a subtlety, discussed properly in Ch. 7, that further limits the manifestation of spin-orbit interaction. In short, since the energy gap between states split by the external magnetic field are proportional to the Zeeman energy E_Z, and the spin-orbit amplitude is proportional to $0.1E_Z$, the coherent transport induced by the transverse spin-orbit terms seems inherently weak. This issue will be addressed by bridging the energy gap with tunable gate electrodes.

The reference [83] derives an effective Hamiltonian for spin-orbit interaction felt by an electron in a two-dimensional quantum dot exhibiting both Rashba and Dresselhaus interactions. The Rashba and two-dimensional Dresselhaus Hamiltonians are, up to first order in p,

$$\hat{H}_R = \alpha(\hat{p}_x\hat{\sigma}_y - \hat{p}_y\hat{\sigma}_x) \text{ and } \hat{H}_D = \beta(\hat{p}_y\hat{\sigma}_y - \hat{p}_x\hat{\sigma}_x), \tag{6.8}$$

where α and β are dimensionless coupling strengths. Having transverse (along spin x and y directions) terms, these Hamiltonians can induce spin-flips. However, as discussed in [29, 84, 85], an external magnetic field E_Z is required to achieve non-vanishing effects. Coining the spin-orbit terms (6.8) with static electric field of

the semiconductor and the Zeeman field yields, after few approximations [83], the effective Hamiltonian for spin-orbit interaction

$$\hat{H}_{SO} = \mu(\vec{B}_{SO} \times \vec{B}_Z) \cdot \vec{\sigma}, \tag{6.9}$$

where μ is the modulus of the spin magnetic moment, $\vec{B}_{SO} \propto \vec{v} \times \vec{E}$ is the effective spin-orbit magnetic field and $\vec{B}_Z$ is the external Zeeman field. The following chapter employs this Hamiltonian to study the spin-orbit interaction in the double quantum dot of a Cooper pair splitter.

7. Spin-orbit interaction in Cooper pair splitter

This chapter presents a quantitative study of spin-flips experienced by electron pairs in a Cooper pair splitter during their stay in the double quantum dot coupled to a superconductor. It is convenient at first to limit the analysis to the part I of the Cooper pair splitter (see Fiq. 5.1), i.e. the superconductor and the double dots. Leaving out the terminal leads is legit as long as the regime of long-lived dot-states (Sec. 5.3.1) is considered. It is assumed that the dot-to-lead tunnelings happen at much slower rate than the superconductor-dots tunneling and the former can hence be ignored for now.

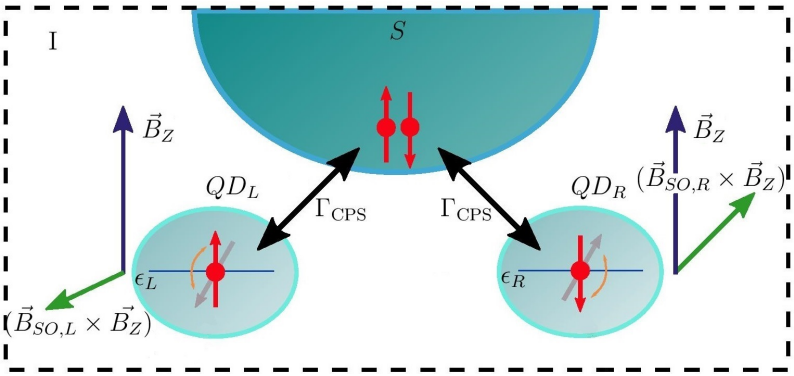

Figure 7.1: (Color online.) Superconductor coupled to quantum dots with active spin-orbit interaction. In the limit of long-lived dot-states (Sec. 5.3.1), the terminal leads of the Cooper pair splitter can be ignored when studying the coherent state delocalized on the superconductor and dots. The quantum dots are subjected to an external magnetic field $\vec{B}_Z$ and they exhibit active spin-orbit interaction, with effective spin-orbit magnetic fields $\vec{B}_{SO,L}$ and $\vec{B}_{SO,R}$, for left and right dot, respectively. The cross products of the Zeeman and spin-orbit fields $(\vec{B}_{SO,L/R} \times \vec{B}_Z)$, denoted by the green arrows, are responsible for the spin-flips experienced by the electrons in the dots; see the Hamiltonian 7.4.

7.1 Hamiltonian of the two-electron spin states

The complete Hilbert space of two-electron spin states is spanned by the singlet-triplet basis

$$
\begin{aligned}
|S\rangle &= \frac{1}{\sqrt{2}}(|\uparrow\downarrow\rangle - |\downarrow\uparrow\rangle), \\
|T_0\rangle &= \frac{1}{\sqrt{2}}(|\uparrow\downarrow\rangle + |\downarrow\uparrow\rangle), \\
|T_+\rangle &= |\uparrow\uparrow\rangle\,, \\
|T_-\rangle &= |\downarrow\downarrow\rangle\,.
\end{aligned} \tag{7.1}
$$

Together with the empty state $|0,0\rangle \equiv |0\rangle$, they constitute the basis vectors for the double quantum dot-states,

$$\{|0\rangle, |S\rangle, |T_0\rangle, |T_+\rangle |T_-\rangle\}. \tag{7.2}$$

The relationships of the states are decoded in the Hamiltonian of the system. This can be separated into a spin-independent part and the spin-dependent part, $\hat{H} = \hat{H}_0 + \hat{H}_s$. The spin-independent Hamiltonian, $\hat{H}_0$ contains the eigenenergies of the dot-states, in addition to the coupling amplitude Γ_{CPS} quantifying the strength of the singlet exchange between the superconductor and dots.

The spin-dependent part $\hat{H}_s = \hat{H}_Z + \hat{H}_{SO}$ includes the Zeeman Hamiltonian (Sec. 3.1.1, Eq. (3.12)) as well as the spin-orbit interaction Hamiltonian (Sec. 6.3, Eq. (6.9)) for both dots ($l = \{L, R\}$), respectively

$$\hat{H}_Z = \sum_{l=\{L,R\}} \mu \vec{B}_Z \cdot \vec{\sigma}_l \quad \text{and} \tag{7.3}$$

$$\hat{H}_{SO} = \sum_{l=\{L,R\}} \mu (\vec{B}_{SO,l} \times \vec{B}_Z) \cdot \vec{\sigma}_l, \tag{7.4}$$

where μ is the modulus of the spin magnetic moment in the dots (assumed identical in both), $\vec{B}_Z$ is the static Zeeman magnetic field, $\vec{\sigma}_l$ is the Pauli vector related to the spin of the electron in quantum dot l. The effective magnetic field $\vec{B}_{SO,l}$ gives the orientation and relative strength of the spin-orbit effect.

The Hamiltonians (7.3) and (7.4) can be written in the basis of states $\{|S\rangle, |T_0\rangle, |T_+\rangle, |T_-\rangle\}$, where the empty state is temporarily suspended, by following the approach of Sec. 3.2, wherein the representation for $\hat{H}_Z$ is derived. Similarly, utilizing $\vec{B}_Z = (0, 0, B_Z)$ and denoting $\vec{\epsilon}_l \equiv \mu(\vec{B}_{SO,l} \times \vec{B}_Z)$, $\hat{H}_{SO}$ can be written as

$$\begin{aligned} \hat{H}_{SO} &= \vec{\epsilon}_L \cdot \vec{\sigma}_L + \vec{\epsilon}_R \cdot \vec{\sigma}_R \\ &= \epsilon_{L,x}\hat{\sigma}_{L,x} + \epsilon_{L,y}\hat{\sigma}_{L,y} + \epsilon_{R,x}\hat{\sigma}_{R,x} + \epsilon_{R,y}\hat{\sigma}_{R,y}. \end{aligned} \tag{7.5}$$

The Pauli matrices of a two-particle Hilbert space spanned by $\{|\uparrow\uparrow\rangle, |\uparrow\downarrow\rangle, |\downarrow\uparrow\rangle, |\downarrow\downarrow\rangle\}$

are obtained as the tensor products

$$\hat{\sigma}_{L,x} = \hat{\sigma}_x \otimes \hat{I} = \begin{bmatrix} 0 & 0 & 1 & 0 \\ 0 & 0 & 0 & 1 \\ 1 & 0 & 0 & 0 \\ 0 & 1 & 0 & 0 \end{bmatrix} \quad ; \quad \hat{\sigma}_{L,y} = \hat{\sigma}_y \otimes \hat{I} = \begin{bmatrix} 0 & 0 & -i & 0 \\ 0 & 0 & 0 & -i \\ i & 0 & 0 & 0 \\ 0 & i & 0 & 0 \end{bmatrix};$$

$$\hat{\sigma}_{R,x} = \hat{I} \otimes \hat{\sigma}_x = \begin{bmatrix} 0 & 1 & 0 & 0 \\ 1 & 0 & 0 & 0 \\ 0 & 0 & 0 & 1 \\ 0 & 0 & 1 & 0 \end{bmatrix} \quad ; \quad \hat{\sigma}_{R,y} = \hat{I} \otimes \hat{\sigma}_y = \begin{bmatrix} 0 & -i & 0 & 0 \\ i & 0 & 0 & 0 \\ 0 & 0 & 0 & -i \\ 0 & 0 & i & 0 \end{bmatrix}. \quad (7.6)$$

The Hamiltonian (7.5) reads then

$$\hat{H}_{SO} = \begin{bmatrix} 0 & \epsilon_{R,x} - i\epsilon_{R,y} & \epsilon_{L,x} - i\epsilon_{L,y} & 0 \\ \epsilon_{R,x} + i\epsilon_{R,y} & 0 & 0 & \epsilon_{L,x} - i\epsilon_{L,y} \\ \epsilon_{L,x} + i\epsilon_{L,y} & 0 & 0 & \epsilon_{R,x} - i\epsilon_{R,y} \\ 0 & \epsilon_{L,x} + i\epsilon_{L,y} & \epsilon_{R,x} + i\epsilon_{R,y} & 0 \end{bmatrix}, \quad (7.7)$$

which can be written in terms of outer products of the basis states as

$$\begin{aligned} \hat{H}_{SO} = {} & (\epsilon_{R,x} - i\epsilon_{R,y}) \left|\uparrow\uparrow\right\rangle \left\langle\uparrow\downarrow\right| + (\epsilon_{L,x} - i\epsilon_{L,y}) \left|\uparrow\uparrow\right\rangle \left\langle\downarrow\uparrow\right| + \\ & + (\epsilon_{R,x} + i\epsilon_{R,y}) \left|\uparrow\downarrow\right\rangle \left\langle\uparrow\uparrow\right| + (\epsilon_{L,x} - i\epsilon_{L,y}) \left|\uparrow\downarrow\right\rangle \left\langle\downarrow\downarrow\right| + \\ & + (\epsilon_{L,x} + i\epsilon_{L,y}) \left|\downarrow\uparrow\right\rangle \left\langle\uparrow\uparrow\right| + (\epsilon_{R,x} - i\epsilon_{R,y}) \left|\downarrow\uparrow\right\rangle \left\langle\downarrow\downarrow\right| + \\ & + (\epsilon_{L,x} + i\epsilon_{L,y}) \left|\downarrow\downarrow\right\rangle \left\langle\uparrow\downarrow\right| + (\epsilon_{R,x} + i\epsilon_{R,y}) \left|\downarrow\downarrow\right\rangle \left\langle\downarrow\uparrow\right|. \end{aligned} \quad (7.8)$$

A change of basis to the singlet-triplet basis is achieved by substituting

$$\begin{aligned} \left|\uparrow\uparrow\right\rangle = \left|T_+\right\rangle \quad ; \quad \left|\uparrow\downarrow\right\rangle = (\left|T_0\right\rangle + \left|S\right\rangle)/\sqrt{2} \\ \left|\downarrow\downarrow\right\rangle = \left|T_-\right\rangle \quad ; \quad \left|\downarrow\uparrow\right\rangle = (\left|T_0\right\rangle - \left|S\right\rangle)/\sqrt{2}. \end{aligned} \quad (7.9)$$

The spin-orbit Hamiltonian is then

$$\begin{aligned}\hat{H}_{SO} =& \frac{\epsilon_{R,x} - i\epsilon_{R,y}}{\sqrt{2}} |T_+\rangle (\langle T_0| + \langle S|) + \frac{\epsilon_{L,x} - i\epsilon_{L,y}}{\sqrt{2}} |T_+\rangle (\langle T_0| - \langle S|) + \\ &+ \frac{\epsilon_{R,x} + i\epsilon_{R,y}}{\sqrt{2}} (|T_0\rangle + |S\rangle) \langle T_+| + \frac{\epsilon_{L,x} - i\epsilon_{L,y}\big)}{\sqrt{2}} (|T_0\rangle + |S\rangle) \langle T_-| + \\ &+ \frac{\epsilon_{L,x} + i\epsilon_{L,y}}{\sqrt{2}} (|T_0\rangle - |S\rangle) \langle T_+| + \frac{\epsilon_{R,x} - i\epsilon_{R,y}}{\sqrt{2}} (|T_0\rangle - |S\rangle) \langle T_-| + \\ &+ \frac{\epsilon_{L,x} + i\epsilon_{L,y}}{\sqrt{2}} |T_-\rangle (\langle T_0| + \langle S|) + \frac{\epsilon_{R,x} + i\epsilon_{R,y}}{\sqrt{2}} |T_-\rangle (\langle T_0| - \langle S|). \end{aligned} \tag{7.10}$$

Collecting terms and using a notation that shortens the sum and difference of spin-orbit fields between the two dots to $\vec{\epsilon}_{s,d} \equiv \vec{\epsilon}_L \pm \vec{\epsilon}_R$ allows finally writing the spin-orbit Hamiltonian in a compact form in the singlet-triplet basis (along with the Zeeman Hamiltonian derived in Sec. 3.2) as

$$\hat{H}_Z = \sum_{\pm} \pm E_Z |T_\pm\rangle \langle T_\pm| \tag{7.11}$$

$$\begin{aligned}\hat{H}_{SO} =& \sum_{\pm} \frac{\epsilon_{s,x} \pm i\epsilon_{s,y}}{\sqrt{2}} |T_0\rangle \langle T_\pm| + \text{h.c.} \\ &+ \sum_{\pm} \frac{\mp\epsilon_{d,x} - i\epsilon_{d,y}}{\sqrt{2}} |S\rangle \langle T_\pm| + \text{h.c.}, \end{aligned} \tag{7.12}$$

where the Zeeman energy is defined as $E_Z \equiv 2\mu|\vec{B}_Z|$. Note that the spin-orbit coupling between the singlet and polarized triplets is proportional to the difference of the spin-orbit fields of the dots, $\vec{\epsilon}_L - \vec{\epsilon}_R$. Hence, for this coupling to be non-zero, it must be possible to set the spin-orbit fields of the two dots to different values. Indeed, the experiments done in [86, 82] support the possibility of individually tuning the spin-orbits fields of each dot by gate electrodes.

Notice the limitations of the spin-orbit coupling terms. They only directly couple the singlet $|S\rangle$ and the neutral triplet $|T_0\rangle$ with the polarized triplets $|T_+\rangle$ and $|T_-\rangle$. This is congruent with the capabilities of a single spin-flip. The singlet and neutral triplet differ only by the inverted phase of the $|\downarrow\uparrow\rangle$ state (see Eq. 7.1) and hence cannot be changed to each other by a spin-flip. Going from one polarized triplet to the other requires two spin-flips, so they are not connected in the first order Hamiltonian (7.13) either.

7.1.1 Matrix form of the Hamiltonian

The two-particle Hamiltonian $\hat{H} = \hat{H}_0 + \hat{H}_s$ can be concisely written in a matrix form in the ordered basis (that now includes the empty state), $\{|0\rangle, |S\rangle, |T_0\rangle, |T_+\rangle, |T_-\rangle\}$, as

$$\hat{H} = \begin{bmatrix} 0 & \Gamma^*_{\mathrm{CPS}} & 0 & 0 & 0 \\ \Gamma_{\mathrm{CPS}} & \nu & 0 & \tilde{\epsilon}^*_d & -\tilde{\epsilon}_d \\ 0 & 0 & \nu & \tilde{\epsilon}^*_s & \tilde{\epsilon}_s \\ 0 & \tilde{\epsilon}_d & \tilde{\epsilon}_s & \nu + E_Z & 0 \\ 0 & -\tilde{\epsilon}^*_d & \tilde{\epsilon}^*_s & 0 & \nu - E_Z \end{bmatrix}, \tag{7.13}$$

where $\nu = \epsilon_L + \epsilon_R$ is the gate-controllable detuning between the empty and two-particle states, $\tilde{\epsilon}_d = -(\epsilon_{d,x} + i\epsilon_{d,y})/\sqrt{2}$ is the spin-orbit coupling between $|S\rangle$ and $|T_\pm\rangle$, and $\tilde{\epsilon}_s = (\epsilon_{s,x} + i\epsilon_{s,y})/\sqrt{2}$ is the spin-orbit coupling between $|T_0\rangle$ and $|T_\pm\rangle$.

The diagonal elements are the energies of the non-interacting two-particle eigenstates and the off-diagonal elements are coherent coupling amplitudes that drive the time evolution of the system. Note the contribution of the Zeeman effect E_Z to the energies of the polarized triplets. Importantly, only the singlet state is coupled to the empty state, via the crossed Andreev reflection amplitude Γ_{CPS}. As stated earlier, spin-orbit couplings connect the singlet and the neutral triplet to the two polarized triplets, with amplitudes proportional to the sum and difference, respectively, of the spin-orbit fields of the individual dots ($\tilde{\epsilon}_s$ and $\tilde{\epsilon}_d$).

As will be reviewed in the following sections, choosing different pairs of resonant values of the electric ν and magnetic E_Z parameters in the Hamiltonian (7.13) lead to different coherent spin states, as a consequence of a mixing caused by the spin-orbit coupling $\tilde{\epsilon}_d$.

7.1.2 Coherent evolution

It is helpful here to recap the way that coherent (undisturbed) quantum systems evolve in time. The state vector of the electron pair on the double quantum dot will in general be the linear superposition of the basis states

$$|\psi(t)\rangle = c_0(t)\,|0\rangle + c_S(t)\,|S\rangle + c_{T_0}(t)\,|T_0\rangle + c_{T_+}(t)\,|T_+\rangle + c_{T_-}(t)\,|T_-\rangle\,. \tag{7.14}$$

The complex probability amplitudes $c_X(t) = \langle X|\psi(t)\rangle$, where $X = \{0, S, T_0, T_+, T_-\}$, dictate the weight of the corresponding eigenstates $|X\rangle$ in the superposition at any given time t. According to the Born's rule, the squared absolute values of the probability amplitudes are identified with the probability of finding the system in the corresponding eigenstates. Hence,

$$|c_0(t)|^2 + |c_S(t)|^2 + |c_{T_0}(t)|^2 + |c_{T_+}(t)|^2 + |c_{T_-}(t)|^2 = 1 \tag{7.15}$$

holds at all times. In the Schrödinger picture [43], the time evolution of the state vector is generated by the Hamiltonian of the system according to the Schrödinger equation

$$i\hbar\frac{\partial}{\partial t}\,|\psi(t)\rangle = \hat{H}\,|\psi(t)\rangle\,. \tag{7.16}$$

The solution $|\psi(t)\rangle = e^{-i\hat{H}(t-t_0)/\hbar}\,|\psi(t_0)\rangle$ indicates oscillating evolution dictated by the Hamiltonian $\hat{H}$ operating on the initial state $|\psi(t_0)\rangle$. It is insightful to track the probability of each eigenstate

$$P_X(t) = |\langle X|\psi(t)\rangle|^2 \tag{7.17}$$

to see which states are taking part in the coherent evolution with given system parameters. For instance, in absence of the spin-orbit couplings the probabilities of the triplet states are zero. Though the coherent evolution of the state vector itself cannot be directly observed, measuring consequential physical observables, such as charge (see Ch. 9), yields information about the electron state on the quantum dots.

In the following sections the coherent evolution of the superconductor-double dot system is studied using the above formalism in the regime of long-lived dot-states. The state and finally the degree of entanglement on the quantum dots at various values of the electric and magnetic field handles ν and E_Z is probed using a following scheme. Three regimes of detuning between the superconductor and dots are considered; zero detuning, intermediate detuning and high detuning. Then in each regime the magnetic field is used to bring the polarized triplets into a resonance point, wherein the spin-orbit effects manifest.

7.2 Transport resonance

The gate controlled detuning ν dictates the strength of Cooper pair exchange between the superconductor and the double quantum dot. The degree of coherent mixing between coupled state vectors depends on the ratio of their energy difference and the coupling amplitude. In the case of Cooper pair tunneling between the superconductor and dots that is $\Gamma_{\mathrm{CPS}}/\nu$, where Γ_{CPS} is the amplitude of the crossed Andreev reflection and the denominator is simply the energy of the singlet state ν, since the energy of the empty state is fixed to zero. At the transport resonance of the Cooper pair exchange $\nu = 0$, the above ratio implies maximal mixing of the eigenstates $|0\rangle$ and $|S\rangle$ via coherent oscillations, which makes the dots to be occupied by an electron pair half of the time on average. Note that in the face of the zero energy gap of resonant states, any coupling is strong enough to cause complete mixing (probability of each state oscillates between zero and one). However, the frequency of the oscillations remains dependent of the coupling amplitude.

The degenerate perturbation theory (see e.g. [43]) proves to be a suitable tool for analysing the Hamiltonian (7.13) of the system. Based on the estimated [82] strength of the spin-orbit couplings in InAs $\tilde{\epsilon}_{d,s} \simeq 0.1E_Z$, these terms can be treated as a small perturbation in the system (provided that the magnetic field

is not too large, $E_Z \simeq \Gamma_{\mathrm{CPS}}$). As a first step of the perturbation approach, the Hamiltonian (7.13) (acting on the basis $\{|0\rangle, |S\rangle, |T_0\rangle, |T_+\rangle, |T_-\rangle\}$) is divided into the unperturbed and perturbing parts $\hat{H} = \hat{H}_0 + \tilde{H}$, where

$$\hat{H}_0 = \begin{bmatrix} 0 & \Gamma^*_{\mathrm{CPS}} & 0 & 0 & 0 \\ \Gamma_{\mathrm{CPS}} & 0 & 0 & 0 & 0 \\ 0 & 0 & 0 & 0 & 0 \\ 0 & 0 & 0 & E_Z & 0 \\ 0 & 0 & 0 & 0 & -E_Z \end{bmatrix}, \tag{7.18}$$

and

$$\tilde{H} = \begin{bmatrix} 0 & 0 & 0 & 0 & 0 \\ 0 & 0 & 0 & \tilde{\epsilon}^*_d & -\tilde{\epsilon}_d \\ 0 & 0 & 0 & \tilde{\epsilon}^*_s & \tilde{\epsilon}_s \\ 0 & \tilde{\epsilon}_d & \tilde{\epsilon}_s & 0 & 0 \\ 0 & -\tilde{\epsilon}^*_d & \tilde{\epsilon}^*_s & 0 & 0 \end{bmatrix}. \tag{7.19}$$

Note that $\nu = 0$ on the diagonal entries at the transport resonance. It is convenient to bring also the upper part of the unperturbed Hamiltonian $\hat{H}_0$ to a diagonal form. Diagonalizing Eq. (7.18) yields eigenvalues $\nu'_{\mp} = \mp\Gamma_{\mathrm{CPS}}$, corresponding to the normalized eigenvectors

$$|S_-\rangle = \frac{1}{\sqrt{2}}(|0\rangle + |S\rangle)$$

and

$$|S_+\rangle = \frac{1}{\sqrt{2}}(-|0\rangle + |S\rangle). \tag{7.20}$$

A new diagonalized unperturbed Hamiltonian for the double dot in the basis $\{|S_-\rangle, |S_+\rangle, |T_0\rangle,$

reads then

$$\hat{H}_0 = \begin{bmatrix} -\Gamma_{\mathrm{CPS}} & 0 & 0 & 0 & 0 \\ 0 & \Gamma_{\mathrm{CPS}} & 0 & 0 & 0 \\ 0 & 0 & 0 & 0 & 0 \\ 0 & 0 & 0 & E_Z & 0 \\ 0 & 0 & 0 & 0 & -E_Z \end{bmatrix}. \tag{7.21}$$

Importantly, the first two eigenstates $|S_-\rangle$ and $|S_+\rangle$ have non-zero eigenenergies. This makes it possible to tune the external magnetic field such that the polarized triplets $|T_-\rangle$ and $|T_+\rangle$ become resonant with the active states $|S_-\rangle$ and $|S_+\rangle$. Evidently, the resonant value for the Zeeman energy equals the crossed Andreev reflection amplitude $E_Z = \Gamma_{\mathrm{CPS}}$. The symmetry of the eigenenergies with respect to the zero-energy (see Fig. 7.2), guarantees that at $E_Z = \Gamma_{\mathrm{CPS}}$, two resonances occur simultaneously. The antisymmetric empty-singlet superposition $|S_-\rangle$ becomes degenerate with the $|T_-\rangle$ triplet at the same Zeeman energy, $E_Z = \Gamma_{\mathrm{CPS}}$, that makes the symmetric superposition $|S_+\rangle$ degenerate with the $|T_+\rangle$ triplet state. As discussed in the next chapter, this equal treatment of the polarized triplets proves to be crucial for improving the average entanglement in presence of the spin blockade on the dots.

7.2.1 The spin blockade

The modest resonant value of the Zeeman energy $E_Z = \Gamma_{\mathrm{CPS}}$ indeed justifies the use of perturbation theory, as it keeps the spin-orbit coupling amplitudes $\tilde{\epsilon}_{s,d}$ an order of magnitude smaller than the energies of the relevant eigenstates. As mentioned earlier, at a resonance point, the mixing of eigenstates is complete and only the frequency of the coherent oscillations depends on the coupling amplitude. The state on the double dot, before introduction of the perturbing spin-orbit coupling, is an equal superposition of the $|S_-\rangle$ and $|S_+\rangle$ states, that themselves are superpositions

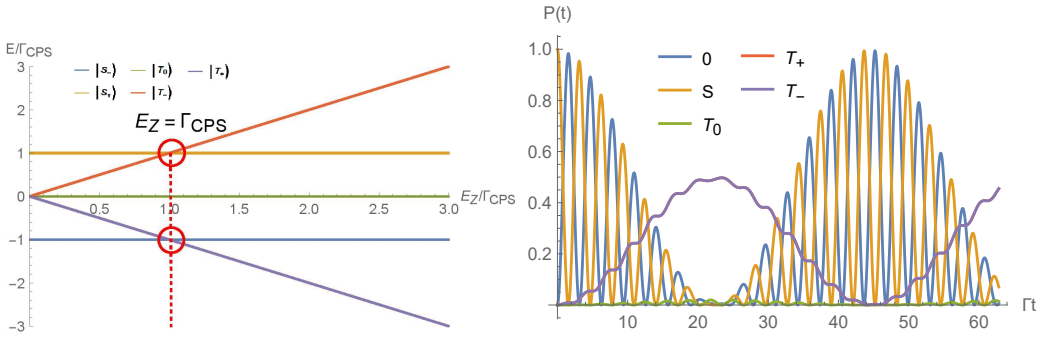

Figure 7.2: (Color online.) Double degeneracy and spin blockade. **Left:** Energies of the two-electron eigenstates at the zero detuning regime as a function of the Zeeman magnetic field E_Z. Two degeneracies coincide at a Zeeman energy $E_Z = \Gamma_{\rm CPS}$. **Right:** Coherent evolution (occupation probability vs. time) of the system at the double degeneracy point in the zero detuning regime ($\nu = 0, E_Z = \Gamma_{\rm CPS}$). The $|T_-\rangle$ and $|T_+\rangle$ states are equally activated by the spin-orbit coupling. Note that the latter is not seen in the plot since it is hidden by the $|T_-\rangle$ curve.

of the $|0\rangle$ and $|S\rangle$ states. The first order perturbation $\tilde{\epsilon}_d$, connects the singlet $|S\rangle$ to both of the polarized triplets $|T_+\rangle$ and $|T_-\rangle$. Thus, the states $|S_-\rangle$ and $|S_+\rangle$ become coherently hybridized with $|T_-\rangle$ and $|T_+\rangle$, respectively. At the resonance $E_Z = \Gamma_{\rm CPS}$, this creates complete coherent oscillations of frequency $\hbar/\tilde{\epsilon}_d$, between the empty-singlet superposition and the polarized triplets.

In view of the original basis states, the evolution of the state vector (7.14) consists of rapid oscillations of frequency $\hbar/\Gamma_{\rm CPS}$ between $|0\rangle$ and $|S\rangle$ (a singlet tunneling back and forth between the superconductor and the dots) accompanied by a slower cycle in and out of an equal superposition of $|T_-\rangle$ and $|T_+\rangle$.

Evidently, the empty state $|0\rangle$ becomes suppressed (along with the singlet) as the probability of a spin-flip increases during the coherent evolution of the double dot experiencing active spin-orbit interaction. The suppression of the empty state follows from the inability of the electrons in spin-triplet to realize the Andreev

reflection; see Sec. 4.3.1. Hence, a double quantum dot housing a triplet state will remain blockaded until a second spin-flip returns the system into singlet state. This effect, called the *spin blockade* [35], turns out to increase the average entanglement available in the double quantum dot of the Cooper pair splitter in the regime of long-lived dot-states. Description of the increased average entanglement (in Ch. 8), as well as a way to observe it (in Ch. 9), will be given after rest of the spin-orbit resonances are discussed. In short, the increase in average entanglement stems from the fact that the activated equal superposition of the polarized triplets is a maximally entangled state. Thus, though in general the activation of triplet states reduces entanglement, in this case the appearance of maximally entangled superposition of triplets, coinciding with the suppression of empty state, increases it.

7.3 Intermediate detuning

Next regime to consider is that of the intermediate detuning $\nu \simeq \Gamma_{\mathrm{CPS}}$. Increasing the chemical potential of the double quantum dot ν above that of the superconductor ($\nu_S = 0$) weakens the coherent mixing of the empty and singlet states. Unlike in the transport resonance, the dot state will now never reach unit probability in regards of the singlet occupation; see Fiq. 7.3. The decrease in the probability of a Cooper pair tunneling into the dots is dependent on the width of the resonance peak, i.e. the crossed Andreev reflection amplitude Γ_{CPS}. For instance, the two lower panels of Fig. 7.3 indicate that at a detuning $\nu = \Gamma_{\mathrm{CPS}}$, the likelihood of the singlet pair residing on the dots is approximately 20 %-units less than it was at the zero detuning. The increased chemical potential of the dots breaks the symmetric energy picture of the transport resonance; see the topmost panel of Fig. 7.3. The energies of the empty-singlet superpositions $|S_-\rangle$ and $|S_+\rangle$ no longer reside equidistantly below and above the zero-energy. This asymmetry means that the value of the resonant magnetic energy E_Z does not coincide for the two triplets $|T_-\rangle$ and $|T_+\rangle$.

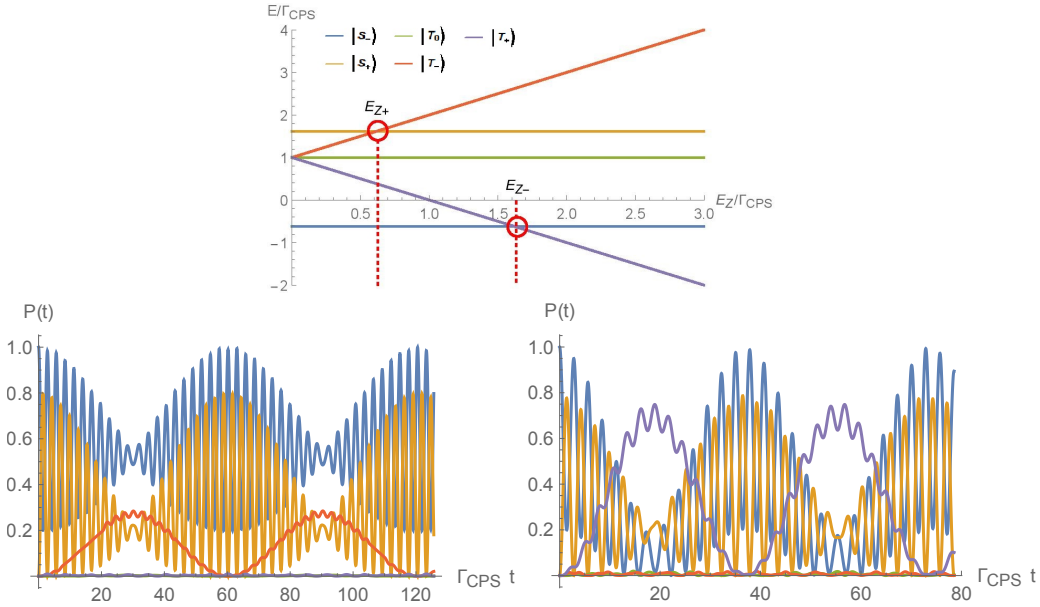

Figure 7.3: (Color online.) Individual triplet activation. **Top:** Energies of the two-electron eigenstates at the intermediate detuning regime ($\nu = \Gamma_{\rm CPS}$) as a function of the Zeeman magnetic field E_Z. The two resonances occur now at different values of the Zeeman field. **Bottom:** The coherent evolution (occupation probabilities vs. time) at the first, $E_Z = E_{Z+}$, and second resonance, $E_Z = E_{Z-}$, respectively. The polarized triplets $|T_+\rangle$ and $|T_-\rangle$ are activated separately and with different amplitudes and frequencies. The states are labelled by the same colours as in the top-figure.

In view of the perturbation theory, the Hamiltonian (7.13) can be treated exactly as in the zero detuning case, as long as the detuning is not too large, $\nu \simeq \Gamma_{\rm CPS}$. Now the eigenstates $|S_-\rangle$ and $|S_+\rangle$ and their eigenenergies ν'_+ and ν'_- attain

more complicated forms in the diagonalization of the unperturbed Hamiltonian,

$$\hat{H} = \begin{bmatrix} 0 & \Gamma^*_{\rm CPS} & 0 & 0 & 0 \\ \Gamma_{\rm CPS} & \nu & 0 & 0 & 0 \\ 0 & 0 & \nu & 0 & 0 \\ 0 & 0 & 0 & \nu + E_Z & 0 \\ 0 & 0 & 0 & 0 & \nu - E_Z \end{bmatrix}. \tag{7.22}$$

After diagonalization the two new eigenenergies are

$$|S_+\rangle = \frac{-\nu - \sqrt{4\Gamma^2_{\rm CPS} + \nu^2}}{\Gamma_{\rm CPS}\sqrt{4 + \left|\frac{\nu + \sqrt{4\Gamma^2_{\rm CPS}+\nu^2}}{\Gamma_{\rm CPS}}\right|^2}} |0\rangle + \frac{2}{\sqrt{4 + \left|\frac{\nu + \sqrt{4\Gamma^2_{\rm CPS}+\nu^2}}{\Gamma_{\rm CPS}}\right|^2}} |S\rangle \tag{7.23}$$

and

$$|S_-\rangle = \frac{-\nu + \sqrt{4\Gamma^2_{\rm CPS} + \nu^2}}{\Gamma_{\rm CPS}\sqrt{4 + \left|\frac{\nu - \sqrt{4\Gamma^2_{\rm CPS}+\nu^2}}{\Gamma_{\rm CPS}}\right|^2}} |0\rangle + \frac{2}{\sqrt{4 + \left|\frac{\nu - \sqrt{4\Gamma^2_{\rm CPS}+\nu^2}}{\Gamma_{\rm CPS}}\right|^2}} |S\rangle\,, \tag{7.24}$$

with eigenenergies

$$\nu'_\pm = \nu/2 \pm \sqrt{(\nu/2)^2 + |\Gamma_{\rm CPS}|^2}. \tag{7.25}$$

Evidently, these forms reduce to their zero detuning counterparts at $\nu = 0$. Now, the two Zeeman resonances of the eigenstates of the two-electron system occur at values $E_{Z+} = \sqrt{(\nu/2)^2 + \Gamma^2_{\rm CPS}} - \nu/2$ and $E_{Z-} = \sqrt{(\nu/2)^2 + \Gamma^2_{\rm CPS}} + \nu/2$ of the Zeeman energy; see. Fig. 7.3. The former value marks a degeneracy between states $|T_+\rangle$ and $|S_+\rangle$ while the second value, corresponding to a higher Zeeman field, renders $|T_-\rangle$ degenerate with $|S_-\rangle$.

The spin-orbit coupling $\tilde{\epsilon}_d$ involves the polarized triplets into the coherent state of the dots, around the now separate resonances $|E_Z - E_{Z-}| \simeq \tilde{\epsilon}_d$ and $|E_Z - E_{Z+}| \simeq \tilde{\epsilon}_d$. There are a few distinctions between the coherent dot-states at the resonances of intermediate and zero detuning regimes, seen in the two lower panels of Fig. 7.3. In the zero detuning regime the probability of the spin blockade periodically reaches

unity. However, as a consequence of the decreased weight of the singlet state in the presence of detuning, the triplet activation, and hence the amount of spin blockade, remains much weaker. Secondly, the individual activation of the polarized triplets ruins the entanglement of the electron pair. However, while involving only one of the polarized triplets destroys entanglement, it also introduces non-zero spin-polarization in the double dot.

7.3.1 Spin-polarization

Spin-polarization is the degree at which spin is aligned with a given direction [49]. In the singlet and neutral triplet states each electron spin has a zero polarization, since they are in a superposition of opposite spins. In contrary, The spins in the polarized triplets are maximally polarized along external field in $|T_+\rangle$ and opposite to it in $|T_-\rangle$. The average spin-polarization on the double quantum dot over a time-period τ is quantified by the integral

$$P_{\text{avg}} = \frac{1}{\tau}\int_0^\tau dt \frac{P_{T_-}(t) - P_{T_+}(t)}{P_S(t) + P_{T_0}(t) + P_{T_-}(t) + P_{T_+}(t)}, \tag{7.26}$$

where $P_X(t)$ are the occupation probabilities of the eigenstates of the (non-empty) dot-state. Fig. 7.4 shows the average polarization as a function of Zeeman energy E_Z. Non-zero polarization appears around the two resonances E_{Z+} and E_{Z-} as a sign of the polarized triplet activation. In the left panel, the polarization is weaker since the singlet state is strongly present in the coherent state. The stronger polarization, seen in the right panel of Fig. 7.4, is achieved in the third energy regime of the superconductor-double quantum dot system; the high detuning regime.

7.4 Regime of high detuning

At a high detuning $\nu \gg \Gamma_{\text{CPS}}$, the empty state gets effectively decoupled from the two-particle states by a large gate-induced potential energy, which highly suppresses

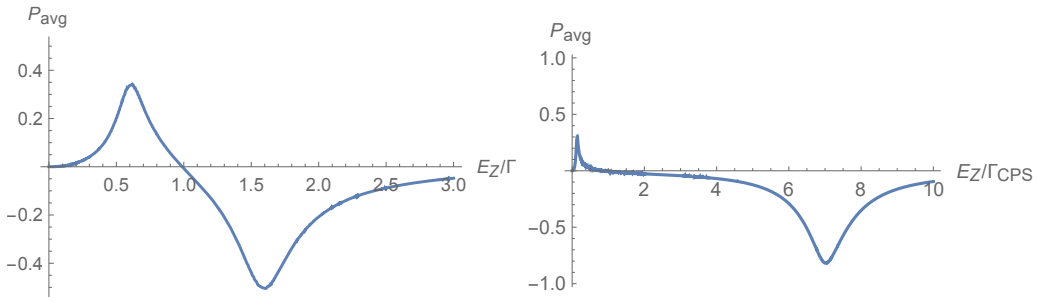

Figure 7.4: (Color online.) Spin-polarization. The average polarization (7.26) of the electron pair on the double quantum dot as a function of Zeeman energy E_Z. **Left:** At the indeterminate detuning regime $\nu = \Gamma_{\rm CPS}$ the average polarization has two peaks with opposite signs, centered at the two resonances $E_Z = E_\pm$, where the polarized triplets $|T_+\rangle$ and $|T_-\rangle$, respectively, become dominant in the coherent state of the electron pair. **Right:** At the high detuning regime $\nu = 7\Gamma_{\rm CPS}$, the second polarization peak becomes greatly emphasized due to suppression of the singlet state, suggesting that a Cooper pair splitter can function as a source of spin current.

the mixing of $|0\rangle$ and $|S\rangle$ states. In the formal treatment of the system, the smallness of $\Gamma_{\rm CPS}$ compared to ν implies that $\Gamma_{\rm CPS}$ should be considered as a perturbing correction term, rather than part of the unperturbed Hamiltonian. Furthermore, as will be seen shortly, an interesting time evolution in this regime occurs when the magnetic Zeeman energy is rather high, $E_Z \simeq 7\Gamma_{\rm CPS}$. This causes the spin-orbit couplings to be comparable with the amplitude of the crossed Andreev reflection $\tilde{\epsilon}_{d/s} \simeq 0.1E_Z \simeq \Gamma_{\rm CPS}$. Hence, it is reasonable to treat them on an equal footing, as

a perturbation $\tilde{H}$, in $\hat{H} = \hat{H}_0 + \tilde{H}$, where

$$\hat{H}_0 = \begin{bmatrix} 0 & 0 & 0 & 0 & 0 \\ 0 & \nu & 0 & 0 & 0 \\ 0 & 0 & \nu & 0 & 0 \\ 0 & 0 & 0 & \nu + E_Z & 0 \\ 0 & 0 & 0 & 0 & \nu - E_Z \end{bmatrix} \tag{7.27}$$

and (7.28)

$$\tilde{H} = \begin{bmatrix} 0 & \Gamma^*_{\mathrm{CPS}} & 0 & 0 & 0 \\ \Gamma_{\mathrm{CPS}} & 0 & 0 & \tilde{\epsilon}^*_d & -\tilde{\epsilon}_d \\ 0 & 0 & 0 & \tilde{\epsilon}^*_s & \tilde{\epsilon}_s \\ 0 & \tilde{\epsilon}_d & \tilde{\epsilon}_s & 0 & 0 \\ 0 & -\tilde{\epsilon}^*_d & \tilde{\epsilon}^*_s & 0 & 0 \end{bmatrix}. \tag{7.29}$$

As a result of the gate-induced Coulomb blockade, the mixing of the eigenstates $|0\rangle$ and $|S\rangle$ is now not present in the unperturbed Hamiltonian. The double quantum dot remains empty as the Andreev reflection is suppressed. Tuning the $|T_+\rangle$ triplet in resonance with the singlet state has no significant effect, due to the suppressed $|0\rangle$ to $|S\rangle$ transport.

However, there is a peculiar way around the Coulomb blockade. Subjecting the quantum dots to a magnetic field with Zeeman energy $E_Z = E_{Z-} \simeq \nu$ brings the $|T_-\rangle$ triplet into resonance with the empty state, as depicted in the left panel of Fiq. 7.5. There is no direct coupling between the two states, as they are separated by two spin-flips, but a second order transport occurring via virtual singlet state indeed connects them. This mechanism enables extraction of strongly spin polarized currents from a Cooper pair splitter.

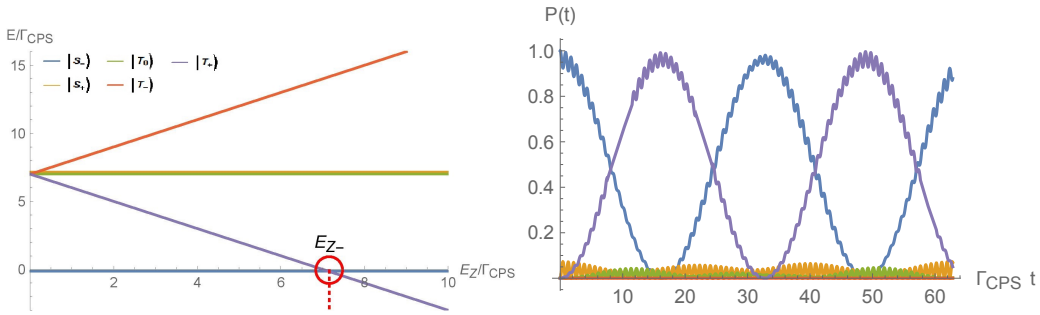

Figure 7.5: (Color online.) Resonance point and coherent evolution at a high detuning $\nu = 7\Gamma_{\mathrm{CPS}}$. **Left:** At a high value of Zeeman energy, $E_Z = \nu$, the polarized triplet $|T_-\rangle$ becomes degenerate with the empty state. **Right:** The spin-orbit coupling enables rotations to the polarized triplet state $|T_-\rangle$, even though the usual tunnelling of singlet Cooper pairs is suppressed by the high detuning. This exchange is maximized at the sweet-spot of $\nu = 7\Gamma_{\mathrm{CPS}}$.

7.4.1 Spin current

The amplitude of the second order tunneling process between $|0\rangle$ and $|T_-\rangle$ is calculated in a manner resembling the single-electron co-tunneling (2.31).

$$\begin{aligned}
\tilde{\epsilon}_{\mathrm{eff}} &\equiv \langle T_-|\, \tilde{H} \frac{1}{E_0 - \hat{H}_0} \tilde{H}\, |0\rangle \\
&= \langle T_-|\, \tilde{H} \frac{1}{E_0 - \hat{H}_0} \Gamma_{\mathrm{CPS}}\, |S\rangle \qquad\qquad \text{where } E_0 = \langle 0|\, \hat{H}_0\, |0\rangle = 0 \\
&= \frac{\Gamma_{\mathrm{CPS}}}{-\nu} \langle T_-|\, \tilde{H}\, |S\rangle \\
&= \frac{\Gamma_{\mathrm{CPS}}}{-\nu} \langle T_-|\, (\Gamma^*_{\mathrm{CPS}}\, |0\rangle + \tilde{\epsilon}_d\, |T_+\rangle - \tilde{\epsilon}^*_d\, |T_-\rangle) \\
&= \frac{\tilde{\epsilon}^*_d \Gamma_{\mathrm{CPS}}}{\nu}.
\end{aligned} \tag{7.30}$$

Though the amplitude of this transport is $\tilde{\epsilon}^*_d/\nu$ times smaller than the that of the first order Cooper pair exchange Γ_{CPS}, at the resonant Zeeman energy $E_Z = \nu$, it dominates the coherent evolution while the Andreev reflection is suppressed by the high detuning. Note that the coherent oscillations between the empty state and polarized triplet happen at a slower frequency than the Cooper pair transfer at its

resonance, $\tilde{\epsilon}_{\rm eff}/\hbar \equiv \tilde{\epsilon}_d^* \Gamma_{\rm CPS}/\nu\hbar \simeq \Gamma_{\rm CPS}/7\hbar$.

Further subtlety follows from the $|0\rangle$ to $|T_-\rangle$ transport being also dependant of the ratio $\Gamma_{\rm CPS}/\nu$, that limits the $|0\rangle$ to $|S\rangle$ part of the transfer. The suppression of the Andreev reflection carries over to the second order process, and consequently, for too high detuning ν, the mixing of $|0\rangle$ and $|T_-\rangle$ becomes partial even at the resonance. The sweet spot for the detuning and corresponding resonant Zeeman energy that realizes the complete mixing seems to be around $\nu = E_Z \simeq 7\Gamma_{\rm CPS}$. At a higher detuning the mixing becomes weaker as transport to $|S\rangle$ diminishes further. At a detuning lower than $\nu = E_Z \simeq 7\Gamma_{\rm CPS}$, the singlet activation starts to become too strong and the system returns to the intermediate detuning regime of the previous section.

Interestingly, the spin-orbit interaction, that was in the previous chapter used to reduce the tunneling between superconductor and the dots (in favour of higher double dot occupancy), now works to lift a tunneling blockade. The *spin-orbit resonance*, occurring at $\nu = E_Z \simeq 7\Gamma_{\rm CPS}$, subverts the blockade with the price of only allowing $|T_-\rangle$ state on the dots. Evidently, this guarantees high spin-polarization of the electrons on quantum dots (see right panel of Fiq. 7.3.1).

This novel observation suggests that a type-I superconductor can be compelled to yield electron pairs in the triplet state with nearly a unit probability. Furthermore, the triplet is guaranteed to be the one anti-aligned with the external field, $|T_-\rangle$. This means, remarkably, that further coupling the double quantum dot to drain leads leads to a *spin current*. More specifically, a Cooper pair splitter can be used as a source of correlated spin-polarized twin currents.

This concludes the discussion of the effects of spin-orbit coupling at various resonances, that were found by varying the electric and magnetic fields, namely the detuning ν and Zeeman energy E_Z inflicted to the dots. Next chapter addresses entanglement, the desired outcome of Cooper pair splitting.

8. Entanglement

Entanglement is a central feature of quantum mechanics, arguably on par with the uncertainty and superposition principles. Entanglement refers to a non-local correlation between seemingly distinct physical systems. It arises in situations where some restriction, say the Pauli exclusion principle or a conservation law, is combined with the quantum uncertainty associated with superposition states.

As an example, consider two electrons that can occupy the same energy state only if they have opposite spins, as dictated by the Pauli exclusion. Unobserved spin of an electron does not have a fixed value, but exists in a coherent superposition of eigenstates (Sec. 3.1). Thus, the total spin of an electron pair sharing an energy level is known to be zero, but the value of each individual spin is undetermined. Once either of the spins is measured, the value of the other spin becomes also immediately known.

The significance of the phenomenon is highlighted by considerations of entangled pairs separated by long distances. The measurement of one particle determines the state of the other with superluminal speed. The effort to capitalize these non-local correlations has motivated the field of quantum information processing, where entanglement is used, for instance, as a resource for new more powerful computational algorithms and encryption methods [11]. Consequently, the production of particles with entangled quantities is an important endeavour for photonics and solid-state physics alike.

8.1 Formalism

Formally, entanglement is a property of a state vector of *composite systems*, that consists of two or more subsystems. By definition, a composite state is entangled if it cannot be expressed as a single tensor product of states of its subsystems. In view of the two-electron states on double quantum dot, it suffices to restrict to two-component, i.e. *bipartite* composite systems. For the state vector of the double quantum dot, the subsystems are the electrons on each single level dot. The states of these electrons are superpositions of the two possible spin orientations along the measuring field

$$|\psi_1\rangle = \alpha_1 |\uparrow\rangle + \beta_1 |\downarrow\rangle$$

and

$$|\psi_2\rangle = \alpha_2 |\uparrow\rangle + \beta_2 |\downarrow\rangle \,, \tag{8.1}$$

respectively for the left and right dot. The composite state vector of the two-electron system is then produced as a tensor product (3.15) of the $|\psi_1\rangle$ and $|\psi_2\rangle$ states.

Coming back to the definition of entanglement, according to the Schmidt decomposition [87], every composite system can always be expressed as a sum of subsystem tensor products. A state of a bipartite system, such as the double quantum dot can be expressed as

$$|\psi\rangle_{12} = \sum_{i,j}^{2} \gamma_{ij} |i\rangle_1 \otimes |j\rangle_2 \,, \tag{8.2}$$

where the $\gamma_{ij} \in \mathbb{C}$ are normalized probability amplitudes of the composite states and $|i\rangle_1$ and $|j\rangle_2$ are the eigenstates of the subsystems one and two. Now, if a composite state can be expressed as exactly *one* tensor product of its subsystem i.e. it has a single-term Schmidt decomposition, the state is *not* entangled. In contrast to these *product states*, the *entangled states* are composite states whose Schmidt decomposition has more than one term. In view of these definitions, writing the

sum of Eq. (8.2) in the spin-notation,

$$|\psi\rangle_{12} = \gamma_{11}\,|\uparrow\rangle \otimes |\uparrow\rangle + \gamma_{12}\,|\uparrow\rangle \otimes |\downarrow\rangle + \gamma_{21}\,|\downarrow\rangle \otimes |\uparrow\rangle + \gamma_{22}\,|\downarrow\rangle \otimes |\downarrow\rangle\,, \tag{8.3}$$

makes it evident that the singlet and neutral triplet are entangled while the polarized triplets are non-entangled product states.

8.1.1 Bell states

The bipartite system with two-level subsystems is the simplest system to exhibit entanglement. There are four maximally entangled bipartite states that span the space of maximally entangled states in composite Hilbert space $\mathbb{C}^2 \otimes \mathbb{C}^2$. Known as the *Bell states*, they are written in the spin notation as

$$\begin{aligned}
|\psi_1^{Bell}\rangle &= \frac{1}{\sqrt{2}}(|\uparrow\downarrow\rangle + |\downarrow\uparrow\rangle) \\
|\psi_2^{Bell}\rangle &= \frac{1}{\sqrt{2}}(|\uparrow\downarrow\rangle - |\downarrow\uparrow\rangle) \\
|\psi_3^{Bell}\rangle &= \frac{1}{\sqrt{2}}(|\uparrow\uparrow\rangle + |\downarrow\downarrow\rangle) \\
|\psi_4^{Bell}\rangle &= \frac{1}{\sqrt{2}}(|\uparrow\uparrow\rangle - |\downarrow\downarrow\rangle).
\end{aligned} \tag{8.4}$$

Evidently, the first and second Bell states are the neutral triplet $|T_0\rangle$ and singlet $|S\rangle$ states of the two-electron system and the latter two are symmetric and antisymmetric superpositions of the polarized triplets; $\frac{1}{\sqrt{2}}(|T_+\rangle + |T_-\rangle)$ and $\frac{1}{\sqrt{2}}(|T_+\rangle - |T_-\rangle)$.

A general quantum state in $\mathbb{C}^2 \otimes \mathbb{C}^2$ space is a superposition of the entangled Bell states and non-entangled product states. Consequently, such states can be only *partially* entanglement. Indeed, the degree of entanglement i.e. non-classical correlation in the measurements outcomes is a continuous variable. In a maximally entangled system, the outcomes of subsystem measurements correlate perfectly, but entanglement can also manifest more subtly as a statistical phenomenon. This calls for a continuous measure of entanglement. While the Von Neumann entropy

[88] is perhaps the most renown measure, a quantity called the *concurrence* [89] is convenient for two-level systems.

8.1.2 Concurrence

The concurrence is defined for pure (as opposed to mixed) bipartite states as [14]

$$C = 2\sqrt{\mathrm{Det}(\gamma\gamma^\dagger)}, \tag{8.5}$$

where the matrix $\gamma = \sum_{ij} \gamma_{ij} |i\rangle \langle j|$, with $i, j = \{\uparrow, \downarrow\}$, contains the probability amplitudes of the superposed two-level states and is normalized by the relation $\mathrm{Tr}(\gamma\gamma^\dagger) = 1$. Concurrence varies from 0 for product states to 1 for maximally entangled states. Thereby, the Bell states (8.4) and their linear combinations have a unit concurrence, whereas superpositions involving both Bell states and product states have concurrence less than one.

Tracking the concurrence of the electron pair on the double quantum dot of a Cooper pair splitter requires writing the matrix $\gamma(t)$ in the basis of spin configurations $\{\uparrow\uparrow, \uparrow\downarrow, \downarrow\uparrow, \downarrow\downarrow\}$. In terms of the time-dependent amplitudes $c_X(t) = \langle X|\psi(t)\rangle$, for $X \in \{S, T_0, T_+, T_-\}$ it reads

$$\gamma(t) = \begin{bmatrix} c_{T_+}(t) & \frac{1}{\sqrt{2}}(c_{T_0}(t) + c_S(t)) \\ \frac{1}{\sqrt{2}}(c_{T_0}(t) - c_S(t)) & c_{T_-}(t) \end{bmatrix}. \tag{8.6}$$

The coherent evolution of the concurrence (8.5) can be now compared to the evolution of the two-electron wavefunction occupation probabilities (7.17). Furthermore, a time-averaged concurrence can be defined as

$$C_{avg} = \frac{1}{\tau} \int_0^\tau dt \; 2\sqrt{\mathrm{Det}[\gamma(t)\gamma^\dagger(t)]}, \tag{8.7}$$

where τ is a macroscopic measuring time.

8.2 Concurrence and spin-orbit interaction

The Cooper pairs supplied by the superconductor are in a spin-singlet state and thus maximally entangled with $C = 1$. In the conventional regime of Cooper pair splitting, these entangled singlets are immediately collected to the terminals. However, in the regime of long-lived dot-states, the coherent evolution occurs faster than the dot-lead tunnelings and a hybridisation of basis states takes place in the double dots and superconductor. In absence of spin-orbit effects, this superposition is a mixture of the empty state and singlet state. At the transport resonance $\nu = 0$, the superposition is equal, and the average concurrence on the dots is $C_{avg} = 0.5$ (the empty state is defined as having zero concurrence for obvious reasons.)

The results of the spin-orbit interaction are seen in the concurrence of the system. As stated earlier, the activation of the polarized triplets $|T_+\rangle$ or $|T_-\rangle$ generally reduces the average entanglement available in the double quantum dot. Indeed, the left panels of Fig. 8.1 shows a decline of concurrence at the two resonances E_{Z+} and E_{Z-} in the regime of intermediate detuning $\nu = \Gamma_{\mathrm{CPS}}$, where the polarized triplets are separately activated. This is contrasted by the resonance at the zero detuning regime, where the equal activation of the polarized triplets introduces an entangled state, $\frac{1}{\sqrt{2}}(|T_+\rangle + |T_-\rangle)$, to the coherent superposition of the electron pair. This equal superposition of triplets can be identified as a fully entangled Bell state from Eq. (8.4). Therefore, as demonstrated by the right panels of Fig. 8.1, the average concurrence of the two-electron state is increased due to the spin blockade.

The next chapter describes how information on the state of the electron pair can be obtained through charge measurements. It turns out that it is possible to distinguish between the coherent states of the quantum dots, discussed in previous sections, by looking at the average charge.

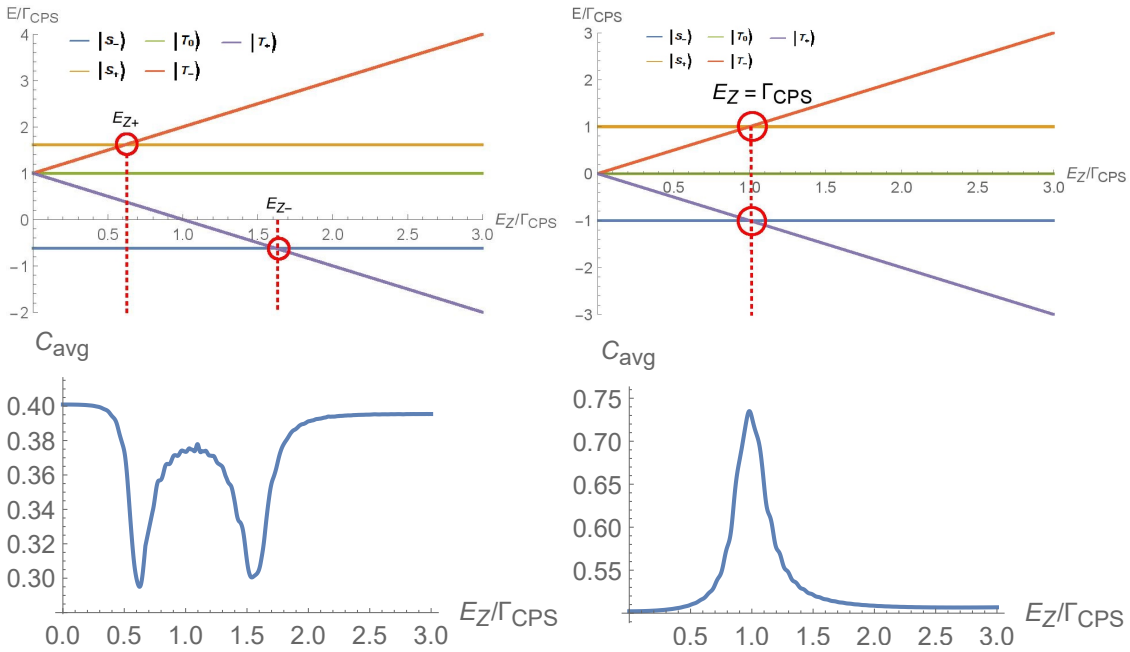

Figure 8.1: (Color online.) Average concurrence. **Top:** The degeneracy points at intermediate ($\nu = \Gamma_{\rm CPS}$) and zero ($\nu = 0$) detuning regimes, respectively. **Bottom:** Corresponding graphs of the average concurrence (8.7) as a function of Zeeman energy. The average concurrence degreases at the degeneracy points $E_Z = E_{Z+}$ and $E_Z = E_{Z-}$, due to activation of triplet states by the spin-orbit coupling. At zero detuning the average concurrence increases on the resonance $\nu = \Gamma_{\rm CPS}$, where the triplets are activated equally in an entangled superposition.

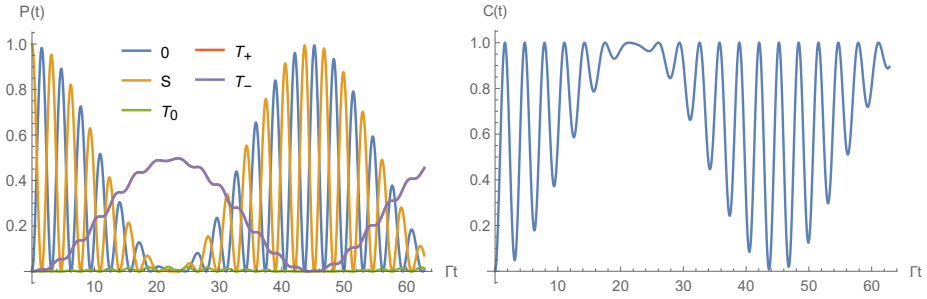

Figure 8.2: (Color online.) Concurrence stabilization. **Left:** At the transport resonance $\nu = 0$ the polarized triplets are activated equally at the double degeneracy point (the probabilities of $|T_+\rangle$ and $|T_-\rangle$ are on top of each other in the graph). **Right:** The oscillations of concurrence (8.6) decrease as the $\frac{1}{\sqrt{2}}(|T_+\rangle + |T_-\rangle)$ state gains presence in the coherent state of the system. The fact that the concurrence stabilizes to unit value at the peak of spin blockade implies that the spin-orbit interaction can indeed produce maximally entangled state.

9. Detection

Spin of a particle is a well isolated quantity due to a weak coupling to the environment, that warrants long coherence times of spin states. Though this allows production of systems well resistant to external disturbances, it also makes the readout of a spin state harder to achieve. The magnetic moment generated by spin is of the order of Bohr magneton (3.11), so its detection by magnetic fields is challenging.

This chapter illustrates how information of the spin state on the double quantum dot of a Cooper pair splitter can be obtained indirectly by looking at the time averaged charge on the dots (in the regime of long lived dot-states; see Sec. 5.3.1). The charge state can be studied either directly by real-time charge detection using a quantum point contact [36, 37] or by performing tunnel spectroscopy i.e. measuring the current arriving to the terminal leads; see Fig. 9.1.

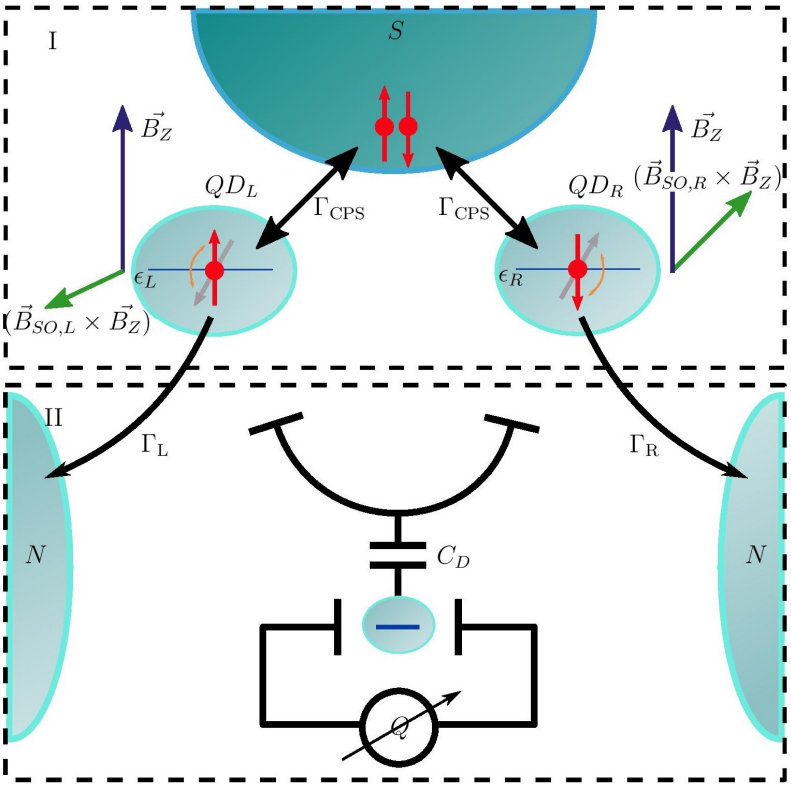

Figure 9.1: (Color online.) Cooper pair splitter and charge measurement. Superconductor (S) and two quantum dots ($\mathrm{QD}_{L,R}$) form the coherent part (I) of the device. The crossed Andreev reflection Γ_{CPS}, electric potentials of the quantum dots $\epsilon_{L,R}$, external static magnetic field $\vec{B}$ and spin-orbit fields $\vec{\gamma}_{L,R} \times \vec{B}$ define the state of the coherent system of part (I). Information of this state can be obtained by weakly coupling the dots either to a capacitive charge measurement device (center of part II) or normal metal leads (N), set to lower potential than the dots. In the regime of long-lived dot-states (Sec. 5.3.1), the coherent state and average entanglement on the dots can be deduced from the current arriving to the lead terminals, or charge measured by capacitive charge measuring device.

9.1 Tunnel spectroscopy

The charge measurements yield information about the spin state for the following reason. Because of the spin blockade effect discussed in Sec. 7.2.1, the probability that the quantum dots are in the empty state anti-correlates with the probability of them being in any of the triplet states. From a charge detection viewpoint, a lower measured average charge implies more time spend in the empty state. Hence, as the empty state can only be reached from the singlet state (with the exception of the spin-orbit transport resonance, introduced in Sec. 7.4.1), greater time-averaged charge can be seen as a sign of the spin blockage resulting from the activation of the triplet states.

9.2 Real-time charge detection

The time-averaged charge on the dots can be quantified as,

$$Q_{avg} = \frac{2e}{\tau}\int_0^\tau dt[P_S(t) + P_{T_0}(t) + P_{T_-}(t) + P_{T_+}(t)], \tag{9.1}$$

where τ is macroscopic measurement time. Equivalently, the average charge can be connected to the probability of the dots *not* being empty, $Q_{avg} = \frac{2e}{\tau}\int_0^\tau dt[1 - P_0(t)]$. In absence of the spin-orbit effects, the time-averaged charge on the double quantum dot is the electron charge e, as the system oscillates symmetrically between the empty state ($0e$) and the singlet ($2e$). The average charge increases when spin-orbit coupling is active at the resonance points, discussed in Secs. 7.2-7.4, and spin rotations to the spin blockaded triplet states ($2e$) are occurring.

Fig. 9.2 shows the average charge (9.1) plotted as a function of the Zeeman energy E_Z in the three detuning regimes discussed in Ch. 7. Corresponding concurrence plots are shown also. In all of the regimes, the average charge on the quantum dots peaks at the resonant values of Zeeman energy. The width of the peak is given by the strength of the spin-orbit coupling ϵ_d.

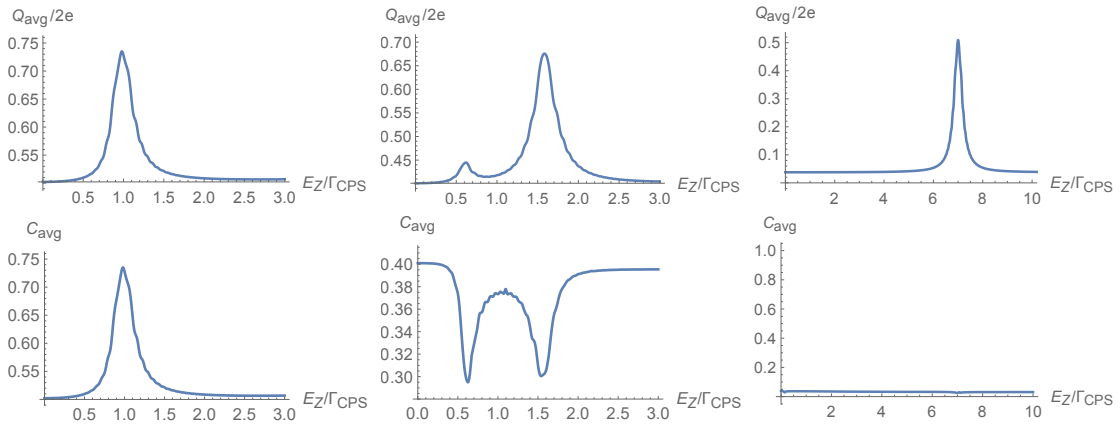

Figure 9.2: (Color online.) Average charge and concurrence. **Top**: average charge (9.1) on the double quantum dot of the Cooper pair splitter at three different detuning regimes: zero detuning, intermediate detuning and high detuning, respectively from left to right. **Bottom**: Corresponding plots of average concurrence (8.7). The average charge can be used to acquire information of the degree of entanglement. In the zero detuning regime the concurrence increases as the average charge grows due to spin-blockade. In the intermediate detuning regime the opposite is seen: concurrence decreases when average charge increases (effect of the individual activation of the polarized triplets). In the high detuning regime the average concurrence remains close zero at all times as the double dot is either empty or houses a non-entangled $|\downarrow\downarrow\rangle$ triplet state.

When only one of the polarized triplets is activated at a given time, as happens with the intermediate and high detuning, the concurrence of the electron pair decreases. Thus, in these regimes the increase of average charge marks a drop in concurrence as a result of spin blockaded product state $|T_+\rangle$ or $|T_-\rangle$ occupying the double dot. At the zero detuning, however, the concurrence increases along with the average charge. This is in agreement with the notion of equal activation of the polarized triplets as an entagled state $(|T_+\rangle + |T_-\rangle)/\sqrt{2}$.

In the regime of long-lived dot-states, the weak coupling between dots and

terminal leads motivates the treatment of the superconductor and double quantum dot as a single hybridized system that outputs electrons to the two leads with rates $\Gamma_{L,R}$ (see the single electron tunneling in Sec. 2.4). Since the tunneling rates from left dot to left lead and right dot to right lead are probabilistic and non-correlated, the double dot will at times hold an unpaired electron. Another Cooper pair can enter the dots from the superconductor only when the lone electron has also tunnelled into a lead. Single electron on the double dot can become de-localised as a result of co-tunneling (Sec. 2.8) through a virtual state in the superconductor.

In view of this, when taking the terminal leads into consideration, the superconductor-dots system is described by an effective non-perturbed Hamiltonian for the even and odd occupation states, $\hat{H}^{(0)}_{CPS} = \hat{H}_e \otimes H_o$, with

$$\hat{H}_e = \begin{pmatrix} 0 & \Gamma_{\mathrm{CPS}} \\ (\Gamma_{\mathrm{CPS}})^* & \epsilon_L + \epsilon_R \end{pmatrix}; \tag{9.2}$$

$$\hat{H}_o = \begin{pmatrix} \epsilon_L & \Gamma_{\mathrm{EC}} \\ (\Gamma_{\mathrm{EC}})^* & \epsilon_R \end{pmatrix}, \tag{9.3}$$

where $\otimes$ signifies the direct product, ϵ_L and ϵ_R are chemical potentials of the left and right dots and the coupling matrix elements Γ_{CPS} and Γ_{EC} are the amplitudes of crossed Andreev reflection and co-tunneling, respectively. The Hilbert bases of the Hamiltonians are $\{|0,0\rangle, |1,1\rangle\}$ and $\{|1,0\rangle, |0,1\rangle\}$ for even and odd occupation, respectively. Luckily, the co-tunneling appearing in the odd occupation Hamiltonian, $\hat{H}_o$, can be suppressed by sufficiently detuning the chemical potentials of the dots $|\epsilon_L - \epsilon_R| \gg 1$. This does not affect the evolution of the even occupation Hamiltonian, $\hat{H}_e$, since there only the sum of the chemical potentials has significance. For instance, the transport resonance for Cooper pair exchange, $\epsilon_L + \epsilon_R = 0$, can be reached even if the dots are detuned, $\epsilon_L \neq \epsilon_R$ [90].

For this reason, the electron co-tunneling can be left out of consideration when deriving a formula for the current resulting from electrons tunneling into the terminal

leads. The double dot will simply deplete its electrons, one to each of the terminals, in a time scale given by dot-lead tunneling rates $\Gamma_{L,R}$. The resulting tunneling spectroscopy current is given by the charge entering the leads per unit of time. The charge in question is the average charge on the double dot determined by the coherent evolution of the superconductor-dots system in its even occupation space i.e. Eq. (9.1). On the other hand, the rate associated with the probing current is independent of the fast coherent evolution induced by Γ_{CPS} as well as the perturbations $\tilde{\epsilon}_{d,s}$ included in the complete Hamiltonian (7.1). By the bottle-neck principle, the rate through the device is equal the slowest rate, that are in this case the dot-to-leads rates $\Gamma_{L,R}$. Hence, in the limit of long-lived dot-states, the current to the terminals is

$$I_N = Q_{\mathrm{avg}}\Gamma_N, \tag{9.4}$$

where the subscript N refers to the combined contribution of the terminal leads ($I_N = I_l + I_r$ and $\Gamma_N = \Gamma_L + \Gamma_R$). So, using the weakly coupled terminal leads to measure the tunneling current from the quantum dots yields information on the charge state, and thus the spin state and entanglement, on the double quantum dot. That is assuming that the tunneling rates $\Gamma_{L,R}$ are known.

In conclusion, evidence of the spin blockade, and arguably of the entanglement, can be obtained by utilizing one of the two schemes presented here, real-time charge detection and tunneling spectroscopy. Both methods work on the limit of weak coupling between the double quantum dot and the terminal leads. The final chapter of this thesis will review the most important results and discuss the implications of active the spin-orbit interaction in the Cooper pair splitter. In particular, the possibility for manipulation of the spin states by time-varying electric fields is considered.

10. Conclusions

The purpose of Cooper pair splitters is to provide spin-entagled electron pairs. In these devices, the spin-entangled Cooper pairs, occurring naturally in superconductors, are made to tunnel through quantum dots into two separate lead terminals. This scheme enables the splitting of Cooper pairs to spatially separated entangled electrons.

The semiconducting quantum dots, used to filter out other transport processes than the desired split tunneling (inverse crossed Andreev reflection), can be made to exhibit active spin-orbit interaction. Spin-orbit interaction is a relativistic effect, where the spin of an electron couples to an electric field (here of the ions of the quantum dot) and rotates as the electron moves in it. Active spin-orbit interaction is achieved by subjecting quantum dots fabricated of specific material, such as InAr or GaAr, that are already commonly used in Cooper pair splitters, to an external static magnetic field.

This thesis investigated the effects of spin-orbit interaction to the state of the electrons in the double quantum dot of a Cooper pair splitter. To enable the measurement of the state in the double quantum dot, the transport through the device is slowed down by suppressing the tunneling between the dots and terminal leads. It was shown in Ch. 9 that measuring the average charge (either capacitively or by tunnel spectroscopy) yields information on the spin state of the electrons in the dots. This is possible due to the spin blockade i.e. the limitation that electron pairs

in the dots that are in the triplet state cannot tunnel back to the superconductor (until spin-flip back to singlet state occurs), and hence occupation of triplet states leads to an increased average charge. Clear fingerprint of the spin-flipping is seen at the transport resonance of the Cooper pairs in Sec. 7.2.1, where the detuning of the quantum dots with respect to the superconductor is zero, when the external Zeeman magnetic field is set equal to the Cooper pair splitting amplitude $\Gamma_{\rm CPS}$.

Under these conditions, the polarized triplets $|T_+\rangle$ and $|T_-\rangle$ both become degenerate with an eigenstate ($|S_+\rangle$ and $|S_-\rangle$ respectively) of the superconductor-dots system. At this resonance, the perturbative spin-orbit coupling terms can hybridize the eigenstates with the triplets, introducing a maximally entangled component $(|T_+\rangle + |T_-\rangle)/\sqrt{2}$ in the coherent superposition of the system. Hence, with the control handles set to $\nu = 0$ and $E_Z = \Gamma_{\rm CPS}$, the increase in the average charge on the dots implies equal increase in the average entanglement; see Ch. 8.

The possibility of utilizing the active spin-orbit interaction of the quantum dots to produce spin-polarized currents was discussed in Sec. 7.4.1. This can be achieved in the regime of high detuning (suppressed singlet-exchange) $\nu = 7\ \Gamma_{\rm CPS}$, when the polarized triplet $|T_-\rangle$ is brought to resonance with $|S_-\rangle$ by Zeeman energy $E_Z = 7\ \Gamma_{\rm CPS}$.

In addition to proposing a way to validate the presence of spin-orbit interaction in the Cooper pair splitter, through charge measurements that observe the spin blockade, the findings of this thesis imply possibility of spin-manipulation in the device. The magnetic and electric fields (gate voltages) considered in this thesis were time-independent. It seems plausible that using time-varying gate-voltages would allow for spin-manipulation via the spin-orbit couplings $\tilde{\epsilon}_{s,d}(t) \propto \vec{B}_{\rm SO}(t) \propto \vec{v} \times \vec{E}(t)$. This would give complete control over the spin state of the electron pair extracted from the Cooper pair splitter. Results of such spin control could then in principle be confirmed using the same charge measurement schemes that were presented here.

References

1 E. Schrödinger, Mathematical Proceedings of the Cambridge Philosophical Society **31**, 555 (1935).

2 R. Horodecki, P. Horodecki, M. Horodecki and K. Horodecki, Reviews of modern physics **81**, 865 (2009).

3 D. N. Page and W. K. Wootters, Physical Review D **27**, 2885 (1983).

4 E. Moreva, G. Brida, M. Gramegna, V. Giovannetti, L. Maccone and M. Genovese, Physical Review A **89**, 052122 (2014).

5 M. Van Raamsdonk, General Relativity and Gravitation **42**, 2323 (2010).

6 R. Ursin et. al., Nature physics **3**, 481 (2007).

7 L. M. Duan, M. D. Lukin, J. I. Cirac and P. Zoller, Nature **414**, 413 (2001).

8 R. Jozsa and N. Linden, Proceedings of the Royal Society of London. Series A: Mathematical, Physical and Engineering Sciences **459**, 2011 (2003).

9 A. Steane, Reports on Progress in Physics **61**, 117 (1998).

10 A. Einstein, B. Podolsky and N. Rosen, Physical review **47**, 777 (1935).

11 M. A. Nielsen and I. Chuang, *Quantum computation and quantum information* (Cambridge University Press, 2002).

12 S. J. Freedman, J. F. Clauser, Physical review letters, **28**, 938 (1972).

13 A. Aspect, P. Grangier and G. Roger, Physical review letters, **49**, 91 (1982).

14 C. W. J. Beenakker, Proceedings of the International School of Physics Enrico Fermi **162** (2006).

15 B. Bhushan, *Springer handbook of nanotechnology* (Springer, 2017).

16 S. Datta, *Quantum transport: atom to transistor* (Cambridge University Press, 2005).

17 Y. V. Nazarov and Y. M. Blanter, *Quantum Transport: Introduction to Nanoscience* (Cambridge University Press, 2009).

18 A. Crépieux, R. Guyon, P. Devillard and T. Martin, Physical Review B **67**, 20 (2003).

19 D. Loss and E. Sukhorukov, Physical review letters **84**, 1035 (2000).

20 G. B. Lesovik, T. Martin and G. Blatter, The European Physical Journal B-Condensed Matter and Complex Systems **24**, 287 (2001).

21 P. G. De Gennes, *Superconductivity of metals and alloys* (CRC Press, 2018).

22 L. N. Cooper, Physical Review **104**, 1189 (1956).

23 J. Bardeen, L. N. Cooper and J. R. Schrieffer, Physical Review **106**, 162 (1957).

24 P. Recher, E. V. Sukhorukov and D. Loss, Physical Review B **63**, 165314 (2001).

25 L. Hofstetter, S. Csonka, J. Nygård and C. Schönenberger, Nature **461**, 960 (2009).

26 M. A. Kastner, Physics Today **46**, 24 (1993).

27 R. C. Ashoori, Nature **379**, 413 (1996).

28 G. Dresselhaus, Physical Review **100**, 580 (1955).

29 A. V. Khaetskii and Y. Y. Nazarov, Physical Review B **61**, 12639 (2000).

30 C. Fasth, A. Fuhrer, L. Samuelson, V. N. Golovach, and D. Loss, Physical review letters **98**, 266801 (2007).

31 L. Thomas, Nature **117**, 514 (1926).

32 L. Thomas, The London, Edinburgh, and Dublin Philosophical Magazine and Journal of Science **3**, 1 (1927).

33 P. A. M. Dirac, Proceedings of the Royal Society of London. Series A, Containing Papers of a Mathematical and Physical Character **117**, 610 (1928).

34 E. Rashba, Soviet Physics, Solid State **2**, 1109 (1960).

35 C. Padurariu and Y. V. Nazarov, EPL (Europhysics Letters) **100**, 57006 (2012).

36 B. J. Van Wees, H. Van Houten, C. W. J. Beenakker, J. G. Williamson, L. P. Kouwenhoven, D. Van der Marel and C. T. Foxon, Physical Review Letters **60**, 848 (1988).

37 D. A. Wharam, T. J. Thornton, R. Newbury, M. Pepper, H. Ahmed, J. E. F. Frost, D. G. Hasko, D. C. Peacock, D. A. Ritchie and G. A. C. Jones, Journal of Physics C: solid state physics **21**, L209 (1988).

38 J. Kessler, *Polarized electrons* (Springer Science & Business Media, 2013).

39 A. Sommerfeld, Zeitschrift für Physik **47**, 1 (1928).

40 D. V. Averin and K. K. Likharev, Journal of low temperature physics **62**, 345 (1986).

41 S. Datta, *Electronic transport in mesoscopic systems* (Cambridge university press, 1997).

42 C. J. Gorter, Physica **17**, 777 (1951).

43 D. J. Griffiths and D. F. Schroeter, *Introduction to quantum mechanics* (Cambridge University Press, 2018).

44 H. Bruus and K. Flensberg, *Many-body quantum theory in condensed matter physics: an introduction* (Oxford university press, 2004).

45 P. A. M. Dirac, Proceedings of the Royal Society of London A **114**, 243 (1927).

46 E. Fermi, *Nuclear physics: a course given by Enrico Fermi at the University of Chicago* (University of Chicago Press, 1950).

47 C. P. Enz and others, *Wave Mechanics: Volume 5 of Pauli Lectures on Physics* (Courier Corporation, 2000).

48 T. Ouisse, *Electron transport in nanostructures and mesoscopic devices: an introduction* (John Wiley & Sons, 2013).

49 S. Bandyopadhyay and M. Cahay, *Introduction to spintronics* (CRC press, 2015).

50 L. E. Ballentine, *Introduction to spintronics* (World Scientific Publishing Company, 1998).

51 W. Gerlach and O. Stern, Zeitschrift für Physik A Hadrons and Nuclei **9**, 349 (1922).

52 D. Hanneke, S. Fogwell and G. Gabrielse, Physical Review Letters **100**, 120801 (2008).

53 A. Landé, Zeitschrift für Physik **5**, 231 (1921).

54 P. Zeeman, Nature **55**, 347 (1897).

55 G. Zehfuss, Zeitschrift für Mathematik und Physik **3**, 298 (1858).

56 W. Heisenberg, Zeitschrift für Physik **38**, 411 (1926).

57 P. A. M. Dirac, Proceedings of the Royal Society of London. Series A, Containing Papers of a Mathematical and Physical Character **112**, 661 (1926).

58 H. Kamerlingh Onnes, Communications from the Physical Laboratory at the University of Leiden b **120**, (1911).

59 P. L. Kapitza, USSR **18**, 21 (1938).

60 L. Landau, Physical Review **60**, 356 (1941).

61 E. Maxwell, Physical Review **78**, 477 (1950).

62 C. A. Reynolds, B. Serin, W. H. Wright and L. B. Nesbitt, Physical Review **78**, 487 (1950).

63 H. Fröhlich, Physical Review **79**, 845 (1950).

64 A. A. Abrikosov, *Fundamentals of the Theory of Metals* (Courier Dover Publications, 2017).

65 M. Tinkham, *Introduction to superconductivity* (Courier Corporation, 2004).

66 P. Debye, Annalen der Physik **344**, 789 (1912).

67 Y. M. Galperin, *Introduction to modern solid state physics* (Citeseer, 2001).

68 N. N. Bogoliubov, Soviet Physics – Journal of Experimental and Theoretical Physics **7**, 41 (1958).

69 J. Pekola, R. Schoelkopf, Robert and J. Ullom, Physics Today **57**, 41 (2004).

70 P. G. de Gennes and E. Guyon, Physics Letters **3**, 168 (1963).

71 P. G. de Gennes, Reviews of Modern Physics **36**, 225 (1964).

72 N. R. Werthamer, Physical Review **132**, 2440 (1963).

73 A. F. Andreev, Soviet Physics – Journal of Experimental and Theoretical Physics **46**, 1823 (1964).

74 M. Eschrig, Reports on Progress in Physics **78**, 104501 (2015).

75 G. Falci, D. Feinberg and F. W. J. Hekking, EPL (Europhysics Letters) **54**, 255 (2001).

76 C. B. Murray, C. R. Kagan and M. G. Bawendi, Annual review of materials science **30**, 545 (2000).

77 K. Bourzac, Nature News **493**, 283 (2013).

78 M. Esposito R. Kawai, K. Lindenberg and C. Van den Broeck, EPL (Europhysics Letters) **89**, 20003 (2010).

79 A. Das, Y. Ronen, M. Heiblum, D. Mahalu, A. V. Kretinin and H. Shtrikman, Nature communications **3**, 1165 (2012).

80 G. Bihlmayer, O. Rader and R. Winkler, New journal of physics **17**, 050202 (2015).

81 S. Nadj-Perge, V. S. Pribiag, J. W. G. Van den Berg K. Zuo, S. R. Plissard, E. P. A. M. Bakkers, S. M. Frolov and L. P. Kouwenhoven, Physical review letters **108**, 166801 (2012).

82 S. Nadj-Perge, S. M. Frolov, E. P. A. M. Bakkers and L. P. Kouwenhoven, Nature **468**, 1084 (2010).

83 V. N. Golovach, M. Borhani and D. Loss, Physical Review B **74**, 165319 (2006).

84 B. I. Halperin, A. Stern, Y. Oreg, J. Cremers, J. A. Folk and C. M. Marcus, Physical review letters **86**, 2106 (2001).

85 I. L. Aleiner, V. I. Fal'Ko, Physical review letters **87**, 256801 (2001).

86 K. C. Nowack, F. H. L. Koppens, Y. V. Nazarov and L. M. K. Vandersypen, Science **318**, 1430 (2007).

87 A. Ekert and P. L. Knight, American Journal of Physics **63**, 415 (1995).

88 J. Von Neumann, *Mathematical Foundations of Quantum Mechanics: New Edition* (Princeton university press, 2018).

89 S. Hill and W. K. Wootters, Physical review letters **78**, 5022 (1997).

90 Z. B. Tan, D. Cox, T. Nieminen, P. Lähteenmäki, D. Golubev, G. B. Lesovik and P. J. Hakonen, Physical review letters **114**, 096602 (2015).